Doctoral Dissertation

博士論文

Developmental studies on the pentaradial body plan in a sea cucumber *Apostichopus japonicus*

(棘皮動物マナマコにおける五放射相称ボディプランの形成機構に関する発生学的研究)

A Dissertation Submitted for the Degree of Doctor of Philosophy

December 2021

令和３年１２月　博士（理学）申請

Department of Biological Sciences, Graduate School of Science,

The University of Tokyo

東京大学大学院理学系研究科

生物科学専攻

Sumio Udagawa

宇田川澄生

Abstract

Echinoderms, which have dramatically changed their body axes from bilateral symmetrical ancestors and have acquired unique body plans with pentaradial symmetry, are an important phylum in terms of understanding the diversification of body plans. In the developmental process of echinoderms, a tissue called hydrocoel first exhibits the pentaradial form. The hydrocoel arises multiples of five projections (hydrocoel lobes) and transforms into a ring-shaped to form the pentaradial pattern. However, the developmental mechanisms underlying the establishment of pentaradial hydrocoel structure was not elucidated. In addition, although it is known that adult tissues are formed around the hydrocoel lobes, involvement of the hydrocoel in the establishment of the pentaradial symmetry of adult tissues were not investigated. I thought that if the hydrocoel regulates the establishment of pentamery of other tissues, formation of the pentaradial structure in the hydrocoel is the determinant of the pentaradial body axis of echinoderms. To elucidate the role of the hydrocoel in the development of pentaradial body plan and the morphogenetic mechanism of the hydrocoel, I performed following studies by using a sea cucumber species *Apostichopus japonicus*, which possess transparent larvae so that the hydrocoel can be easily observed. Firstly, I showed that the ablation of a hydrocoel lobe prevent the formation of pentaradial nervous system, suggesting that the hydrocoel lobes regulate the formation of the pentaradial nervous system. Then, I investigated the behavior of epithelial cells during the hydrocoel-lobe formation, suggesting that the lobe formation is accomplished by radial cell intercalation of epithelial tissues. Finally, in order to identify genes involved in the hydrocoel-lobe formation, analyses on genes

specifically expressed in the hydrocoel were carried out. As the results, it was implied that several transcription factors and genes related to the Wnt pathway were involved in the regional differentiation inside the hydrocoel. Moreover, inhibition of the Wnt pathway indicated that the pathway is involved in the hydrocoel morphogenesis. Taken together, it was revealed that the pentaradial body plan of the focal sea cucumber is established by the pentaradial hydrocoel formation via the Wnt signaling and radial intercalation and, that induces the pentaradial symmetry of other tissues.

Contents

General Introduction

Echinoderms possess pentaradial body plan.

Metazoans have acquired a wide variety in body plans and understanding the diversification of body plans has been one of the important goals in evolutionary developmental biology (Tusscher and Hogeweg, 2011). Echinodermata, a phylum including animals such as sea stars, sea urchins and sea cucumbers, is thought to have evolved from a bilateral ancestor, and the pentaradial symmetry is a novel trait acquired in echinoderms (A B Smith et al., 2004). This dramatic evolution in body axis is of interest since the body symmetry is the defining feature of animal body plan (Raff, 1996). However, the developmental mechanisms and evolutionary process of this unique body plan have long puzzled zoologists (Hyman, 1955).

The developmental process of the pentaradial body plan: the hydrocoel is the first pentaradial structure

In the development of echinoderms, it is known that the bilateral larvae metamorphose into pentaradial juveniles. During this process, a tissue called hydrocoel first takes the pentaradial form (Ferkowicz and Raff, 2001; Koop et al., 2017; Minsuk and Raff, 2002a). Hydrocoel is the mesodermal coelom on the left side of the larva and multiples of five projections called hydrocoel lobes are formed on the hydrocoel. The hydrocoel becomes the water vascular system, which is an organ involved in circulatory, locomotion, and feeding of echinoderms (Hyman, 1955). It is known that adult tissues such as nerves tissue, muscle and ossicles are formed around the hydrocoel lobes so it has been suggested that

the hydrocoel may induce the formation of these tissues (Dolmatov I . Yu . and Yushin V . V, 1993; Minsuk and Raff, 2002a). However, there is no experimental evidence showing that the hydrocoel regulates the establishment of pentamery in these tissues, and thus the developmental role of hydrocoel in the pentaradial body plan formation has remained unclear.

If the hydrocoel regulates the establishment of pentamery of other tissues, formation of the pentaradial structure in the hydrocoel is the determinant of the pentaradial body axis of echinoderms. Analyses of fossil species also suggested that changes in the morphology of the water vascular system are involved in the evolution of echinoderm symmetry (Sumrall and Wray, 2007). Thus, understanding the mechanisms underlying the formation of pentaradial hydrocoel is an important issue to understand the development and evolution of the pentaradial body plan (Byrne et al., 2016a; S. V. Rozhnov, 2014). However, the mechanisms underlying the hydrocoel morphogenesis remains unclear.

It is known that echinoderms changed their symmetry from bilateral to triradial, and then became pentaradial during their evolution (Smith and Zamora, 2013) and it is thought that these changes in body symmetry may be achieved by the duplication of body axes (Raff and Popodi, 1996). Considering these issues, the examination of whether the hydrocoel contributes to the establishment of pentamery in other tissues is thought to lead to the understanding of body axis formation in pentaradial echinoderms. At the same time, investigation of the mechanism underlying morphogenesis and pattern formation in the hydrocoel itself will provides us an important insight into the duplication of body axes.

Sea cucumber as material to elucidate the developmental functions and morphogenetic mechanisms of the hydrocoel

In this study, the sea cucumber *Apostichopus japonicus* was used as material species. In developmental studies of echinoderms, so far, sea urchins have often been used (Cary and Hinman, 2017). However, it is difficult to observe the development of the hydrocoel since the sea urchins form the structure called adult rudiment, which covers the hydrocoel (Smith et al., 2008). On the other hand, in auricularia larvae of indirect developing sea cucumbers such as *A. japonicus*, the hydrocoel is apart from other tissues and no covering structure is formed around the hydrocoel. Therefore, the process of hydrocoel lobe formation can be easily observed and the hydrocoel can be manipulated without destroying other tissues.

Furthermore, since *A. japonicus* is an important species in fisheries, genome sequences and developmental transcriptome are available (Li et al., 2018; Zhang et al., 2017) and methods to induce spawning and rearing systems are well established. (Kato et al., 2009; Qiu et al., 2015; Yoshida et al., 2001). This species is distributed around the Misaki Marine Biological Station, many individuals were easily obtained for experiments.

Content of this study

In order to elucidate the developmental mechanism underlying pentaradial body plan formation in sea cucumber *A. japonicus*, I conducted analyses on the role of hydrocoel in the development of pentaradial body plan and the morphogenetic mechanism underlying the formation of pentaradial structure in the hydrocoel itself. In Chapter 1, I examined whether the hydrocoel regulates the pentamery of other tissues. The ablation effect of a hydrocoel lobe on the formation of adult pentaradial body plan was evaluated. In Chapter

2, the morphogenetic process of the hydrocoel lobe formation was investigated in detail and the contribution of cell proliferation and migration in the process of lobe formation were observed. In Chapter 3, I tried to identify genes responsible for the formation of pentameric hydrocoel. Expression analyses of regulatory factors in development and the functional assay of signaling pathways were carried out.

Chapter 1.

The pentameric hydrocoel lobes organize adult pentaradial structures in a sea cucumber, *Apostichopus japonicus*.

The content of this chapter has already been submitted as Udagawa, S, Nagai, A, Kikuchi, M, Omori, A, Tajika, A, Saito, M, Miura, T, Irie, N, Kamei, Y & Kondo, M. The pentameric hydrocoel lobes organize adult pentaradial structures in a sea cucumber, *Apostichopus japonicus.* (Under revision)

Abstract

Despite being one of the bilaterians, the body plan of echinoderms shifts from bilateral symmetry to five-fold radial, or pentaradial symmetry during embryogenesis or their metamorphosis. While the clarification of the developmental mechanism behind this transition will be a basis for understanding their unique body plan evolution, it is still poorly understood. With this regard, the hydrocoel, a mesodermal coelom formed on the left side of bilateral larva, would be a clue for understanding the mechanism as it is the first pentaradial structure that appears before metamorphosis and develops into the water vascular system of adults. By analyzing the development of a sea cucumber, *Apostichopus japonicus*, I found that the hydrocoel expresses genes related in muscle and neural formation such as *myosin heavy chain*, *tropomyosin*, *soxC,* and *elav*, implying that cells of the hydrocoel contributes to muscle and neural structures in the adult. Furthermore, ablation of one of the hydrocoel lobes led to incomplete development of adult pentaradial structures, which include tentacles, radial canals and radial nerve cords. My findings suggest that the hydrocoel lobes may serve as a potential organizing center for establishing the pentaradial body plan in echinoderms.

Introduction

The phylum Echinodermata, comprised of sea urchins, sea stars and its allies, is a group in Bilateria, displaying a unique pentaradial (five-fold radial) body plan in their adult phase. This exceptional body plan develops from bilateral larvae through metamorphosis (reviewed in Omori et al., 2018). The developmental process behind the establishment of this unique body plan has long puzzled scientists since body symmetry is the most basic component of animal body plans. Evolutionarily, pentaradial echinoderms are considered to have emerged from bilateral ancestors. Thus, echinoderms are an interesting and suitable model to study the evolution of animal body plans due to the switch in their body plan during development and in the course of evolution. However, the developmental mechanisms, especially the organizing center for the determination of the pentaradial body axis remains to be clarified.

In echinoderms, a variation exists in how the pentaradial body plan is formed from a bilateral larva. For example, a sea urchin *Strongylocentrotus purpuratus* develops its pentaradial body from an adult rudiment that appears in the bilateral larvae, whereas a sea cucumber *Apostichopus japonicus* does not form an adult rudiment but develops a pentaradial body plan by reorganizing the whole larval body (see Smith et al., 2008 and Qiu et al., 2015 for details on development). Despite the diversity in development, a common structure can be observed during the metamorphosis processes. In *S. purpuratus*, prior to metamorphosis, a mesodermal coelom, or the hydrocoel, appears on the left side of the archenteron, and together with the vestibular ectoderm, the hydrocoel contributes to the adult rudiment (Smith et al., 2008). Similarly, *A. japonicus* develops a hydrocoel in bilateral auricularia larvae, although an adult rudiment does not develop (Qiu et al., 2015). The hydrocoel differentiates into the water vascular

system in adults, an organ used for locomotion and circulation in echinoderms and is a major characteristic feature of echinoderms.

In order to study the development of the hydrocoel, I used the sea cucumber, *A. japonicus*. *A. japonicus* is an indirect developer, which develops through feeding larval stages during development. Its transparent larvae up to metamorphosis and accessible genome and transcriptomic information (Li et al., 2020, 2018; Zhang et al., 2017) makes this species an emerging model for echinoderm developmental studies. In addition, its hydrocoel has no overlying tissue such as vestibule ectoderm. Therefore, the development of the hydrocoel is easily observable under the microscope. Moreover, it is relatively easy to observe the development and manipulate the hydrocoel without damaging other tissues.

In the laboratory, spawning may be induced by using a peptide, cubifrin (Kato et al., 2009). After fertilization, *A. japonicus* embryos undergo cleavage and develop into bilateral auricularia larvae (Fig. 1-1a). Through metamorphosis, late auricularia larvae transform into barrel-shaped doliolaria larvae with a pentaradial body plan. Metamorphosis of sea cucumbers is a gradual process and is not as distinct as in sea urchins (Dolmatov et al., 2016; Raff and Byrne, 2006; Smiley, 1986), but reorganization of the ciliary band is one of the features of the initiation of metamorphosis. The larvae further differentiate into pentactula and then into juveniles. Focusing on the hydrocoel, it first appears on the left side of the digestive tract of auricularia larvae, as a sac with a smooth surface (Fig. 1-1b). As development progresses, hydrocoel lobes (bulges arising from the hydrocoel) develop in late auricularia. The number of lobes is a multiple of five, which suggests that pentamery (five-fold symmetry) is being established at this stage. The hydrocoel elongates into a

horseshoe shape and then forms the ring canal surrounding the esophagus to build the first apparent pentaradial structure during metamorphosis (Fig. 1-1b). The five initial lobes (lobes I to V in Fig. 1-1b) extend anteriorly and give rise to the five water vascular canals of the tentacles. Another five lobes (i to v) develop between the first lobes and extend posteriorly, eventually giving rise to radial canals after metamorphosis (Fig. 1-1b) (Hyman, 1955; Smirnov, 2014a). The extension of five radial canals is not synchronized; the mid-ventral radial canal, which runs along the midline of the ventral side, extends first and forms the primary podia at the tip (Dolmatov et al., 2016), and the other four canals follow. In juveniles, the five radial canals of the water vascular system associated with longitudinal muscle bands and the radial nerve cords constitute the major pentaradial structures (Fig. 1-1c).

Of note, the water vascular system originating from the hydrocoel is the first structure that shows pentaradial symmetry, and thus, the hydrocoel could be regarded as an attractive candidate of an organizing center that determines the body plan with pentaradial symmetry. Actually, it has been suggested that the hydrocoel itself is indispensable in the formation of the adult rudiment of a sea urchin *Heliocidaris erythrogramma* (Minsuk and Raff, 2002b). Moreover, possible associations between the hydrocoel lobes and development of pentaradial structures such as the nerve cords and the longitudinal muscle bands of sea cucumbers has been pointed out by previous studies using histological approaches. For example, Dolmatov and Ivantey (1993) pointed out that the radial canal could be inducing the development of longitudinal muscle bands, because the formation of the radial canals precedes the development of paralleling longitudinal muscle bands (Dolmatov and Ivantey, 1993). Induction of nervous system development by the signal from the hydrocoel has also been implicated,

since the formation of the nervous system strongly correlates to that of the hydrocoel (Mashanov et al., 2007).

Nevertheless, whether the pentaradial structure of the hydrocoel, namely the hydrocoel lobes, govern pentaradial axis formation of the entire body remains to be clarified. To answer this question, in this study, I focused on the development of the whole body including the pentaradial structures of the sea cucumber *A. japonicus*, using molecular markers to visualize the differentiation of adult tissues and observing the effect of ablation of a hydrocoel lobe. Due to the difficulty of manual dissection of small tissues, laser ablation was employed for the experiment. My results indicate that the hydrocoel is a key tissue for development, not only by developing into the water vascular system, but also by providing a possible platform where the pentaradial adult organs form. Furthermore, the hydrocoel may act as the source of cells that differentiate into the adult nervous and muscular tissues.

Materials & Methods

Animal culture and sampling of larvae

Adult sea cucumbers, *Apostichopus japonicus* (black type), were collected by SCUBA in Sagami Bay, Kanagawa, Japan and Onahama Port, Fukushima, Japan. The animals were kept in the laboratory and larvae were collected as previously described (Kikuchi et al., 2015). Briefly, spawning was induced by injection of cubifrin (Kato et al., 2009) into females and mature eggs were artificially fertilized. The larvae were cultured in the laboratory of Misaki Marine Biological Station, kept in filtered sea water (20°C) and fed diatoms (*Chaetoceros calcitrans*; Marinetch, Tahara, Japan).

Identification and cloning of molecular marker genes

Sequences for *Strongylocentrotus purpuratus elav*, *soxB1*, *soxC*, *myosin heavy chain* (*mhc*), *tropomyosin* were used as queries (listed in Supplementary Table 1) to search homologous sequences in an *A. japonicus* EST database (Kikuchi *et al*., unpublished). Based on the identified sequences, specific PCR primers were designed (Supplementary Table 2), with which partial sequences were amplified from cDNA of mixed larval stages and cloned into plasmid vectors (pGEM-T easy, Invitrogen).

Whole mount *in situ* hybridization

For whole mount *in situ* hybridization (WISH), larvae were fixed in fixation buffer (4% paraformaldehyde, 0.1 M MOPS, 0.5 M NaCl) and stored in 70% ethanol at -20°C until use. Digoxigenin-labeled RNA probes were synthesized from cloned cDNAs and WISH was performed as previously described (Kikuchi et al., 2015). For more detailed observations, some of the WISH samples were embedded in Technovit 7100 (Heraeus

Kulzer) and sliced into 10 μm sections and counter-stained with Nuclear Fast Red (Sigma-Aldrich).

Ablation of the hydrocoel lobe

The Infrared Laser-Evoked Gene Operator system (IR-LEGO 1000, Sigma-Koki, Saitama Japan) (Kamei et al., 2009) with 1,460 nm infrared (IR) laser (HPU10X09-001, Furukawa Electric, Tokyo Japan) and 20x objective (Olympus Uapo/340 20x, Olympus, Tokyo, Japan) was used for laser ablation (Kimura et al., 2013; Okuyama et al., 2014; Zeng et al., 2021). Just before irradiation, a single larva was temporarily immobilized on the bottom of a glass bottom dish (Matsunami #D11140H, Matsunami Glass, Osaka, Japan) with 0.5 μg/l protamine sulfate in artificial sea water (REI-SEA marine, Iwaki, Osaka, Japan). Then, one of the hydrocoel lobes was irradiated with a high-power IR laser (duration 1/60 sec, power 80 mW, following (Kimura et al., 2013; Okuyama et al., 2014)) several times changing the target location to ablate the tissue. Three types of controls were prepared: larvae which were immobilized but without irradiation, larvae whose hydrocoel lobe was irradiated with low-power IR laser (1/60 sec, 10 mW) and larvae irradiated with high power (1/60 sec, 80 mW) in the right side of the larvae (opposite to the hydrocoel) where no obvious internal tissue is present. After irradiation, protamine sulfate was removed by washing the larvae with filtered sea water and the larvae were individually kept in glass vials (4-6 mL) with filtered sea water containing 75 mg/l of penicillin and streptomycin and fed diatoms.

Immunohistochemistry

Larvae were fixed in methanol overnight. Specimens were incubated with primary antibody against sea star *Asterina pectinifera* synaptotagmin B (1E11, (Nakajima et al., 2004) and (Burke et al., 2006)) at 4°C overnight. After the incubation, samples were washed four times with PBST and then incubated with Alexa fluor 488 conjugated goat anti-mouse IgG (H+L) (Invitrogen) as the secondary antibody, at room temperature for 3 hours. Nuclei (DNA) were labeled with DAPI. Stained samples were observed with confocal laser scanning microscopy (Nikon A1Rsi).

Results

Identification of molecular marker genes for neural and muscle development in *A. japonicus*

Molecular marker genes for muscle differentiation, *tropomyosin* and *myosin heavy chain* (*mhc*) were used in identifying differentiated myoblasts. In *S. purpuratus*, expression of these terminal differentiation markers starts from gastrula at the oral vegetal region and in prism and pluteus stages (Andrikou et al., 2013; Wessel et al., 1990). These are also coexpressed in the circumesophageal muscles (Andrikou et al., 2013). Based on the similarities of predicted amino acid sequences with those of *S. purpuratus*, I identified the homologous sequences from *A. japonicus* (Table 1-1). Similarly, *A. japonicus* homologs for *elav*, *soxB1*, and *soxC* (Table 1-1) were also identified. The involvement of these gene products in neurogenesis have been reported in other echinoderms such as sea urchin *S. purpuratus* and sea star *Patiria miniata* (Garner et al., 2016; Wei et al., 2016, 2011; Yankura et al., 2013). These genes have also been investigated in hemichordates *Saccoglossus kowalevskii* and *Ptychodera flava* (Lowe et al., 2003; Taguchi et al., 2002). Though there may be slight differences in their roles between species, based on their expression, *elav* is designated as a marker for differentiated neurons and neural progenitors, *soxC* as a marker for neurons or neural differentiation, and *soxB1* to function in maintaining pluripotency of neural progenitors (Garner et al., 2016; Wei et al., 2016, 2011; Yankura et al., 2013).

Possible contribution of hydrocoel cells toward muscle and neural lineage

The prominent pentaradial structures in adult sea cucumbers besides the radial

canals are nerve cords and the longitudinal muscle bands. To observe the development of these structures and how the formation of pentaradial structures are related to each other, I analyzed the spatial and temporal expression patterns of muscle-related genes and neurogenesis-related genes.

Expression of *mhc* detected by whole mount *in situ* hybridization (WISH) suggested the existence of myoblasts in the developing larvae and juveniles (Fig.1-2a-c). At an early stage (mid-auricularia), expression of *mhc* was seen in the esophagus (Fig. 1-2a), indicating that circumesophageal muscles are being formed. In juveniles, *mhc* was expressed in the mesocoel wall adjacent to radial canals, where the longitudinal muscle bands are formed (Fig. 1-2c). The longitudinal muscle bands developed along the radial canals and extended posteriorly, following the formation of radial canals. This close association of radial canals and longitudinal muscle bands is consistent with the previous histological observation in the direct-developing sea cucumber, *Eupentacta fraudatrix* (Dolmatov and Ivantey, 1993).

An unexpected finding was that *mhc* expression was detected in an even earlier stage, the late auricularia (Fig. 1-2a), in which *mhc* was expressed in the initial five hydrocoel lobes. *mhc* was also detected in the hydrocoel lobes in metamorphosing individuals (Fig. 1-2a) and in the water vascular canals of the tentacles in doliolaria (Fig. 1-2b, see the cross-section). These results indicate that the five initial hydrocoel lobes directly contribute to the muscles in tentacles of juveniles and the differentiation of hydrocoel lobe cells into muscle starts at late auricularia, prior to the formation of tentacles. Essentially the same results were obtained for the expression pattern of another muscle structure gene, *tropomyosin* (Fig. 1-2d).

Interestingly, a similar tendency was observed for the development of nervous

tissues. *soxC*, encoding a transcription factor known to be involved in neural development, and *elav,* a marker gene for neurons, were detected not only in the hydrocoel of mid-auricularia but also in the hydrocoel lobes of late auricularia (Fig. 1-3a, arrowheads). In the meanwhile, another neurogenesis-related gene *soxB1* was not detected in the hydrocoel region. Why not all genes that have been implicated in neurogenesis were detected require further studies. Nevertheless, the expression patterns of *soxC* and *elav* suggest that the hydrocoel could also provide cells of neural lineages.

In doliolaria larvae, strong *elav* expression was detected in the ring canal region, tentacles, and also along the radial canals, which could be the developing radial nerve cords (Figs. 1-3a and b). The location of the signals in the posterior part of the larva was lateral to the elongating radial canal, on the outer side of the canal (see Fig. 1-3b-1, sagittal section). Since the mid-ventral radial canal develops first, followed by the two dorsal-lateral radial canals (Mashanov et al., 2007), only three of the five radial canals have developed in the larva shown in Fig. 3B-2. The signal for *elav* expression can be detected close to all three radial canals in the anterior slice (Fig. 1-3b-2), but only at the mid-ventral canal in posterior slices (Figs. 1-3b-3 and 4), presumably in the radial nerve cords. In addition, the radial canal itself appears to express *elav* in the distal (posterior) region or at the tip of the elongating canal (Fig. 1-3b-3, 4). That the expression of *elav* is stronger towards the distal tip of the forming canals strongly suggests that some of the cells of the canal differentiate into or acquire the potential to become nervous precursor cells as the canal elongates; as these cells differentiate into nervous tissue, they lose their precursor characteristics, thus *elav* expression becomes weaker.

Ablation of the hydrocoel lobe disrupts development of pentaradial structures

The expression of muscle and neural marker genes are suggestive of the direct involvement of the hydrocoel to development of adult muscles and nerve cords. To test whether the pentaradial structure of the larval hydrocoel is essential to the formation of adult pentaradial structures, I performed hydrocoel lobe ablation experiments. The infrared laser-evoked gene operator (IR-LEGO) system has originally been developed to induce heat-shock induced gene expression in target single cells (Kamei *et al.,* 2009). This system also can be applied to the ablation of target cells, since irradiation overdose can cause heat injury to cells (Kimura et al., 2013; Okuyama et al., 2014). The transparency of *A. japonicus* larvae and the fact that the hydrocoel is not associated with any other internal tissues are of great advantage to performing such experiments.

One of the hydrocoel lobes in late auricularia stage larva was irradiated with infrared laser. I selected to target either the primary lobe I, which will be one of the water vascular canal of tentacles, or the lobe i, which will be the mid-ventral radial canal and primary podia (Fig. 1-1b). The targeted lobe (lobe i in Fig. 4A and B) after irradiation shows grain-like components (Fig. 1-4b), possibly the damaged cells. The ablation of cells was confirmed this by the loss of DAPI signals in another trial (lobe I in Fig. 1-4c, d).

While some of the ablated larvae died after ablation (10 survived and developed into juveniles among the 60 Lobe I-ablated larvae, and 17 out of 50 lobe i-ablated larve), the survival rate was comparable to those in negative control (4 out of 10 survived with mock-ablation procedure on the right side of the larva. Survival ratio of experimental group vs control was not statistically significant tested by Fisher's exact test.). Lobe-ablated larvae that survived to juvenile showed interesting phenotypes. For example, I

found that some of the lobe I-ablated larvae showed reduced numbers of the tentacles into three or four (Fig.4e, f, Table 1-1). Similarly, lobe i-ablated larvae showed loss of the primary podia (the tip of the mid-ventral radial canal, one of the radial canals which extends to the posterior direction), suggesting that the mid-ventral radial canal is also lost, eventually leading to disruption or incomplete formation of pentaradial structures. Among the 27 surviving juveniles (from either lobe I or lobe i ablation), 25 showed either loss of the tentacle(s) (Fig. 1-4e, three tentacles; 4f, four tentacles) or loss of the primary podia (Table 1-1). These findings indicate that the hydrocoel lobe is necessary for the development of these pentaradial structures. In contrast, two juveniles showed normal phenotypes with respect to pentaradial structures (Fig. 1-4g, Table 1-1). In normal development, it is considered that lobe I develops into a tentacle, whereas lobe i develops into a radial canal and primary podia. However, I found cases in which the destruction of lobe I resulted in loss of primary podia, as well as lobe i-targeted larvae showing loss of tentacles. In addition, even though only lobe I was targeted, some juveniles showed loss of two tentacles. The reason for these inconsistencies is not clear, however, one possibility would be that the irradiation exerted wider effects, such as not only disrupting the targeted lobe, but also affecting adjacent lobes. In addition, sometimes the ablation may not have been sufficient to destroy a single lobe completely.

In my study, I was only able to obtain a small number of juveniles whose lobe of the hydrocoel was ablated. However, the results were consistent in that in most of the treated animals showed changes in morphology, especially with regard to pentaradial structures. Therefore, despite the low number of samples, I may conclude that ablation of a lobe affects the development of pentaradial structures such as the tentacles and radial canals.

Observation of the nervous system in the ablated larvae

To further study the effect of the ablation toward other pentaradial structures, I next focused on the development of the radial nerve cords, which makes up the adult nervous system with the circumoral nerve ring and tentacle nerves (Dolmatov et al., 2016; Hyman, 1955; Smiley, 1986). 1E11 anti-synaptotagmin monoclonal antibody, which can specifically visualize the nervous system in echinoderms (Burke et al., 2006; Nakajima et al., 2004; Nakano et al., 2006), was used for this observation.

Synaptotagmin is present in the nerve tracts along the ciliary bands of auricularia larvae (Fig. 5A left), as has been reported by Nakano *et al*. (2006). At this stage, the hydrocoel does not show any immunoreactivity to 1E11, though my WISH showed expression of several neurogenesis-related gene transcripts. In doliolaria, 1E11-positive nerve tracts are positioned along the ciliary bands that are rearranged into five rows around the body (Fig. 5A middle). During metamorphosis, the ciliary bands are lost, and in juveniles, the nerve tracts of the circumoral nerve ring, tentacles, the mid-ventral radial nerve cord, and those branching to the primary and secondary podia are prominent (Fig. 5A right, 5B). Weaker signals were observed in the other four radial nerve cords (Fig. 5B). To test whether radial canals are essential for the formation of the radial nerve cords, I immunostained juveniles which lack primary podia from hydrocoel lobe-ablation. Since the primary podia is formed at the tip of the mid-ventral radial canal, individuals without the primary podia were expected to lack the mid-ventral canal. As shown in Fig. 1-5c, the number of radial nerve cords was also reduced from five to four in the posterior region of the ablated juvenile (Fig. 1-5c). All of the five observed juveniles presented loss in one of the five radial nerve cords. These results clearly show that the development of the radial nerve cord is linked to that of

the radial canal and further indicates that the hydrocoel lobes are essential for the formation of the pentaradial nervous system in *A. japonicus*.

Discussion

Expression of neural and muscle marker genes in the hydrocoel

My WISH experiments showed that hydrocoel express genes related to muscle and cells of neural lineages (Figs. 1-2 and 1-3), such as *mhc, tropomyosin, soxC,* and *elav*. The expression precedes metamorphosis or even the formation of the ring canal. These results imply that the hydrocoel contains myoblasts and neural precursor cells in rather early stage of development.

Considering that myosin heavy chain and tropomyosin are structural proteins of differentiated muscle, and initial hydrocoel lobes develop into the water vascular canals of the tentacles, it is likely that hydrocoel cells could be contributing directly to the cells of the tentacle muscle. The expression patterns of *mhc,* which was detected adjacent to the radial canal, implies that the formation of the longitudinal muscle bands follows the formation of the radial canals. The inductive role of radial canals in the formation of longitudinal muscle bands was implied in a previous report; the primordia of the longitudinal muscle band was histologically observed at sites where the radial canals come into contact with the somatocoel (Dolmatov and Ivantey, 1993). My results support this idea.

The expression of neurogenesis-related genes such as *elav* and *soxC* suggest the direct contribution of the hydrocoel to neural progenitor cells. This provides an insight toward the long debate on the origin of the adult radial nerve cord. My results are consistent with Cobb (1985) that described that the hyponeural layer of the radial nerve cord of eleutherozoan echinoderms (including sea cucumber) is of mesodermal origin (Cobb, 1985). Conversely, based on the fine histological observation in a different sea

cucumber *E. fraudatrix*, Mashanov *et al.* (2007) claimed that it is solely made up of ectodermal cells that ingress into the body cavity from the vestibule, forming a rudiment from which nerves grow out (Mashanov et al., 2007). I did not observe in *A. japonicus* any other distinct nerve rudiment as in *E. fraudatrix* nor was the hydrocoel located close to the vestibule. This may be a difference between species, but my results did not suggest an exclusive ectodermal origin of nerve cells; rather, my observations are in favor of a mesodermal origin. Considering that that progenitors of the pharyngeal neuron in the embryo of a sea urchin *S. purpuratus* arise from endodermal tissue, i.e., the foregut (Wei et al., 2011), it is possible that the nervous tissue of echinoderms are made from all three germ layers and differ by species.

Immunostaining of Synaptotagmin did not show the presence of mature neurons in the hydrocoel (Nakano et al., 2006 and my result), so at least before metamorphosis, the hydrocoel cells are not differentiated into mature neurons. In *A. japonicus*, the hyponeural layer of the nervous system is reported to be formed between the water vascular canals and the ectoneural part of radial nerve cords after metamorphosis (Dolmatov et al., 2016). Thus, it may be possible that some of the cells in the radial canal contribute to the formation of hyponeural tissue in this phase, which could explain the observation of *elav* expression in some parts of the radial canal during elongation, although a further thorough histological examination is required.

The genes tested in my study are limited, but I have selected genes whose involvement in neurogenesis and myogenesis have been reported in different echinoderm classes and hemichordates, as mentioned in the introduction. Comprehensive expression analyses on a wider variety of genes related to neurogenesis and myogenesis are required to further deepen our knowledge of the role of the

hydrocoel. Though I have not succeeded in use of the Cas-9 system in sea cucumber, Cas-9 tests on gene function may reveal in detail the involvement or role of the hydrocoel in adult body formation during and/or after metamorphosis.

The effects of hydrocoel lobe ablation

Although there are many studies on the echinoderm body axes, not many studies have tackled how the pentaradial body shape itself develops. In my study, I revealed the possible involvement of the hydrocoel toward pentaradial structures by ablating one of the hydrocoel lobes. The results indicated that the hydrocoel lobe is essential for the development of pentaradial structures, namely, the radial canal and the radial nerve cord (Fig. 1-5, Table 1-1). These suggest that the radial canal may play a role as a scaffold for forming pentaradial structures, presumably by giving rise to cells that make up tissues of the pentaradial structures. In addition, it is also possible that the five radial canals may also have a potential to induce the formation and differentiation of nervous and muscular tissues, by acting as an organizing center or signaling center.

My ablation experiments clearly indicated that the hydrocoel lobes or the elongating radial canal is required for the development of adult pentaradial structures in *A. japonicus*. To my knowledge, this is the first experimental examination which supported the hypothesis that the pentaradial hydrocoel lobe is an organizing center for pentaradial structures. In the meanwhile, this hypothesis may further be supported by gain-of-function experiments, for example, transplantation of microdissected hydrocoels or the elongating radial canals into host larvae, to test if these could lead to additional formation of nerve cords and longitudinal muscle bands. However, as of now, due to the very small size of *A. japonicus* larvae, methods to accomplish these procedures are unavailable and

remains to be developed. Nonetheless, as the hydrocoel of *A. japonicus* has no other overlying tissues, I might be able to purely study the function of the hydrocoel or its lobes by transplantion experiments in this species. Other methods such as cell lineage tracing, in vitro organ cultures, or bioinformatics-based approaches may also help understanding of the origin of the pentaradial structures other than the radial canals. Especially, approaches like Koop *et al*. (2017), which found expression of genes associated with Nodal and BMP2/4 signaling in hydrocoel lobes of a sea urchin *H. erythrogramma* (Koop et al., 2017), would provide important hints toward the actual molecular components during the formation of pentaradial structures.

Although my experiments dealt with the possible role of the hydrocoel lobe being a signalling center in establishing the adult pentaradial structures, the big question of how the pentaradiality of the hydrocoel is initially formed still needs to be tackled. There may or may not be a basic organizer that regulates pentaradial pattern formation of the hydrocoel. Though there are no apparent tissues that are directly in contact with the developing hydrocoel in *A. japonicus*, it is possible that distantly located cells, tissues, or even extracellular matrices induce the pentaradiality of the hydrocoel. These issues remain important ones to be considered in order to reveal the developmental mechanism of echinoderm pentaradiality.

Based on my findings, I propose that the five hydrocoel lobes are not only the first pentaradial structure that develops in *A. japonicus* but is also responsible for development of the adult pentaradial structures. In addition, I propose the hydrocoel as a potential organizing center of the pentaradial body plan of echinoderms. Considering that the hydrocoel is a conserved structure in echinoderms, it is tempting to know if this also applies to other echinoderm species. Meanwhile, the actual molecular mechanism of how

the hydrocoel develops its lobes to form the initial pentaradial structure remains to be elucidated. Further studies are awaited to clarify the precise mechanism behind the development of the pentaradial body plan, which will reveal how echinoderms evolved to possess their unique shapes.

Table 1-1. Phenotype of ablated larvae.

This table shows the number of individuals that showed each phenotype after ablating the hydrocoel lobe I or i. Only larvae which reached juvenile after the ablation experiment are counted here. Among the 10 lobe I-targeted larvae, 8 showed reduced tentacles (6 with 4 tentacles, and 2 with 3 tentacles). Among the 17 lobe i-targeted larvae, 15 showed phenotypes without primary podia (p.p.).

Ablated lobe	phenotype				
	5 tentacles with p.p. (normal)	5 tentacles without p.p.	4 tentacles with p.p.	4 tentacles without p.p.	3 tentacles without p.p
I	1	1	2	4	2
i	1	2	1	8	5

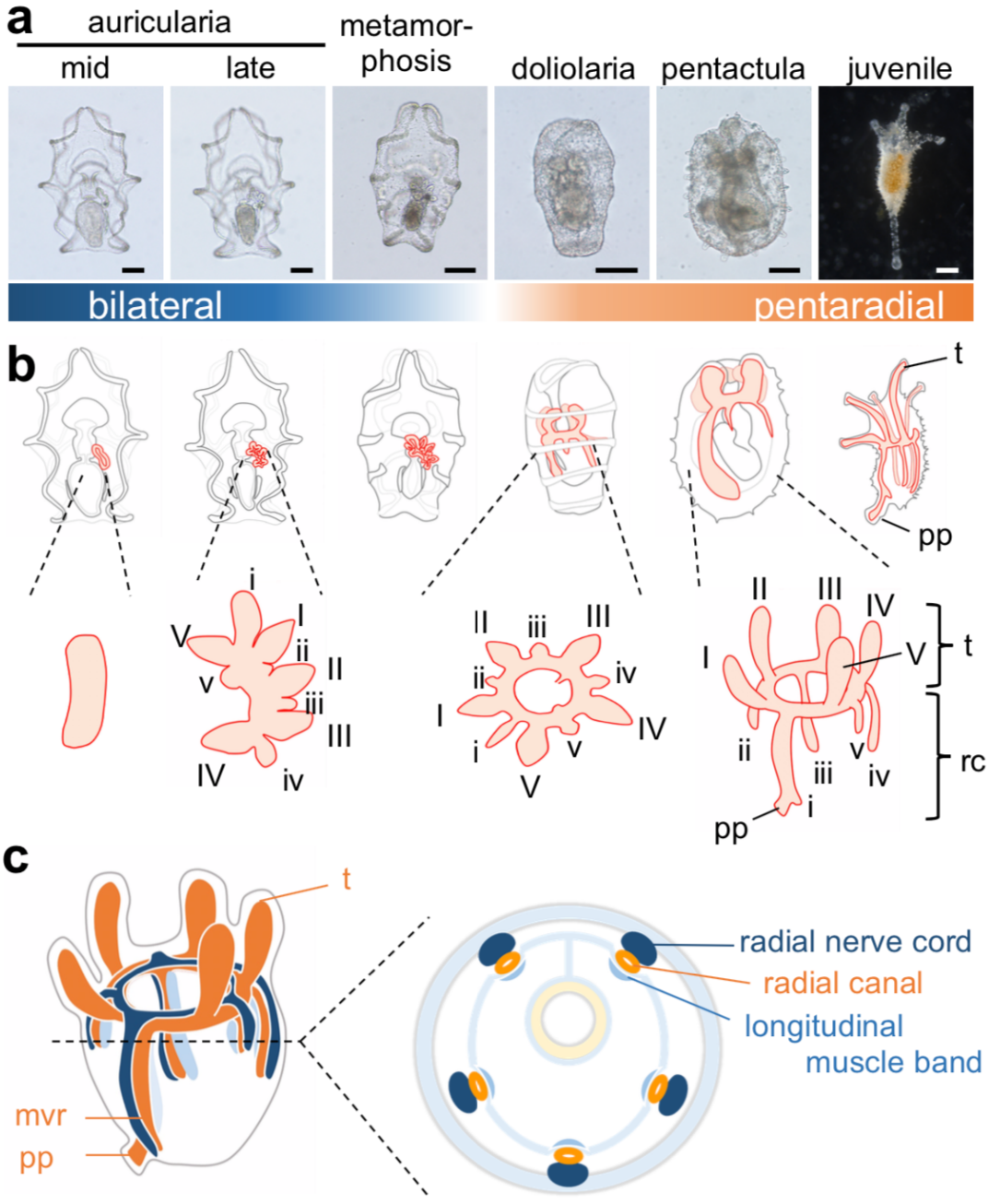
a
auricularia
mid
late
metamor-
phosis
doliolaria
pentactula
juvenile
bilateral
pentaradial
b
t
pp
i
I
ii
II
iii
III
iv
IV
V
v
II
iii
III
ii
iv
I
IV
i
v
V
II
III
IV
I
V
t
ii
v
iii
iv
i
pp
rc
c
t
mvr
pp
radial nerve cord
radial canal
longitudinal
muscle band

Figure 1-1. Development of pentaradial structures in a sea cucumber *A. japonicus.*

(a) Development of *A. japonicus* larvae before and after metamorphosis. While larvae are anatomically bilateral before metamorphosis, it gradually transforms into a pentaradial body plan during metamorphosis. (b) Schematic illustration of hydrocoel development. The hydrocoel first develops on the left side of the larva and forms the five initial lobes (I-V), followed by the formation of another five lobes (i-v) between each initial lobe. The hydrocoel then surrounds the digestive tract to form the ring canal. The five initial lobes of the ring canal contribute to the tentacles around the mouth, while the five additional lobes extend toward the posterior direction to form the radial canals. At the pentactula stage, radial canal i (which develops into the mid-ventral radial canal) extends and forms the primary podia. Numbering of the hydrocoel lobes follows Smirnov (2014). **C**. Longitudinal muscle bands, radial canals, and radial nerve cords of *A. japonicus* juveniles showing pentaradial structures. In juveniles, the hydrocoel develops into the water vascular system (red), which serves as a locomotion and circulation system. Five radial nerve cords extend from the circumoral nerve ring (dark blue). Five longitudinal muscle bands (light blue) are arranged along the radial canals. pp: primary podia, rc: radial canal, mvr: mid-ventral radial canal, t: water vascular canal of the tentacle. Scale bar: 100 μm.

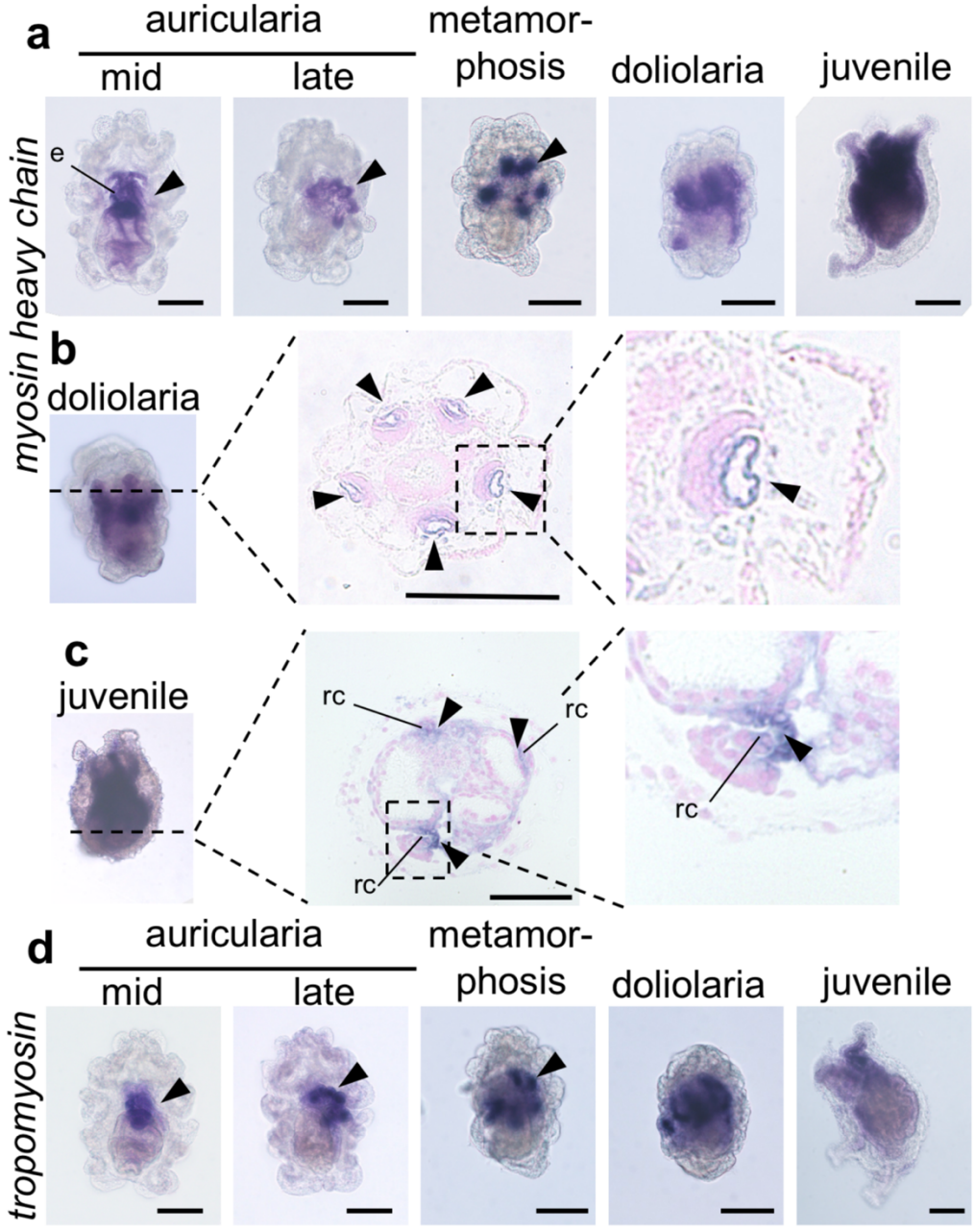
a
auricularia
mid
late
metamor-
phosis
doliolaria
juvenile
myosin heavy chain
e
b
doliolaria
c
juvenile
rc
rc
rc
rc
d
auricularia
mid
late
metamor-
phosis
doliolaria
juvenile
tropomyosin

Figure 1-2. Expression of muscle-related genes in the hydrocoel and its related structures.

(a) WISH detection of *myosin heavy chain* (*mhc*) expression during mid auricularia to juvenile. Note that larvae at the mid-auricularia stage show *mhc* expression is only in the esophagus (e) and not in the hydrocoel (arrowhead). In late auricularia, *mhc* expression was detected in the initial hydrocoel lobes (arrowheads), and this expression continues during metamorphosis and later stages. (b) Histological sections of doliolaria after WISH. *mhc* is detected in the water vascular canal inside the tentacles (b, arrowheads), which is the derivative of the initial hydrocoel lobes. (c) Histological sections of a juvenile after WISH. *mhc* expression is detected in the mesocoel walls (arrowheads) adjacent to the radial canals (rc), where the longitudinal muscle bands are formed. In this section, only three of the five radial canals are observed, since the other two are not yet extended. (d) Expression pattern of *tropomyosin*, another muscle-related gene. Similar to *mhc*, it is detected in the hydrocoel lobes and tentacles (arrowheads). Larvae of auricularia, doliolaria and metamorphosis stages are ventral views, whereas juveniles are left lateral views. Anterior to the top. Scale bar: 100 μm.

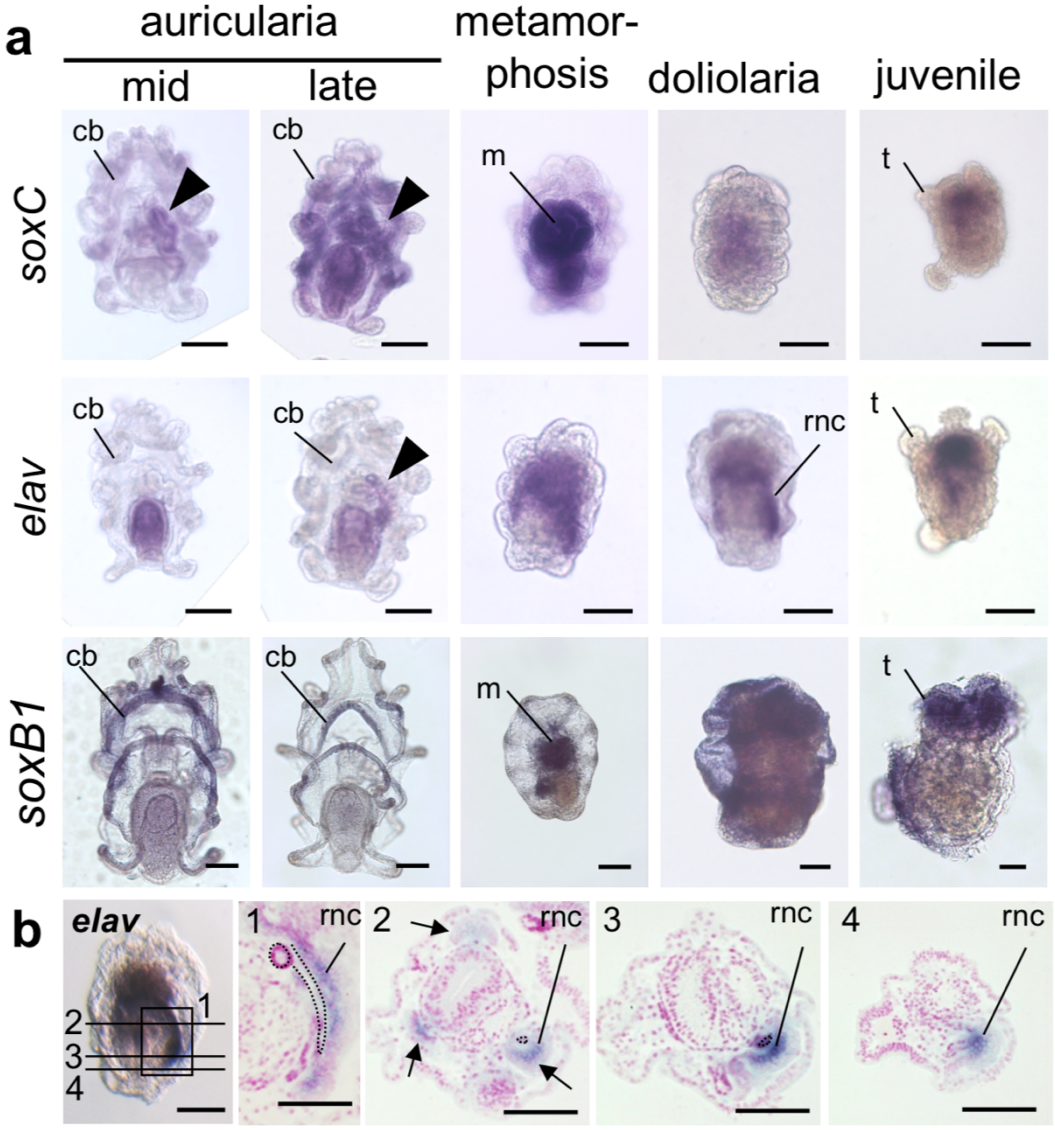
a
auricularia
mid
late
metamor-
phosis
doliolaria
juvenile
soxC
elav
soxB1
cb
m
t
rnc
b
elav
1
2
3
4

Figure 1-3. The expression of the nervous tissue-related genes in the hydrocoel.

(a) Expression of nervous tissue-related genes (*soxC, elav* and *soxB1*) analyzed by whole mount *in situ* hybridization during mid-auricularia to juvenile stages. Note that expression of *soxC* and *elav* are detected in the hydrocoel of auricularia (arrowheads). *soxB1* is detected in the ciliary bands (cb) in auricularia, around the mouth (m) during metamorphosis, and tentacles (t) in juveniles. (b) *elav* expression in doliolaria larvae. The leftmost figure is a representative larva. A sagittal section of one individual (1) and a series of cross sections (2, 3, and 4) from a different larva are shown. The radial canals are dotted. Arrows in cross-section 2 indicate the location of the developing radial canals with related adult tissues. Larvae of auricularia, doliolaria and metamorphosis stages are ventral views, whereas juvenile are left lateral views. Anterior to the top. Scale bar: 100 μm.

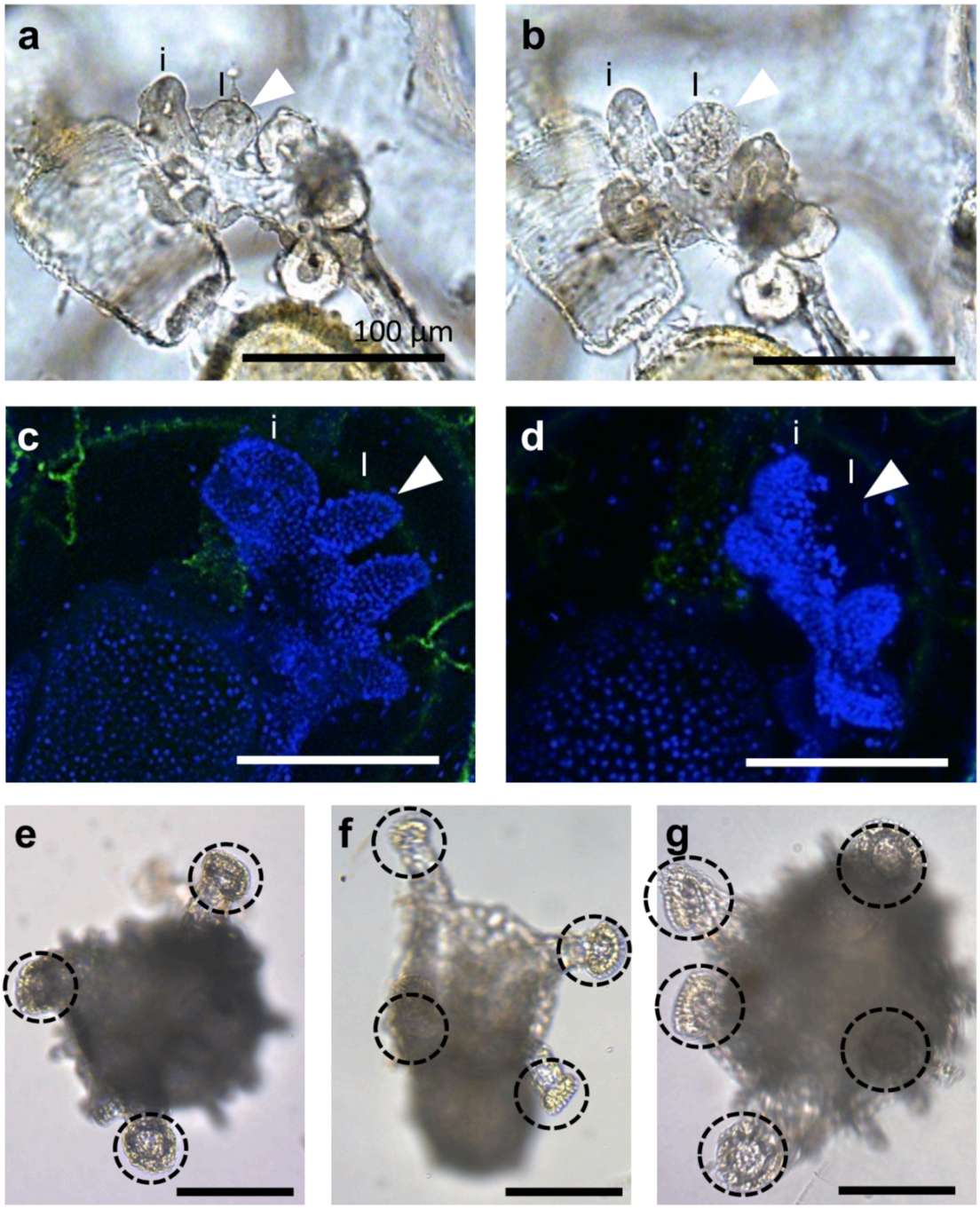
a
i
l
100 µm
b
i
l
c
i
l
d
i
l
e
f
g

Figure 1-4. Laser ablation of the hydrocoel lobe results in the failure of pentaradial structure development of the water vascular system.

(a-d) A single hydrocoel lobe I (arrowheads) of late auricularia was targeted for the ablation. A and C: before irradiation; B and D: after irradiation. After laser irradiation, the cells in the targeted hydrocoel lobe were destructed (b, arrowhead). DAPI staining shows that the targeted lobe was destructed. (e-g) Phenotypes observed after the ablation experiment. The number of pentaradial structures of the water vascular system in some juveniles was reduced to 3 or 4 (e, f), though some individuals developed 5 tentacles even after the ablation (g). Significant morphological differences other than the number of tentacles and primary podia were not observed. Scale bar: 100 μm.

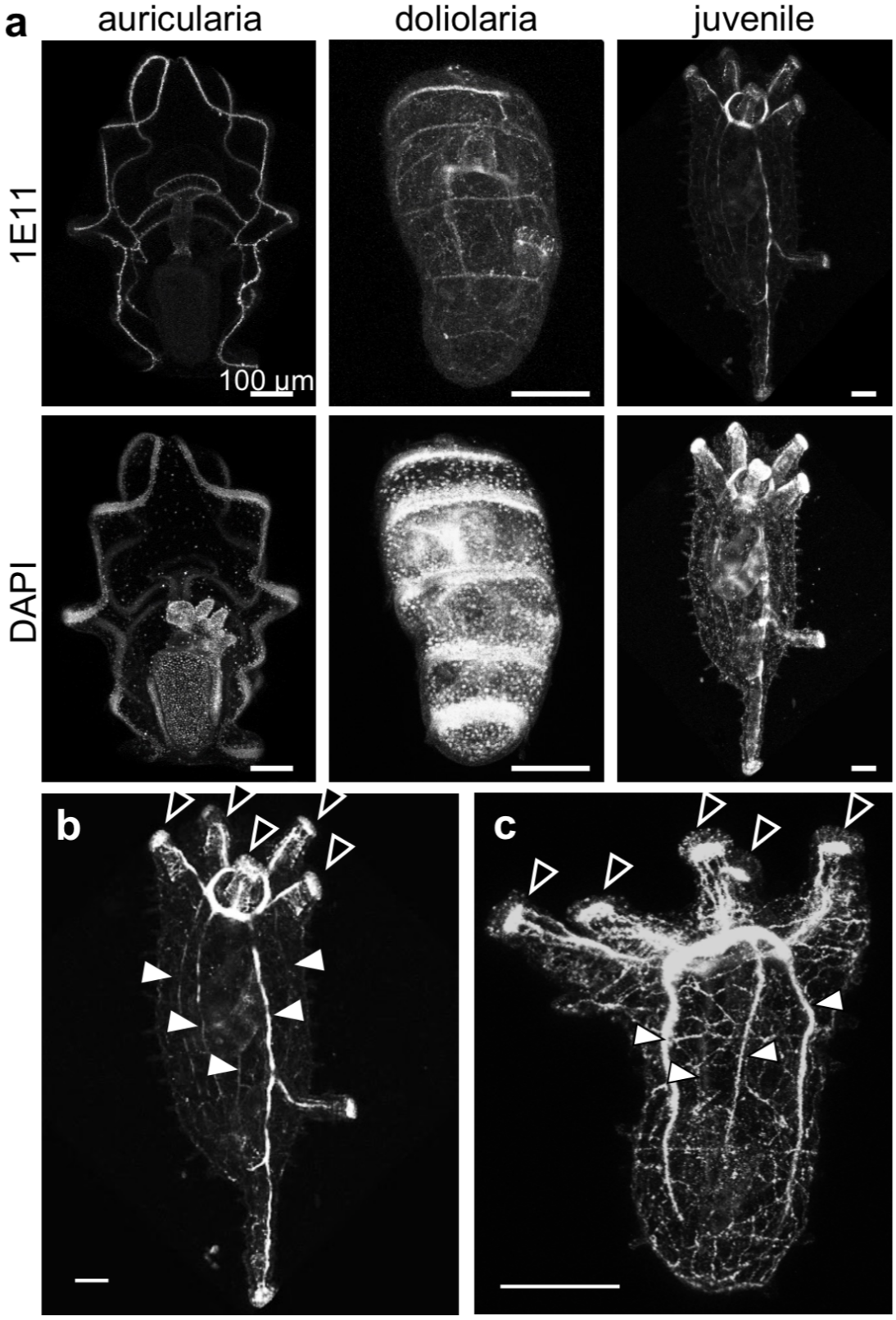
a
auricularia
doliolaria
juvenile
1E11
DAPI
100 µm
b
c

Figure 1-5. Reduced numbers of nerve cords in a lobe-ablated larva.

(a) Immunostaining of the nervous tissue with 1E11 and DAPI counterstaining of auricularia, doliolaria, and juvenile. Note that 1E11 signals are not detected in auricularia larvae, recapitulating the previous report by Nakano *et al.,* (2006) that the adult nervous tissue starts to be formed from the doliolaria stage. (b) A normal juvenile showing five tentacles (black arrowheads) and five radial nerve cords (white arrowheads). (c) A lobe-ablated juvenile with five tentacles (black arrowheads) and four radial nerve cords (while arrowheads). Note that the ablated juvenile in C has a reduced number of nerve cords despite that it has five tentacles. Scale bar: 100 μm.

Chapter 2.

Hydrocoel morphogenesis forming the pentaradial body plan in a sea cucumber, *Apostichopus japonicus*.

The content of this chapter has already been submitted as Udagawa, S, Ikeda, T, Oguchi, K, Kohtsuka, H & Miura, T. Hydrocoel morphogenesis forming the pentaradial body plan in a sea cucumber, *Apostichopus japonicus*. (Under revision)

Abstract

Echinoderms constitute an animal phylum characterized by the pentaradial body plan. During the development from bilateral larvae to pentaradial adults, the formation of the multiple of five hydrocoel lobes, i.e., the buddings from the mesodermal coelom, is the firstly emerging pentameral character. The developmental mechanism underlying the hydrocoel-lobe formation should be revealed to understand the evolutionary process of this unique and highly derived body plan of echinoderms, although the morphogenetic mechanisms of hydrocoel lobes is largely uninvestigated. In this study, using the sea cucumber *Apostichopus japonicus,* in which the hydrocoel is easily observable, the developmental process of hydrocoel lobes was described in detail, focusing on the cell proliferation and rearrangement. Cell proliferation was not specifically distributed in the growing tips of the hydrocoel lobes and inhibition of the cell proliferation did not affect the lobe formation. During lobe formation, epithelium of the hydrocoel lobes were firstly stratified and then transformed into single-layered, suggesting that radial cell intercalation contributes to hydrocoel-lobe formation.

Introduction

Species belonging to the phylum Echinodermata constitute a deuterostome clade that shows unique pentaradial body plans. Echinoderms are thought to have evolved from a bilateral ancestor (Andrew B. Smith et al., 2004). Therefore, the developmental process forming the pentaradial symmetry is an important issue to understand the diversification of animal forms, although the developmental mechanisms underlying the establishment of the pentaradial body plan remain to be elucidated (Byrne et al., 2016a; Raff, 1996).

In both extant and fossil species, the primary body axis of echinoderms is defined based on the arrangement of the ambulacrum, a region associated with the water vascular system (Sumrall and Wray, 2007). The water vascular system is a synapomorphy of echinoderms that is involved in locomotion, circulation and feeding. The water vascular system exhibits a pentaradial structure forming a tubular network consisting of a ring canal around the mouth and radial canals that extend from the ring canal (Hyman, 1955). Thus, the water vascular system is an essential key character for considering the echinoderm body plans (S. Rozhnov, 2014).

The water vascular system is formed from the hydrocoel, i.e., a mesodermal coelom that emerges on the left side of a bilateral larva (Hyman, 1955; Omori et al., 2018b). In echinoderms, bilateral larvae are transformed into juveniles with pentaradial body plans through metamorphosis. At the time of metamorphosis, multiples of five buds (hydrocoel lobes) are projected from the hydrocoel, and the whole hydrocoel encircles the mouth, forming a ring and resulting in a pentaradial water vascular system (Fig. 1-1). It is known that in many echinoderm species the emergence of a multiple of five lobes on the hydrocoel is the first pentameral character in the ontogeny. The outline of

the hydrocoel development has so far been described in many echinoderms, and recent advances in microscopy enable us to observe the detailed structures inside an embryo(Morris, 2016). However, the morphogenetic mechanisms underlying the hydrocoel formation, especially histological transitions and behaviors of hydrocoel cells, have not yet been unraveled.

Although many of the studies on echinoderm development have been carried out in sea urchins as the study materials (Cary and Hinman, 2017), no studies have so far been conducted on the morphogenetic processes of hydrocoel-lobe formation in sea urchins due to their biological characteristics. For example, in *Strongylocentrotus purpuratus* showing indirect development, it takes a month from fertilization to the hydrocoel-lobe formation and its hydrocoel overlaps with the vestibule invagination which contributes to the adult rudiment (Smith et al., 2008), making observations on the hydrocoel difficult. On the other hand, sea cucumbers (Holothuroidea) such as *Apostichopus japonicus*, showing indirect development, are suitable models to observe hydrocoel development, since their larva is transparent and does not form the hydrocoel-associated structures such as the adult rudiment, so the hydrocoel-lobe formation is easily observable.

The hydrocoel of *A. japonicus* is formed from the archenteron on the left side of the auricularia larva around 4 days post-fertilization (dpf). The larvae develop relatively quickly as indirect developers, so the hydrocoel lobes are formed on the hydrocoel approximately 10 dpf (Qiu et al., 2015; Yoshida et al., 2001). In this species, as in other holothurians, 10 hydrocoel lobes are formed on the hydrocoel. Five major lobes (I-V) develop into water vascular canals of tentacles. Another five minor lobes (i-v), which are formed between each of the major lobes, extend posteriorly and develop into radial

canals of the water vascular system (Fig. 1b) (Smiley, 1986; Smirnov, 2014a). The hydrocoel becomes horseshoe-like shaped after the lobe formation and then forms the ring canal surrounding the digestive tract to establish the pentaradial structure. At the same time of ring canal formation, metamorphosis starts and the whole larval body is rearranged to become a doliolaria larva.

After the hydrocoel-lobe formation, pentaradial structures of adult sea cucumber such as longitudinal muscle bands and radial nerve cords are formed along the radial canals, which are formed from hydrocoel lobes (Dolmatov et al., 2016; Dolmatov and Ivantey, 1993; Mashanov et al., 2007). Other echinoderms such as sea urchins also form pentaradial adult tissues around the hydrocoel (Hyman, 1955), which suggests that the hydrocoel lobes might induce the formation of pentaradial structures of echinoderms and contribute to the establishment of the pentaradial body axis also in these species. Thus, the spatial control of hydrocoel lobe formation and the determination of the number of hydrocoel lobes is thought to be critical to the development of the pentaradial body plan.

In general, histological changes during morphogenesis involve changes in cell number, cell shape and cell arrangement (Heisenberg and Bellaïche, 2013). In particular, branching or budding morphogenesis is driven by the contribution of cell proliferation and collective migration to the morphogenesis (Spurlin and Nelson, 2017). Therefore, it was considered that either, or both, of these cellular processes should be involved in the hydrocoel-lobe formation.

In this study, therefore, to reveal the morphogenetic process underlying the hydrocoel lobe formation in *A. japonicus*, detailed observations at the cellular level were carried

out focusing on changes in cell proliferation and cell arrangement during the formation process.

Methods

Animals

Mature adults of *A. japonicus* were collected between April and June of 2019-2021 from sandy bottom of the sea at the depth of 3-10 m around the Misaki Marine Biological Station, Kanagawa or at Onahama Port, Fukushima (36° 94' N, 140° 90' E) by SCUBA diving. All the collected individuals were morphologically diagnosed as the black type of the focal species, that was recently redescribed as *A. armatus* (Woo et al., 2017) although it is still treated as *A. japonicus* in many recent studies. Collected individuals were kept in the laboratory tank at 17 ºC to maintain the sexually mature condition. Gonads of collected individuals were dissected from inside the body wall to discriminate sex and maturity. Mature ovary is vivid orange and mature testis is white. Egg spawning was induced by the injection of 500 µL of 10 µM cubifrin (Kyusyu TLO Company, Fukuoka, Japan), a peptide known to induce oocyte maturation and spawning in *A. japonicus* (Kato et al., 2009). Sperms were obtained by dissecting matured testes in sea water.

Embryo culture was conducted based on Kikuchi et al., 2015. Briefly, embryos were kept in 10 L of filtered sea water in a plastic container with circulation at 20 ºC, and daily fed *Chaetoceros calcitrants* diatoms. The density of individuals was kept as 1 embryo/mL, and sea water was changed every two days. Embryos become bilateral auricularia larva at 2 dpf. The hydrocoel emerges at the left side of the digestive tract around 6 dpf and the hydrocoel lobes can be observed around 10 dpf[11]. Individuals during this period were used for observations. After the formation of hydrocoel lobes, larvae metamorphose into doliolaria and pentactula juveniles, and settle down on the

container bottom.

Morphological observation of the hydrocoel

For observations of the overall shape of hydrocoel, larvae were fixed using Fix1 (4% PFA/ 0.1M MOPS, pH 7.0/ 0.5M NaCl) (Kikuchi et al., 2015). Specimens were stained with 4',6-Diamidino-2-phenylindole (DAPI) (Nakalai Tesque, Kyoto, Japan) for observation of the overall morphology of the hydrocoel. For observations of cell arrangements and cell shapes, *N*-(4,4-Difluoro-5,7-Dimethyl-4-Bora-3a,4a-Diaza-s-Indacene-3-Pentanoyl) Sphingosine (BODIPY FL C_5-Ceramide) (Life Technologies, Carlsbad, CA, USA) was used. Larvae were kept alive in BODIPY FL C_5-Ceramide （100 μM in sea water,） for 6 hours at 20 °C. Based on a previous study (Vidavsky et al., 2016), specimens were embedded on the glass bottom dish using 1% low temperature melting agarose. The specimens were then observed using a confocal laser scanning microscope（FV3000, Olympus, Tokyo, Japan） and an optical microscope (TE300 Nikon, Tokyo, Japan) equipped with a camera (DP27, Olympus, Tokyo, Japan).

Detection and inhibition of cell proliferation

To observe the localization of cell proliferation, the intake of thymidine analogue 5-ethynyl-2'-deoxyuridine (EdU) was detected using a Click-iT^{TM} EdU Cell Proliferation Kit for Imaging (Life Technologies, Eugene, OR, USA). EdU labeling was conducted based on Sharma & Ettensohn, 2011 with some modifications. EdU was diluted to 10 μM in filtered sea water according to the manufacturer's instruction. Auricularia larvae

at each phase were incubated in 10 mL of EdU sea water for 3 hours at 20 ºC. Larvae were fixed with Fix1 soon after the treatment. Detection of EdU was conducted based on the manufacturer's instructions and cell nuclei were stained with DAPI. Then, the stained specimens were observed using a confocal laser scanning microscope.

Cell proliferation was inhibited using DNA polymerase I inhibitor aphidicolin (Adipogen, Liestal, Switzerland). This reagent is known to inhibit cell proliferation in a sea urchin, *Lytechinus pictus* (Stephens, 1986), as in many other eukaryotes. The treatment method was based on Smith et al., 2009 . Aphidicolin was dissolved at a concentration of 10 mg/ml in dimethyl sulfoxide (DMSO) and diluted to 0.5 µl/ml in filtered sea water. Auricularia larvae before lobe formation were incubated in aphidicolin sea water for 20 hours at 20 ºC. Control experiments were conducted by incubating in the same condition using 0.5 µl/ml DMSO in filtered sea water. For the evaluation of the effect of aphidicolin on the hydrocoel lobe formation, phase 2 larvae were randomly divided into 6 groups. 3 of the groups were kept in aphidicolin sea water and the other 3 groups were kept in DMSO sea water (control). Larvae were fixed after 20 h treatment and the number of larvae which formed the hydrocoel lobes (phase 3 and phase 4) were counted (10-18 larvae in each group). Two-sided Fisher's exact test was carried out with R 4.0.3.

Results

Staging of hydrocoel lobe formation

Firstly, the overall process of hydrocoel-lobe formation in auricularia larvae was observed, focusing on morphological characteristics. Fixed specimens were observed under an optical microscope and a confocal laser scanning microscope after staining with DAPI (Fig. 2-1). During the formation process, 4 developmental phases were defined based on the hydrocoel morphology (Table 2-1).

Phase 1: The hydrocoel primarily emerged at the left side of the digestive tract, showing a spindle-like shape (Fig. 2-1a-a’’’).

Phase 2: The entire hydrocoel extended up to 100 μm along its longitudinal axis of the spindle shape and became a slightly curved columnar shape (Fig. 2-1b-b’’’).

Phase 3: The hydrocoel lobes started to form (Fig. 2-1c-c’’’). The lobes were formed in a line along the AP axis of a larva. Each of 5 minor hydrocoel lobes which will become radial water vascular canals were respectively formed between the 5 major hydrocoel lobes which became water vascular canals of tentacles.

Phase 4: The lobes continuously extended to form tubular structures (Fig. 2-1d-d’’’). Each hydrocoel formed a tubular structure surrounded by epithelial tissue, and these tubular structures later formed the tubular network of the water vascular system.

There were no other obvious morphological changes in other parts of an auricularia larva, such as the digestive tract and ciliate bands, throughout these phases.

Observations of cell proliferation

To examine whether cell proliferation contributes to the hydrocoel morphogenesis, we

observed the distribution patterns of cell-proliferation signals by EdU during the process. Larvae were incubated in 10 μM EdU sea water for 3 hours. In all of the observed phases, cell proliferation was detected (Fig. 2-2).

In phases 1 and 2, the EdU signal was distributed throughout the whole hydrocoel, and observations of both z-stack images and optical sections indicated that the signal was equally localized throughout the hydrocoel (Fig. 2-2a-b, a'-b''). The cell proliferation was also observed in phases 3 and 4 (Fig. 2-2c-d, c'-d'). Both z-stack images and optical sections showed that the EdU signals were not specifically localized at certain region such as the lobe tips (Fig. 2-2c-d, c'-d', arrowheads).

To examine whether cell proliferation is required for the hydrocoel-lobe formation, larvae at phase 2 was treated with the cell proliferation inhibitor aphidicolin. Administration of 0.5 μg/mL aphidicolin was shown to completely inhibit the EdU incorporation into the hydrocoel tissues, confirming the effect of aphidicolin (Fig. 2-3d). Then auricularia larvae at phase 2, just prior to the hydrocoel-lobe formation, were treated with 0.5 μg/ml aphidicolin (Fig. 2-3a). At 20 hours after the onset of treatment, the hydrocoel lobes were successfully formed, as in untreated animals (Fig. 2-3b). There was no significant difference in the ratio of larvae in which hydrocoel lobes were formed (phase 3 or 4) to larvae in which hydrocoel lobes were not formed yet (phase 2) between the treated and control groups (Two-sided Fisher's exact test, $p = 0.144$, Fig. 2-3c).

Observations on cell arrangement

To observe the changes of cell shape and cell arrangement in the hydrocoel epithelium,

the cell membrane of live larvae was stained with bodipy FL C5-ceramide. At phase 1, the hydrocoel was surrounded by a single layer of columnar epithelial cells (Fig. 2-4a). At phase 2, the hydrocoel epithelium was stratified, which was observed throughout the whole hydrocoel (Fig. 2-4b). At phase 3, when the lobe formation started, stratified epithelial tissue became single-layered epithelium again at the tip of the hydrocoel lobes (Fig. 2-4c-d). The tissue between the lobes was still multi-layered and started to be bent. At phase 4, when the hydrocoel lobes extended, the epithelium between the lobes also became single-layered, being sharply bent, and consequently the lobe shape became more constricted (Fig. 2-4e-f).

The positions of hydrocoel lobes were the same in all of the observed individuals, and all of the hydrocoel lobes formed synchronously (Fig. 2-4). Although the lobes for water vascular canals of tentacles (i.e., lobe I, II, III, IV and V) were relatively larger than those for radial canals (i.e., lobe ii, iii, and iv) except for lobe i, the transitions in cell arrangement from multi-layered to monolayered epithelium were observed in all of the lobes regardless of lobe size (Fig. 2-4, 2-5).

Discussion

In general, developmental mechanisms of the formation of branching or budding structures in the epithelium can be classified into 3 categories, i.e., single cell extension, collective migration and non-migratory branching (Spurlin and Nelson, 2017). Since the hydrocoel lobes are multicellular structures, the mechanism underlying the hydrocoel morphogenesis should be driven by cell migration or non-migratory mechanisms. The non-migratory branching is typically observed during the morphogenesis of vertebrate kidney and mammalian lung (Spurlin and Nelson, 2017). The morphogenesis of ureteric buds in kidney is driven by localized proliferation at the tip of the branch (Spurlin and Nelson, 2017). In the hydrocoel-lobe formation, cell proliferation was evenly distributed throughout the hydrocoel, and no specific localization of proliferation, such as concentration at hydrocoel-lobe tips, was observed in relation to the lobe formation (Fig. 2-2b, c). It is still possible that cell proliferation drives the formation of hydrocoel lobes even if no specific localization of cell proliferation was detected. In the case of lung branching in mammals, global proliferation drives the budding process in coordination with cell shape change and localized muscle cell differentiation (Spurlin and Nelson, 2017). In the hydrocoel-lobe morphogenesis, however, cell proliferation seems to be unnecessary for the hydrocoel-lobe budding, since the inhibition of cell proliferation during phase 2 and phase 4 did not prevent the lobe formation (Fig. 2-3).

A previous research in a direct-developing sea urchin, *Heliocidaris erythrogramma*, showed that the cell proliferation is not necessary for the formation of the hydrocoel itself (Smith et al., 2009). However, the stratification and the successive intercalation of epithelial cells are suggested to be driving forces for the hydrocoel morphogenesis

as discussed below. Since cell proliferation is known to be required for the stratification of epithelium(Li et al., 2016), the cell proliferation between phase 1 and phase 2 is suggested to contribute indirectly to the hydrocoel lobe morphogenesis.

Based on my observations on cell shape and cell arrangement in the hydrocoel, intercalation of epithelial cells is suggested to contribute to budding morphogenesis in the hydrocoel-lobe formation. At phase 1, the hydrocoel epithelium consisted of a single-layered cell sheet, but then it was stratified at phase 2 (Fig. 2-4). Multi-layered epithelial cells became single-layered arrangement again specifically at the lobe-tip position (phase 3, Fig. 2-4). This change in cell arrangement is supposed to be achieved by cell intercalation. After the tip intercalation and the lobe extension, intercalation occurred at the proximal part of each lobe, (phase 4, Fig. 2-4). This time-dependent difference of cell intercalation depending on the positions in the hydrocoel lobes suggests that the cell intercalation occurs sequentially from the tip of the hydrocoel lobe to the proximal part. Cell intercalation observed in these phases can be categorized as “radial intercalation”, in which cells intercalated in the direction perpendicular to the epithelium and the multiple cell layers were transformed into a single layer (Keller, 1980). Radial intercalation is thought to leads to tissue spreading (Neumann et al., 2018), so the tissue expansion caused by the sequential radial intercalation might contribute to budding and elongation of hydrocoel lobes. Thus, the radial cell intercalation seems to be involved in the morphogenetic process of hydrocoel lobes, and it can be said that the morphogenetic process of hydrocoel lobes consist of branching driven by cell migration though further testing such as inhibition of cell migration is needed. In addition, the tissue was curved sharply at the tips of hydrocoel lobes and between the hydrocoel lobes as the hydrocoel lobes developed, although it is

not clear whether these changes in epithelial tissue constitute an active process to form the hydrocoel lobes or a passive result of morphogenetic processes such as cell intercalation.

The result of this study is the first report suggesting the involvement of radial intercalation in echinoderm development. In the sea urchin *Lytechinus pictus*, in which cell behavior during gastrulation has been well studied, it is known that the cell-shape change and the convergent extension caused by mediolateral intercalation are involved in gastrulation (Ettensohn, 1985; Hardin and Cheng, 1986; Kimberly and Hardin, 1998), while stratification and radial intercalation should not be involved, since the archenteron is single-layered epithelium in this species. In the branching morphogenesis of the mouse mammary gland, it is known that simple epithelium becomes transiently stratified and is then resolved to simple epithelium again to form the branching structure (Ewald et al., 2012), and tube elongation is achieved by radial intercalation (Neumann et al., 2018). Hydrocoel-lobe morphogenesis resembles these processes. On the other hand, indispensable structures in mammary ductal elongation such as the myoepithelium which covers the ducts (Neumann et al., 2018) or the growth zone like terminal end bud, which is stratified and shows a high proliferation rate (Hinck and Silberstein, 2005; Williams and Daniel, 1983) were not observed in the sea cucumber hydrocoel.

It is known that radial intercalation is driven by cell chemotaxis in amphibian epiboly (Szabó et al., 2016). Therefore, in the focal sea cucumber, sequential radial intercalation during the hydrocoel-lobe formation could also be driven by chemotaxis. If so, the diffusion pattern of attractants and/or the localization of their source might determine the number and the position of hydrocoel lobes. Alternatively, specific localization of

gene expression might regulate the responsiveness of epithelial cells to the attractants, leading to the sequential intercalation. Future studies on the molecular mechanisms involved in hydrocoel-lobe morphogenesis will help us to understand the developmental mechanisms underlying the pentaradial body plans in echinoderms.

Table 1. Features of hydrocoel tissue in each phase of the hydrocoel lobe morphogenesis.

phase	Feature
phase 1	Spindle shape (hydrocoel lobes are not formed.) Single layered cell sheet
phase 2	Bean shape (hydrocoel lobes are not formed) Stratified cell sheet
phase 3	Emergence of the hydrocoel lobe Single layered at the tip of the hydrocoel lobes
phase 4	Extension of the hydrocoel lobe Single layered in the entire hydrocoel lobes

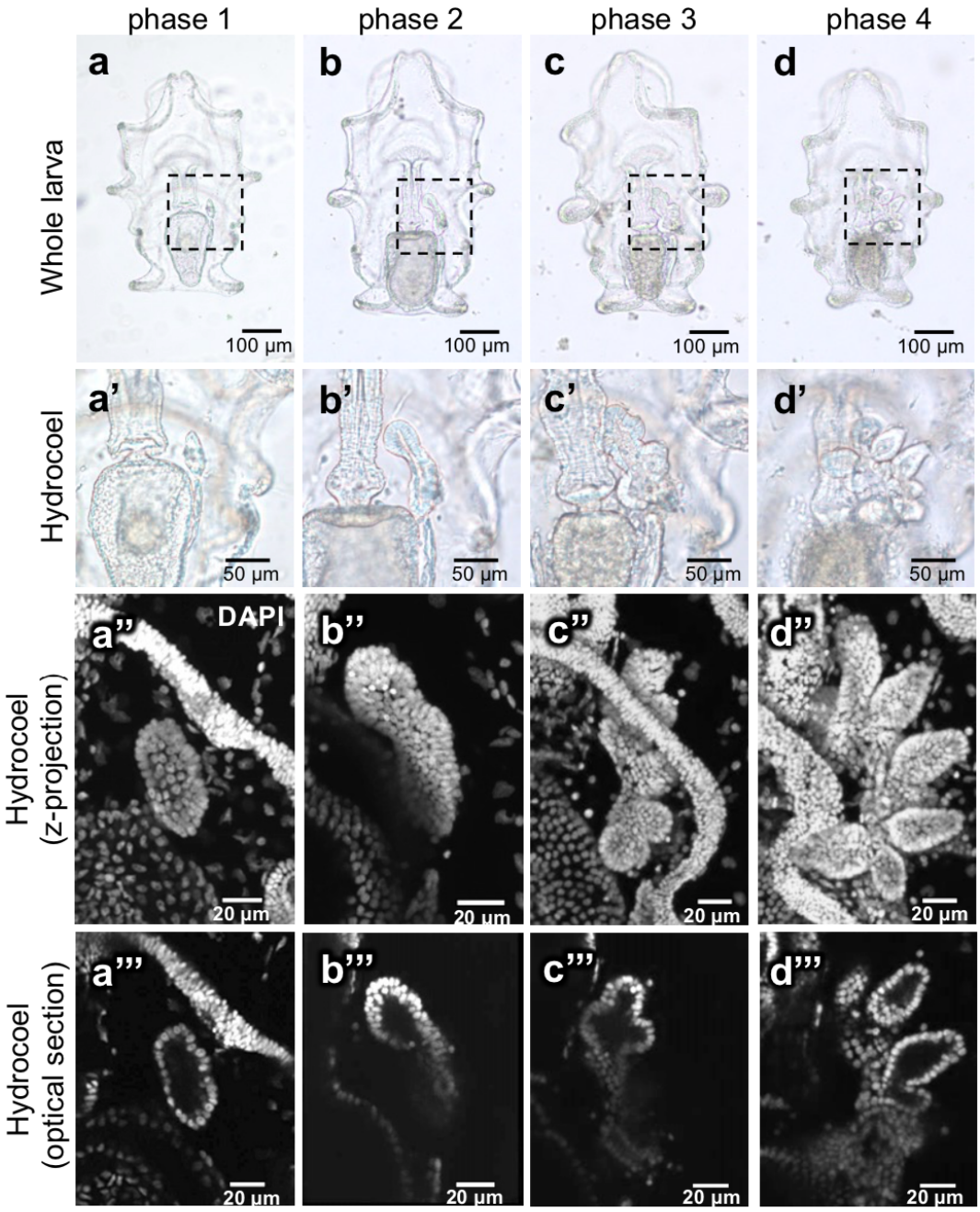

Figure 2-1 Observation of the overall morphology of the developing hydrocoel lobes.

(**a-d**) show the whole embryo under the microscope (ventral view, anterior top) from phase 1 to phase 4. (**a'-d'**) show the hydrocoel of a-d. The dotted lines in (**a-d**) indicate the region shown in

(**a'-d'**). The hydrocoel of the specimens stained with DAPI are shown in (**a"-d'**: z-stack images) and (**a'"-d'"**: optical sections). In phase 1, the hydrocoel was spindle shaped and then it extended up to 100 μm along the longitudinal axis in phase 2. The hydrocoel lobes started to form in phase 3 and the lobes extended in phase 4. During phase 1 and phase 4, no significant change in the overall morphology of entire larva other than the change in the hydrocoel was observed.

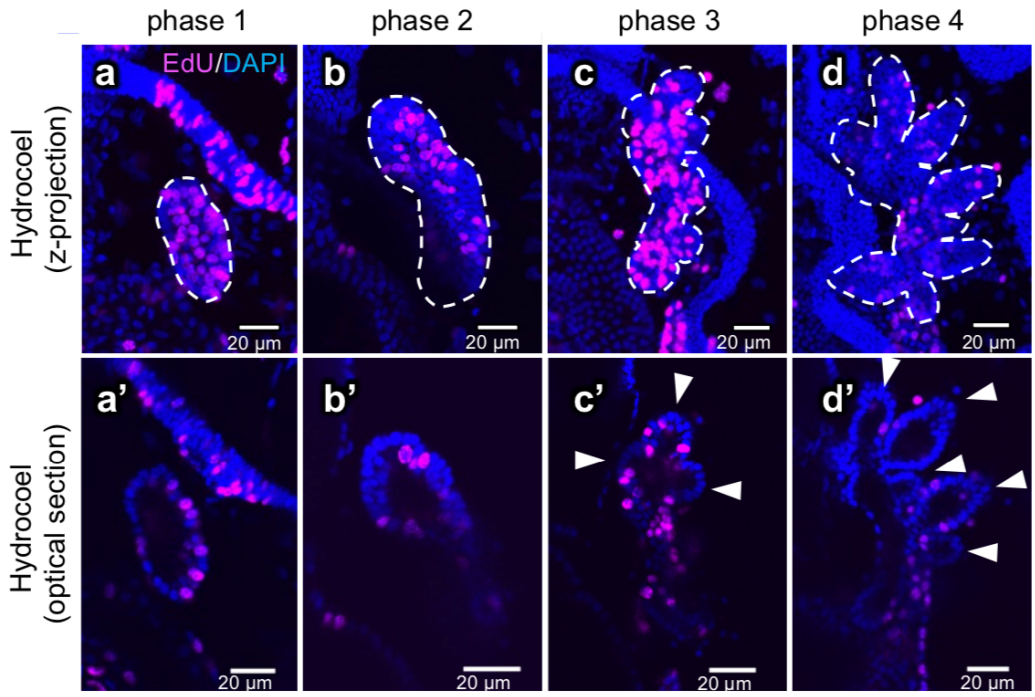

Figure 2-2. The spatial distribution of cell proliferation in the hydrocoel during the hydrocoel lobe morphogenesis.

The cell proliferation in the hydrocoel from phase 1 to phase 4 was detected using EdU after a 3-hour EdU treatment (**a-d**). The hydrocoel is indicated by the dotted lines. (**a'-d'**) show the optical sections of a-c. The position of the hydrocoel lobe is indicated by arrowheads. The EdU signal was detected equally throughout the whole hydrocoel during phase 1 and phase 4 and specific localization was not observed.

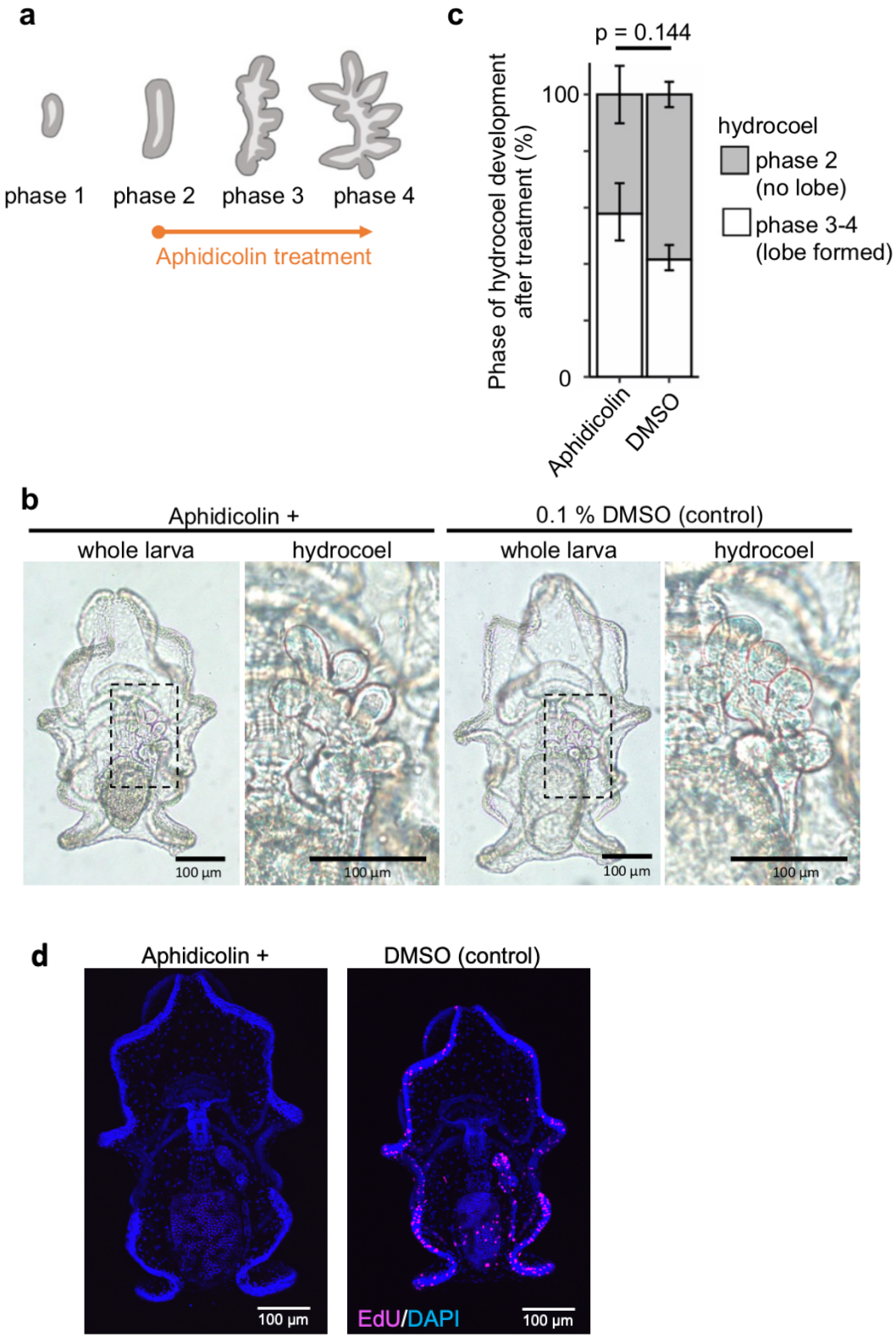
a
phase 1
phase 2
phase 3
phase 4
Aphidicolin treatment
c
p = 0.144
Phase of hydrocoel development after treatment (%)
100
0
Aphidicolin
DMSO
hydrocoel
phase 2 (no lobe)
phase 3-4 (lobe formed)
b
Aphidicolin +
0.1 % DMSO (control)
whole larva
hydrocoel
whole larva
hydrocoel
100 µm
100 µm
100 µm
100 µm
d
Aphidicolin +
DMSO (control)
100 µm
EdU/DAPI
100 µm

Figure 2-3. Inhibition of cell proliferation by aphidicolin treatment during the hydrocoel lobe morphogenesis.

(a) Experimental design for aphidicolin treatment. Auricularia larvae were treated with aphidicolin beginning at phase 2 and the phenotype was observed at 20 hours. (b) Phenotype resulting from aphidicolin treatment. Hydrocoel lobe was formed both in aphidicolin treatment and DMSO treatment (control) larvae. The number or shape of hydrocoel lobes (arrowhead) was not affected by the aphidicolin treatment compared to DMSO treatment. (c) Ratio of phase 3-4 larva (lobe formed) to phase 2 larva (lobe not formed)in treated and control groups at 20 h after the initiation of treatment. There was no significant difference (Student's t-test, $p = 0.06457$). Graph represents the mean ± s.d. from 3 independent experiments. (d) Cell proliferation was detected using EdU after a 3-hour treatment with aphidicolin. In larvae incubated with EdU and 0.5 % DMSO (control), EdU signal was detected in the whole body. On the other hand, EdU signal was not detected in larvae incubated with EdU and aphidicolin.

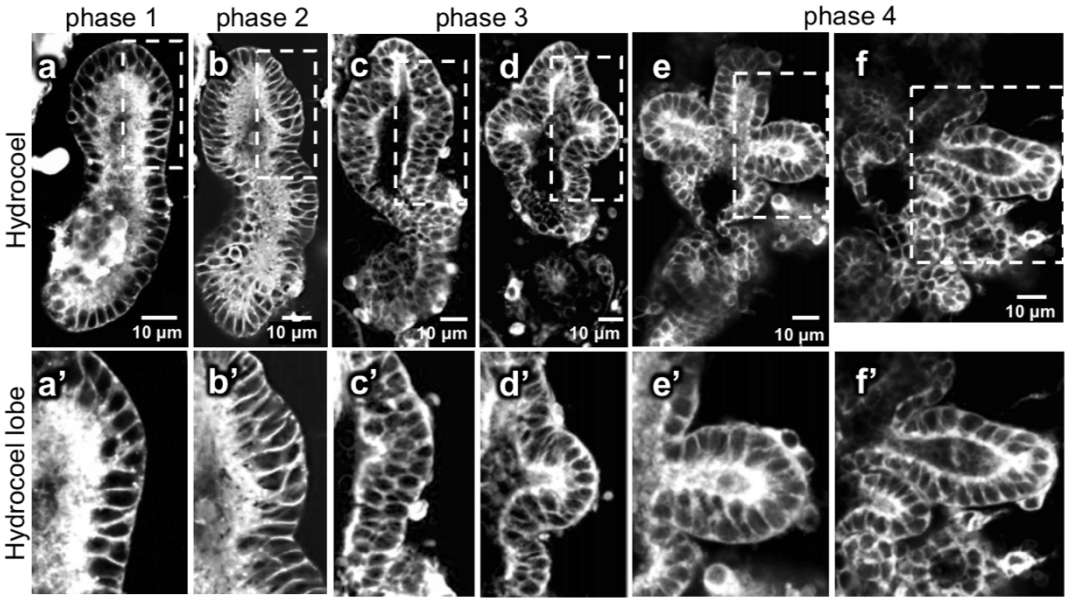

Figure 2-4 The observed changes in cell shape and cell arrangement during the lobe formation in the hydrocoel.

Cell membrane of larvae was stained by BODIPY FL C_5-Ceramide and observed using confocal laser scanning microscopy from phase 1 to phase 4. (**a-f**) are optical sections of the hydrocoel in each phase (ventral view, anterior top). The time-course and stages are indicated in the figure. (**a'-f'**) show the magnification of regions indicated in (a-f), respectively. Hydrocoel epithelium was a single cell layer in phase 1 and then became stratified in phase 2. In phase 3, the tissue became single layered again at the tip of the lobe (arrowhead in C'-D') and then in the whole hydrocoel lobe.

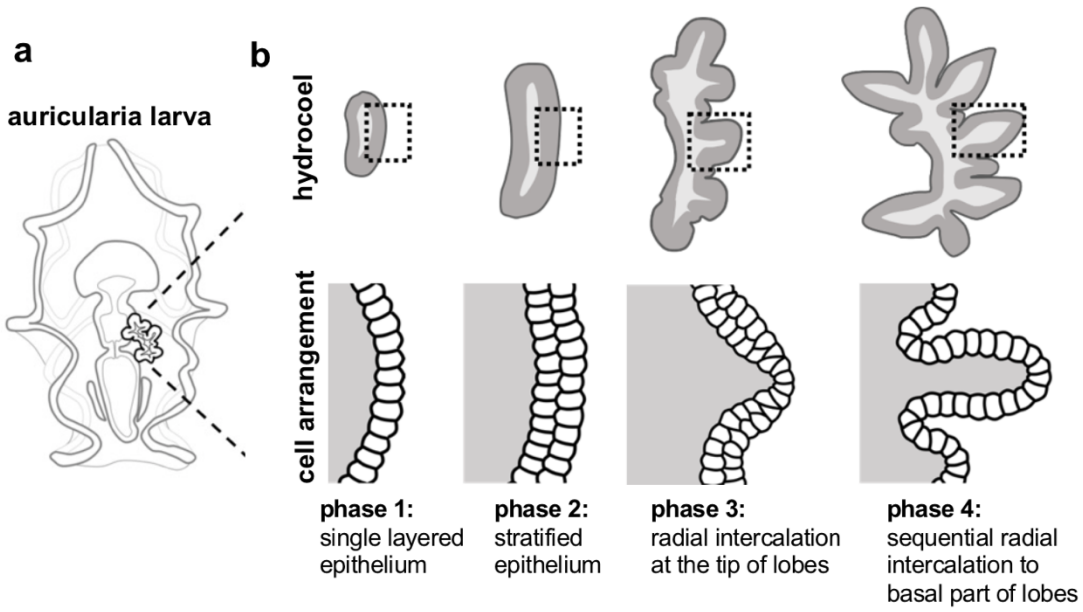

Figure 2-5. Schematic illustration of change in cell arrangement during the hydrocoel lobe morphogenesis.

(**a**) represents an auricularia larva and (**b**) represents the development of its hydrocoel. Upper panel is the overall shape of the hydrocoel, and the cell arrangement of hydrocoel epithelium in dotted areas is shown in the lower panel. The hydrocoel at phase 1 consists of a single cell sheet, and it becomes stratified at phase 2. As the formation of the hydrocoel lobe proceeds, the cell sheet becomes single layered again sequentially from the tip of the hydrocoel lobe (phase 3) to the proximal part of the lobe (phase 4).

Chapter 3.

Identification of genes responsible for the pentaradial pattern formation of hydrocoel in a sea cucumber *Apostichopus japonicus.*

Abstract

In echinoderms, bilateral larvae metamorphose into juveniles with pentaradial symmetry. Prior to the metamorphosis, multiples of five projections (hydrocoel lobes) are formed on a hydrocoel, showing the first pentaradial structure in development. The pattern formation process of hydrocoel lobes is thought to be critical for determining primary body axis of the pentaradial body plan, but the underlying mechanism is completely unknown. In this study, in order to identify genes involved in the pentaradial pattern formation of hydrocoel, hydrocoels were isolated from auricularia larvae of sea cucumber, and hydrocoel-specific RNA-seq analysis was carried out. The results were further confirmed by *in situ* hybridization, showing that several transcription factors, such as *foxC* and *zic,* and genes involved in signaling pathways, such as Wnt and Notch, were expressed in the hydrocoel. In particular, the Wnt receptors *frizzled1/2/7* and *frizzled4* were expressed in different parts of the hydrocoel, and the patterns of expression became more complex in the later stages. In addition, other genes such as *ap2a, six1/2* and *bmp3*, were heterogeneously expressed in the hydrocoel. Moreover, inhibition of Wnt signaling led to failure of the hydrocoel development. These results indicate that Wnt signaling is involved in the regulation of hydrocoel morphogenesis and that the regional differentiation of the hydrocoel proceeds with development.

Introduction

Echinoderms possess pentaradial body plan and they are thought to have evolved from a bilateral ancestor (Andrew B. Smith et al., 2004). This drastic change in the body plan accompanied by changes in the body axis has been of interest in terms of the diversification of animal morphologies (Raff, 1996). In order to understand how this novel body plan was acquired, it is important to understand the developmental mechanisms underlying this unique body plan.

In the developmental process of echinoderms, it is known that bilateral larvae metamorphose into pentaradial juveniles. Prior to the metamorphosis, multiples of five projections is formed on a hydrocoel, i.e., hydrocoel lobes, exhibiting the first pentaradial structure observed during development (S. Rozhnov, 2014). The hydrocoel becomes the pentaradial water vascular system, which is the circulation system of echinoderms (Hyman, 1955). Since adult tissues such as nervous system, muscles, and ossicles are formed around the hydrocoel lobes, it has been suggested that the hydrocoel may induce the formation of other tissues (Dolmatov and Ivantey, 1993; Minsuk and Raff, 2002a). In Chapter 1, I found that the hydrocoel lobes are essential for the formation of the pentaradial nervous system. In other words, it is suggested that the hydrocoel governs the establishment of pentamery of the other tissues, resulting in the pentaradial adult body. Based on this background, it can be said that the mechanism of pattern formation of hydrocoel itself is the mechanism which determines the unique body patterns seen in echinoderms.

However, the mechanism of pattern formation in the hydrocoel is still unknown (Byrne et al., 2016b). There are no reports disrupting the pattern formation of hydrocoel or altering the number of emerging hydrocoel lobes by any chemical treatments or

surgical manipulations.

Therefore, there are no clues to reveal the mechanisms underlying the pentaradial pattern formation in the hydrocoel. What are the possible mechanisms of pattern formation in the hydrocoel? When the pattern formation occurs in the hydrocoel, genes involved in the regulation of developmental process such as transcription factors, ligands and receptors of signaling pathways should show the expression pattern localized to a certain region of the hydrocoel, prior to the formation of the hydrocoel lobes. In other words, the genes involved in pattern formation in the hydrocoel can be identified by searching for the genes heterogeneously expressed in a hydrocoel.

In this study, to identify the genes involved in the pattern formation of hydrocoel in sea cucumber *Apostichopus japonicus*, I searched for genes that showed heterogeneous expression pattern in the hydrocoel before the lobe formation, and further analyzed its functions. As in chapters 1 and 2, I used *A. japonicus* since the developmental process of the hydrocoel can be easily observed. I conducted the comprehensive analyses to select candidate genes involved in the patterning process in the hydrocoel. As defined in Chapter 2, the developmental process of hydrocoel can be divided into four phases (Fig. 3-1a). At each of these phases, the hydrocoel was isolated, and hydrocoel tissue specific RNA-seq analysis was conducted (Fig. 3-1b). Based on the RNA-seq analysis, candidate genes which specifically expressed in the hydrocoel were obtained, and *in situ* hybridization to test the detailed expression pattern and chemical treatment to investigate the involvement in pattern formation in the hydrocoel were conducted.

Materials and Methods

Animals

Mature adults of *A. japonicus* were collected between April and June of 2019-2021 from sandy bottom of the sea at the depth of 3-10 m around the Misaki Marine Biological Station, Kanagawa or at Onahama Port, Fukushima (36° 94' N, 140° 90' E) by SCUBA diving. All the collected individuals were morphologically diagnosed as the black type of the focal species, that was recently redescribed as *A. armatus* (Woo et al., 2017) although it is still treated as *A. japonicus* in many recent studies. Collected individuals were kept in the laboratory tank at 17 ºC to maintain the sexually mature condition. Gonads of collected individuals were dissected from inside the body wall to discriminate sex and maturity (Liu et al., 2015). Mature ovary is vivid orange and mature testis is white. Egg spawning was induced by the injection of 500 µL of 10 µM cubifrin (Kyusyu TLO Company, Fukuoka, Japan), a peptide known to induce oocyte maturation and spawning in A. japonicus (Kato et al., 2009). Sperms were obtained by dissecting matured testes in sea water.

Embryo culture was conducted based on Kikuchi et al., 2015. Briefly, embryos were kept in 10 L of filtered sea water in a plastic container with circulation at 20 ºC, and daily fed *Chaetoceros calcitrants* diatoms. The density of individuals was kept as 1 embryo/mL, and sea water was changed every two days. Embryos become bilateral auricularia larva at 2 dpf. The hydrocoel emerges at the left side of the digestive tract around 6 dpf and the hydrocoel lobes can be observed around 10 dpf. Individuals during this period were used for observations. After the formation of hydrocoel lobes, larvae metamorphose into doliolaria and pentactula juveniles, and settle down on the container

bottom.

RNA-seq data analysis and candidate selection

RNA was extracted from both the excised hydrocoel and the rest of the body in each of the four developmental phases (Fig. 3-1a, b). Larvae were stored in RNA later (Thermo Fisher Scientific, Waltham, MA, USA) and dissected with a tungsten needle under a stereomicroscope. Biological replicates were taken in triplicate, and RNA from 20-50 individuals was pooled into each sample. Dissected tissues were lysed using buffer RLT (Qiagen, Hilden, Germany), and RNA was purified using RNA XP clean beads (Beckman Coulter, Brea, CA, USA). Toral RNA concentrations were determined on a Qubit 2.0 fluorometer (Thermo Fisher Scientific, Waltham, MA, USA) using the Qubit RNA HS Assay Kit (Thermo Fisher Scientific, Waltham, MA, USA). RNA quality was measured using the RNA6000 pico kit (Agilent Technologies, Santa Clara, CA, USA) on a Bioanalyzer (Agilent Technologies, Santa Clara, CA, USA), and samples with RIN < 9 were used.

The obtained RNA was reverse transcribed and amplified by the Quartz-seq method (Sasagawa et al., 2013). Library preparation was performed using the Nextera XT DNA library kit (Illumina, San Diego, CA, USA). cDNA and library quantification were performed using the Qubit dsDNA HS Assay Kit (Thermo Fisher Scientific, Waltham, MA, USA) and High sensitivity DNA kit (Agilent Technologies, Santa Clara, CA, USA) was used for quality check. The pooled libraries were sequenced at the paired end using HiSeq 1500.

The obtained sequence data were quality checked with FastQC -0.11.9 (http://www.bioinformatics.bbsrc.ac.uk/projects/fastqc) and Trimmomatic -0.39

(Bolger et al., 2014) to remove adapter sequences. Sequence data were mapped to sea cucumber genome data (Zhang et al., 2017) with Hisat2 -2.1.0 (Kim et al., 2019). Expression level were obtained with StringTie v2.1.1 (Pertea et al., 2015), and prepDE.py was used to obtain read counts. All parameters of these tools were default. DEseq2 (Love et al., 2014) was used for gene expression variation analysis. Hierarchical clustering among genes was drawn using the heatmap.2 function of the R package gplots.

For GO annotation, we used three tools: blast2GO (Conesa et al., 2005), pannzer2 (Törönen et al., 2018), and eggNOG-mapper (Huerta-Cepas et al., 2017). In addition, reciprocal blasts were performed against sea urchin *S. purpuratus* genes (Tu et al., 2012) to pick up the GO term for reciprocal top hits. The results obtained by these four methods were integrated and used in this study. For GO enrichment analysis, a database was created using annotation forge (Carlson and Pagès, 2020) and analyzed and visualized using cluster profiler (Wu et al., 2021).

Whole mount in situ hybridization

For whole mount *in situ* hybridization (WISH), larvae were fixed using Fix1 (4% PFA/ 0.1M MOPS, pH 7.0/ 0.5M NaCl) and stored in 70% ethanol at -20°C until use (Kikuchi et al., 2015). Digoxigenin-labeled RNA probes were synthesized from cDNAs and WISH was performed as previously described (Kikuchi et al., 2015; Shoguchi et al., 2000) with modification. Hybridization process was extended from 16 h to 7 days based on protocols of sea urchins (Yaguchi et al., 2016). Specimens were observed under an optical microscope (TE300 Nikon, Tokyo, Japan) equipped with a camera (DP27, Olympus, Tokyo, Japan).

Chemical treatment

To examine the involvement of the Wnt, TGF-β super family, and Notch signaling pathways in pattern formation and morphogenesis in the hydrocoel, chemical treatment was conducted (Table 3-3).

For Wnt pathway, C59 (5 μM), which interferes with Wnt protein secretion by inhibiting post-translational modifications of Wnt (Cui et al., 2014; Proffitt et al., 2013) was used. Since the Wnt pathway is known to have multiple downstream pathways, in addition to C59, inhibition experiments for each downstream pathway were conducted. For canonical pathway, CHIR99021(10 μM) and lithium chloride (LiCl, 3 mM) were used as activators (Vonica et al., 2000) and PNU-74654 (20 μM) and IWR-I-endo (20 μM) were used as inhibitors(Chen et al., 2009; Demilly et al., 2013; Lu et al., 2009). For PCP pathway, Y27632 (75 μM), which inhibits downstream Rho kinase (ROCK) (Croce et al., 2006; Riento and Ridley, 2003), and SP600125 (20 μM), which inhibits downstream c Jun N-terminal kinase (JNK) (Bennett et al., 2001; Dush and Nascone-Yoder, 2013) were used. For Wnt/Ca2+ pathway, bisindolylmaleimide I (10 μM) (Chou and Howard, 2002; Croce et al., 2006; Koyanagi et al., 2005) was used. For inhibition of the TGF-β super family pathway, I used dorsomorphin (20 μM) , which inhibits Alk2/3/6, the receptor for BMP2/4 (Hao et al., 2008; Luo and Su, 2012; Yu et al., 2008), and SB431452 (5 μM), which inhibits Alk4/5/7, the receptor for ActivinB, BMP3, and Univin (Inman et al., 2002; Piacentino et al., 2015). For inhibition of the Notch pathway, YO-010127 (10 μM) (Hasebe et al., 2017; Milano et al., 2004) was used.

Larvae were reared in glass dishes with 10 mL of filtered seawater containing the drug or 0.1 % DMSO as control. The number of larvae per dish was 10-20, and the seawater was changed every two days. Water temperature and feeding conditions were the same

as in normal rearing. Since the regulation of morphogenesis and pattern formation in the hydrocoel is thought to be initiated before the hydrocoel formation, chemicals were added to phase 1 larvae and reared them until they showed a clear phenotype or reached phase 4 (Fig. 3-13a). For the drugs with strong phenotypes, the concentration was reduced to 1/5 or 1/10 and the experiment was repeated. Specimens were observed under an optical microscope (TE300 Nikon, Tokyo, Japan) equipped with a camera (DP27, Olympus, Tokyo, Japan).

Results

Data analysis of RNA-seq

In the principal component analysis, the samples of the hydrocoel (H) and other parts of the body (B) were plotted in different regions and generally plotted in the order of phase 1 to phase 4 (Fig. 3-2a). Samples were generally divided into hydrocoel and body clusters in hierarchical clustering. However, h2-3 (hydrocoel, phase 2, replicate 3) and h3-3 (hydrocoel, phase 3, replicate 3) were placed in the body cluster (Fig. 3-2b).

To identify genes that are specifically expressed in the hydrocoel, differentially expressed genes (DEGs) that were highly expressed in the hydrocoel (fold change > 2, padj > 0.01) compared to the body at each phase (Fig. 3-3a). To identify genes whose expression varied during the developmental stage, DEGs between each phase (fold change > 2, padj > 0.01) were selected (Fig. 3-3b). The total number of genes in both groups was 637.

To understand the overall expression dynamics of the DEGs, hierarchical clustering between DEGs was conducted. When DEGs were divided into four groups, subcluster 1 was highly expressed in the early hydrocoel and subcluster 2 was highly expressed in the late hydrocoel. Subcluster 3 was upregulated in the late phase in both the hydrocoel and body, and subcluster 4 was upregulated in the early phase in both the hydrocoel and body (higher expression in body) (Fig. 3-3c).

GO enrichment analysis and candidate gene selection based on GO terms

I integrated the results of 4 methods and got 26248 genes (87%) out of total 30205 genes annotated (Fig. 3-4a). GO enrichment analysis showed that genes related to membrane transport and ribosomes were particularly abundant in subcluster 1. In

subcluster 2, genes involved in muscle formation, remodeling of the extracellular matrix, and regulation of peptidase activity were particularly abundant (Fig. 3-4b).

To select candidate genes involved in the regulation of pattern formation and morphogenesis in the hydrocoel, selection based on GO terms from 637 DEGs selected above was conducted. Genes containing GO:0003700: DNA-binding transcription factor activity or its offspring GO were selected as transcription factors. Genes containing GO:0048018 receptor agonist, GO:0048018 receptor agonist activity, GO:0005102 signaling receptor binding, GO:0038023 signaling receptor activity, or their offspring GO were selected as genes involved in intercellular signaling. As a result, 80 genes were selected. From these genes, I selected 21 genes that may be involved in developmental regulation by checking the expression pattern and the content of GO (Fig. 3-5, Table 3-1).

in situ hybridization of candidate genes

The spatial expression patterns of 20 candidate genes were examined from phase 1 to phase 4 by *in situ* hybridization, except for bmp2/4 , which was described in a previous study (Harada et al., 2002).

Among the 7 transcription factors examined, *activating enhancer binding protein 2 alpha (ap2a), forkhead box C (foxC), msh homeobox (msx), sineoculis homeobox homolog 1/2 (six1/2)*, and *zinc finger protein (zic)* were expressed in the hydrocoel (Table 3-1). Signal of *ap2a* was observed in the entire hydrocoel at phase 1 and 2. Weak signal was observed in the entire hydrocoel, and stronger signal was observed in lobe i at phase 3 (arrowhead). At Phase 4, signal was observed in lobes ii, iii, iv, and v in addition to lobe i, while no signal was observed in lobes I-V (white arrowheads, Fig. 3-

6). Signal of *foxC* was observed in the entire hydrocoel at phases 1-2, and the signal became weaker in the hydrocoel at phases 3-4. The signal was also found in the ventral region of ciliate band (Fig. 3-6). For *msx*, weak signal was observed in the whole body in phases 1-4, and stronger signal was observed in the whole hydrocoel in phase 4 (Fig. 3-6). For *six1/2*, signal was observed in the entire hydrocoel at phase 1, in the posterior side of the hydrocoel at phase 2, in the posterior side of the hydrocoel and lobes V and I at phase 3 (arrowheads), and in the entire hydrocoel at phase 4 (Fig. 3-7). For *zic*, signal was observed in the entire hydrocoel throughout phases 1-4 (Fig. 3-7). No clear signal was observed for *Alx homeobox 1 (alx1)* and *LIM dimain only protein (lmo)* (Fig. 3-6).

Next, the expression patterns of genes of TGF-β superfamily and their related factors were examined (Table 3-1). For *activinB,* very weak signal only in the hydrocoel at phase 1 was detected (Fig. 3-7). For *bone morphogenetic protein 3 (bmp3),* signal was detected in lobe i at phase 4 (black arrowhead) and a signal in hydropore canal, a tube connected to the hydrocoel, at phase 1-4 (white arrowheads) (Fig. 3-7). There was no clear signal for *univin* and *gremlin* (Fig. 3-7,8).

As for Wnt and its related factors, signal was observed in five genes: *wnt3, wnt8, frizzled1/2/7, dickkopf1,* and *secreted frizzled related protein5 (sfrp5)* (Table 3-1). Weak signal was observed for *wnt3* and *wnt8* throughout the body, but the signal was not localized to specific tissues or regions (Fig. 3-8). For *frizzled1/2/7*, signal was detected in the anterior side of the hydrocoel at phase 2 and in the region of the hydrocoel except for lobes v and ii at phase 3 (white arrowhead). At phase 4, signal was observed in the whole body (Fig. 3-8). *dickkopf1* signal was detected in the hydropore canal at phase 2-3 (white arrowhead). At phase 4, the signal of *dickkopf1*

was observed in the entire hydrocoel. It was also expressed in a part of the ventral ciliary band (arrowhead, Fig. 3-9). Weak signal of *sfrp5* were observed in the whole body including the hydrocoel and digestive tract from phase 1 to 4 (Fig. 3-9).

Expression of other signaling molecules, such as *notch, cysteine rich transmembrane BMP regulator (crim), and slit guidance ligand 1 (slit1)*, were also detected (Table 3-1). Signal of notch was observed in the hydrocoel and digestive tract throughout phases 1-4 and in phase 4, signals were observed in the whole body (Fig. 3-9). For *crim*, a weak signal was observed in the hydrocoel in phase 4. In addition, signals were observed in the digestive tract from phase 1 to 3 (Fig. 3-9). The signal of *slit1* was observed in the digestive tract from phase 1 to 4 (Fig. 3-9).

in situ hybridization of genes related to the candidate genes

Genes involved in TGF-β super family, Wnt, and Notch pathway were found to be expressed in the hydrocoel, so further investigation on expression patterns of genes related to these pathways was conducted. Only the genes that were predicted to be expressed in the hydrocoel based on RNA-seq data were analyzed (Table 3-2).

For TGF-β super family, the expression patterns of a*ctivin receptor-like kinase 3/6 (alk3/6)*, which is one of the receptors, and a ligand *bmp1* were investigated. The signal of *alk3/6* was observed in the hydrocoel at phase 1-3 and in the whole body at phase 4 (Fig. 3-10). Weak signal of *bmp1* was observed in the hydrocoel at phase 4 (Fig. 3-10).

For Wnt pathway, ligands *wnt5, wnt7*, and *wnt9*, receptors *frizzled4* and *frizzled5/8*, and the *low-density lipoprotein receptor-related protein5/6* (*lrp5/6*, co-receptor of the canonical Wnt pathway), *retinoic acid-related orphan receptor (ror)* and *receptor tyrosine kinase (ryk)*, which are co-receptors of the planar cell polarity (PCP) and Wnt-

Ca2+ pathways(Mehta et al., 2021), were examined (Table 3-2). Signal of *wnt5* and *wnt7* was detected in the digestive tract, but no clear signal in the hydrocoel was detected. *wnt9* signal was detected throughout the body from phase 1 to 4, but especially strong signals in the hydrocoel at phase 2 (Fig. 3-10). *frizzled4* signal was observed in the entire hydrocoel at phase 1, in the hydrocoel except for the anterior and posterior ends at phase 2, in the hydrocoel at phase 3 around the lobe v, lobe ii (arrowheads), and the region where the hydropore canal connects (Fig. 3-11). *frizzled5/8* signal was detected in the digestive tract at phase 2-3 and in the whole body at phase 4, but no specific signal was observed in the hydrocoel (Fig. 3-11). Among the coactivators of the Wnt pathway, *ror* showed weak signals throughout the body in phases 1 to 4, and stronger signals in the hydrocoel at phases 1 and 2. In contrast, signal of *lrp5/6* and *ryk* was not detected in the hydrocoel (Fig. 3-11).

For the Notch pathway, the expression patterns of *delta* and *serrate* were examined (Table 3-2). For *delta*, no clear signal was observed, while for *serrate*, signal was observed throughout the hydrocoel at phases 1-3 and throughout the body at phase 4 (Fig. 3-12).

Functional analysis of Wnt pathway, TGF-beta pathway, and Notch pathway

For the Wnt pathway, C59 treatment (5 μM) resulted in the disassociation of cells from the hydrocoel and hydrocoel tissue was disrupted. In addition, the ciliary band was slightly shrunk and the morphology was simpler than that of control (Fig. 3-13, Table 3-3). As for the activation/inhibition of the canonical pathway, no phenotype was observed in LiCl (3 mM) or PNU-74654 (20 μM), and larvae became phase 4 with no defects in the morphology of the hydrocoel. With the activator CHIR99021 (5 μM), the

larvae showed a severe degeneration of the whole-body tissues. IWR-1-endo (20 μM), an inhibitor of the canonical pathway, also caused the whole-body shrinkage. Inhibition of the PCP pathway by Y27632 (75 μM) showed no phenotype, and larvae developed to phase 4 with no defects in the morphology of the hydrocoel. Inhibition of the PCP pathway by SP600125 (20 μM) showed the same phenotype as C59, where cells in the hydrocoel was disassociated and hydrocoel tissue was collapsed. For inhibition of the Ca^{2+} pathway, bisindolylmaleimide I (10 μM) caused a disintegration of larval body surface, but no effect on hydrocoel or digestive tract was observed. When the concentrations of the inhibitors that produced the phenotypes were reduced to 1/5 or 1/10 of the original concentrations (to 1 μM for C59 and CHIR99021, bisindolylmaleimide I, and 2 μM for IWR-1-endo and SP600125), larvae developed normally and became phase 4. The number and the position of the hydrocoel lobe were unaffected.

Dorsomorphin (20 μM) caused a shrinkage of the hydrocoel and other tissues throughout the body, while SB431452 (5 μM) caused a shrinkage of body surface tissues but had no effect on the hydrocoel (Fig. 3-13). When the concentrations of dorsomorphin and SB431452 were reduced to 1/5, i.e., 4 μM and 1 μM, respectively, the effect on the body surface disappeared and the hydrocoel developed normally.

No phenotype was observed with YO-010127 (10 μM), and larvae developed to phase 4 with no abnormalities in hydrocoel morphology (Fig. 3-13).

Discussion

RNA-seq analysis and selection of candidate genes

The PCA plots between the samples showed that samples in same part and phases were of high similarity, so it a can be said that the sampling for RNA-seq was properly completed (Fig. 3-2a). Enrichment analysis showed that subcluster 2, which was upregulated specifically in the hydrocoel in the latter phase (Fig. 3-3c), contained genes related to extracellular matrix remodeling and muscle tissue development (Fig. 3-4b) and this is consistent with the fact that the formation of the hydrocoel lobe in phase 3-4 results in dynamic changes in tissue morphology, and that muscle-related genes are expressed in the hydrocoel lobe (Chapter 1).

In candidate selection, several neurotransmitters and immune-response factors were excluded from this analysis since these molecules are not responsible for pattern formation during development (Fig. 3-5).

Expression patterns of transcription factors

Among the transcription factors selected as candidate genes (Table 3-1), *foxC, zic* and *msx* are known to be expressed in the hydrocoel or its primordium of sea urchins (Adachi et al., 2018; Koop et al., 2017; Su, 2014), consistently with my results in *A. japonicus* (Fig. 3-6, 7). In other words, the expression patterns of these transcription factors are generally a conserved feature between the two groups. However, since these transcription factors did not show the heterogeneous expression before the lobe formation, involvement in the determination of location and number of hydrocoel lobes was not suggested.

Since *ap2a* at was also expressed in the whole hydrocoel at phases 1-2, *ap2a* is unlikely to be involved in the hydrocoel pattern formation (Fig. 3-6). On the other hand, *ap2a* was expressed in only five of the ten lobes, that were future radial canals, suggesting that *ap2a* is involved in the determination of hydrocoel lobe identity (Fig. 3-14b).

The only transcription factor that showed a localized expression pattern in the hydrocoel prior to the lobe formation was *six1/2* (Fig. 3-6). The expression pattern of six1/2 shows that it is expressed in a single region in the hydrocoel (phase 1 and 2) and then in multiple regions (phase 3) (Fig. 3-14b). *six1/2* may be involved in a mechanism that mediates pattern formation in response to diffusive molecules, or it is possible that the number and distribution of cells expressing *six1/2* are important in pattern formation. However, in the sea urchin *H. erythrogramma*, the expression of *six1/2* continues even in the tube feet of larvae formed from hydrocoel lobes (Byrne et al., 2018). This suggests that *six1/2* is involved in the process of hydrocoel tissue differentiation, but not in pattern formation. It is necessary to further investigate the detailed expression pattern of *six1/2*, for example, by fluorescence *in situ* hybridization and functional analysis to verify whether six1/2 is involved in the pattern formation. Since *six1/2* plays important roles in the embryogenesis (Andrikou et al., 2015), it is necessary to temporally knockdown or knockout *six1/2*. Not only in the sea cucumber but also in other echinoderms, systems of conditional knockdown in the larvae have not been well developed, so the development of functional analysis will be an important issue.

Role of TGF-β super family, Notch and other signaling pathway in hydrocoel lobe formation

Based on the results of *in situ* hybridization and inhibitor treatment, it is unlikely that the TGF-β super family pathway is involved in the hydrocoel pattern formation (Fig. 3-7, 10, 13). On the other hand, *bmp3* was expressed only in hydrocoel lobe i, suggesting that *bmp3* may be involved in determination of the identity of hydrocoel lobes and in the tissue formation that occurs around the hydrocoel lobe (Fig. 3-14b).

As for the Notch pathway, expressions of *notch* and *serrate* suggest that the Notch pathway is constantly activated in the hydrocoel from phase 1 to phase 4(Fig. 3-9, 12), although the inhibition of the notch pathway (Table 3-3, Fig. 3-13) suggested that the notch pathway is not involved in the pattern formation in hydrocoel.

Wnt pathway in the hydrocoel morphogenesis and pattern formation

Interestingly, Wnt receptors *frizzled1/2/7* and *frizzled4* were expressed in a nested manner in the hydrocoel and their spatial expression patterns became more complex as development progresses (Fig. 3-8, 11, 14a). In addition, a Wnt antagonist *dickkopf* was expressed in the hydropore canal adjacent to the hydrocoel, implying that the diffusion of Wnt and antagonist and regulation of Wnt pathway might be involved in the pattern formation. The Wnt pathway is a complex signaling pathway that encompasses three major pathways: canonical pathway, PCP pathway, and Wnt/Ca^{2+} pathway (Mehta et al., 2021), and is known to be involved in various pattern formation phenomena during development (Pond et al., 2020). It is also known that in echinoderms, the feedback loop through the canonical pathway and PCP pathway, which is transmitted by Frizzled

receptors, establishes regional divisions along the anterior-posterior axis of embryo (Range, 2018).

The expression patterns of co-receptors suggests that the PCP pathway or Wnt/Ca2+ pathway is activated in the hydrocoel (Table 3-2, Fig. 3-11). Inhibition of JNK, a downstream factor of the PCP pathway and inhibition of Wnt secretion suggested that Wnt-PCP-JNK pathway is involved in the morphogenesis of the hydrocoel.

The involvement of the Wnt pathway in the morphogenesis of the hydrocoel was firstly revealed in this study. It is difficult to infer the exact function of PCP pathway in hydrocoel. However, an interesting implication is obtained from gut elongation in *Xenopus laevis* driven by radial cell intercalation, in which PCP pathway maintains the tissue integrity (Dush and Nascone-Yoder, 2013). As shown in Chapter 2, radial cell intercalation is thought to contribute to the formation of hydrocoel lobes. Taken together, it is also suggested that the Wnt-PCP-JNK pathway may be involved in the maintenance of tissue integrity in the sea cucumber hydrocoel.

On the other hand, the inhibition of Wnt pathway (Table 3-3, Fig. 3-13) suggested that Wnt pathway itself does not determine the number and position of hydrocoel lobe, suggesting that the complex expression pattern of *frizzled* is likely to be a downstream phenomenon of pattern formation by other upstream factors. However, even if the Wnt pathway itself is not responsible for pentameral pattern formation, the increasing complexity of the spatial expression patterns of *frizzled* during phases 1 and 4 are likely to reflect the distribution of upstream factors. In other words, the patterns of *frizzled* expression, which gradually divided into different regions, suggests that the pentameral pattern of hydrocoel is likely to be formed gradually through intercellular signals via

diffusible ligands, rather than being determined at the very early phase of hydrocoel development.

Pattern formation mechanism in the hydrocoel

The hypothesis that the pentameral pattern in the hydrocoel is gradually formed through development is also supported by the expression patterns of other genes. Transcription factors *ap2a* and *six1/2* were found to be expressed throughout the hydrocoel in phase 1, whereas in phases 2 to 4, they showed heterogeneous expression patterns (Fig. 3-14).

At present, mechanism of pattern formation in the hydrocoel is still unknown. In future studies, investigations of additional candidate genes to find other genes with heterogeneous expression in the hydrocoel, and functional analyses of those candidates will provide the deeper insights about the mechanisms of pentaradial pattern formation.

It will also be important to compare the results of this study with other echinoderms. The morphology of the hydrocoel differs among echinoderm lineages. In an extreme example, direct developing sea urchin *Holopneustes purpurescens* has two separate hydrocoel, a dorsal hydrocoel and a ventral hydrocoel (Morris, 2007). In many echinoderms other than sea cucumbers, the initial number of lobes in a hydrocoel is five rather than ten. The investigation on expression patterns of genes such as *frizzled, six1/2* and *ap2a* in the hydrocoel of other echinoderms will provide important insights into the conserved mechanism of pentaradial pattern formation in the hydrocoel.

It is also necessary to consider whether the hydrocoel pattern formation occurs independently or under the regulation by other tissue. For example, in auricularia larva of *A. japonicus*, the hydrocoel is located adjacent to the

hydropore canal, somatocoel, and esophagus. It is important to conduct tissue culture of isolated hydrocoel or analyses on the genes expressed in adjacent tissues to evaluate the effect of other tissue.

Table 3-1. List of candidate genes and its expression pattern.

Based on Fig. 3-6 to 3-9. Expression in the hydrocoel is shown in red characters.

Type	ID	Character	Signal
TF	PIK56440	*alx1*	not detected
TF	PIK51735	*ap2a*	specific part of the hydrocoel
TF	PIK49661	*foxC*	hydrocoel, ciliary band
TF	PIK57316	*lmo*	not detected
TF	PIK54978	*msx*	hydrocoel lobes (slight), whole body
TF	PIK55398	*six1/2*	specific part of the hydrocoel
TF	PIK54868	*zic*	hydrocoel
TGF (ligand)	PIK48233	*activin B*	hydrocoel (slight)
TGF (ligand)	PIK45926	*bmp2/4*	hydrocoel lobes (based on Harada *et al., 2002*)
TGF (ligand)	PIK37799	*bmp3*	specific hydrocoel lobe, hydropore canal
TGF (ligand)	PIK56113	*univin*	not detected
TGF (antagonist)	PIK53087	*gremlin*	digestive tract
Wnt (ligand)	PIK45647	*wnt3*	whole body
Wnt (ligand)	PIK51024	*wnt8*	hydrocoel, whole body
Wnt (receptor)	PIK40213	*frizzled1/2/7*	specific part of the hydrocoel
Wnt (receptor)	PIK53113	*frizzled9/10*	digestive tract
Wnt (antagonist)	PIK40341	*dickkopf1*	hydropore canal, ciliary band
Wnt (antagonist)	PIK36412	*sfrp5*	digestive tract
Notch (receptor)	PIK60374	*notch*	hydrocoel
ligand	PIK40094	*crim*	digestive tract
ligand	PIK34757	*slit1*	digestive tract

Table 3-2. List of genes related to TGF-β super family, Wnt and Notch pathway and its expression pattern.

Based on Fig. 3-10 to 3-12. Expression in the hydrocoel is shown in red characters.

Type	ID	Character	Signal
TGF-β (receptor)	PIK51009	*alk3/6*	hydrocoel, whole body
TGF-β (ligand)	PIK43870	*bmp1*	hydrocoel lobe (slight)
Wnt (ligand)	PIK40288	*wnt5*	digestive tract
Wnt (ligand)	PIK56278	*wnt7*	digestive tract
Wnt (ligand)	PIK51469	*wnt9*	hydrocoel, whole body
Wnt (receptor)	PIK41264	*frizzled4*	specific part of the hydrocoel
Wnt (receptor)	PIK60968	*frizzled5/8*	whole body
Wnt (co-receptor)	PIK59538	*lrp5/6*	digestive tract
Wnt (co-receptor)	PIK40732	*ror*	hydrocoel, whole body
Wnt (co-receptor)	PIK59541	*ryk*	not detected
Notch (ligand)	PIK54747	*delta*	not detected
Notch (ligand)	PIK34472	*serrate*	hydrocoel, whole body

Table 3-3. List of chemicals for perturbation analysis and its phenotype.

Based on Fig. 3-13.

Reagent	Purpose	Function	Phenotype
C59	Inhibition of Wnt secretion	Porcupine inhibitor	Loss of the tissue integrity in the hydrocoel
CHIR99021	Activation of canonical Wnt pathway	GSK3 inhibitor	Distraction of body surface
lithium chloride	Activation of canonical Wnt pathway	GSK3 inhibitor	No effect
IWR-1-endo	Inhibition of canonical Wnt pathway	Wnt antagonist	Shrinkage of body surface
PNU74654	Inhibition of canonical Wnt pathway	TCF inhibitor	No effect
Y27632	Inhibition of Wnt/PCP pathway	ROCK inhibitor	No effect
SP600125	Inhibition of Wnt/PCP pathway	JNK inhibitor	Loss of the tissue integrity in the hydrocoel
bisindolylmaleimide I	Inhibition of Wnt/Ca^{2+} pathway	PKC inhibitor	Distraction of body surface
SB431452	Inhibition of TGF-β pathway	alk4/5/7 inhibitor	Shrinkage of body surface
dorsomorphin	Inhibition of TGF-β pathway	alk2/3/6 inhibitor	Shrinkage of body surface
YO-01027	Inhibition of Notch pathway	γ-secretase inhibitor	No effect

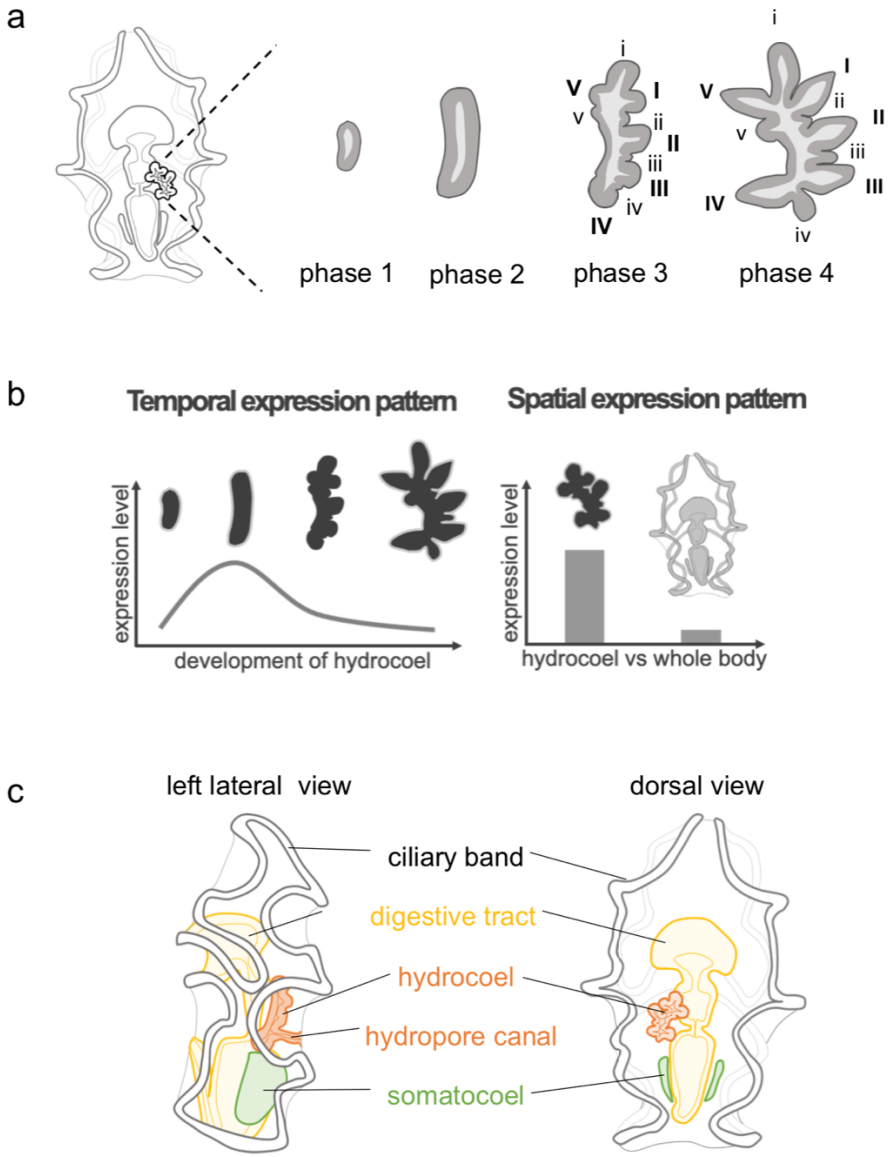

Figure 3-1. Auricularia larva of *A. japonicus* and its hydrocoel.

(a) Development of hydrocoel in auricularia larva based on chapter 2. Numbering of the hydrocoel lobe is based on Smirnov, 2014. (b) Strategy of RNA-seq analysis. Differentially expressed genes between hydrocoel between each phase (temporal expression pattern） and highly expressed genes in the hydrocoel (spatial expression pattern) were obtained. (c) Schematic diagram of auricularia larva and its body structure.

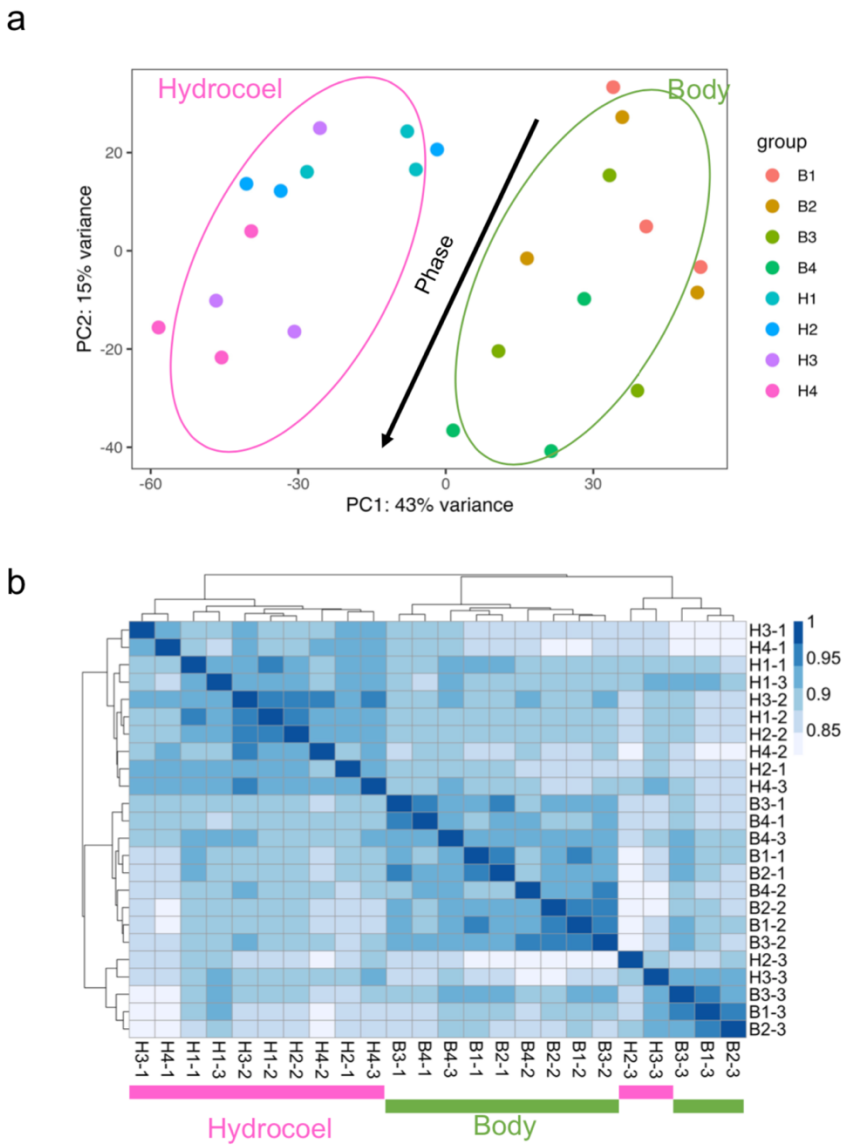

Figure 3-2. Investigation of the similarities between samples used in RNA-seq analysis.

(a) Plots showed PC1 and PC2 of principal component analysis between samples. Group means the body part and phases (B means body and H means hydrocoel. Numbers show phase.) (b) Hierarchical clustering between samples. B and H means body part. Numbers show phase and replicate. For example, H3-1 means hydrocoel, phase 3, replicate 1.

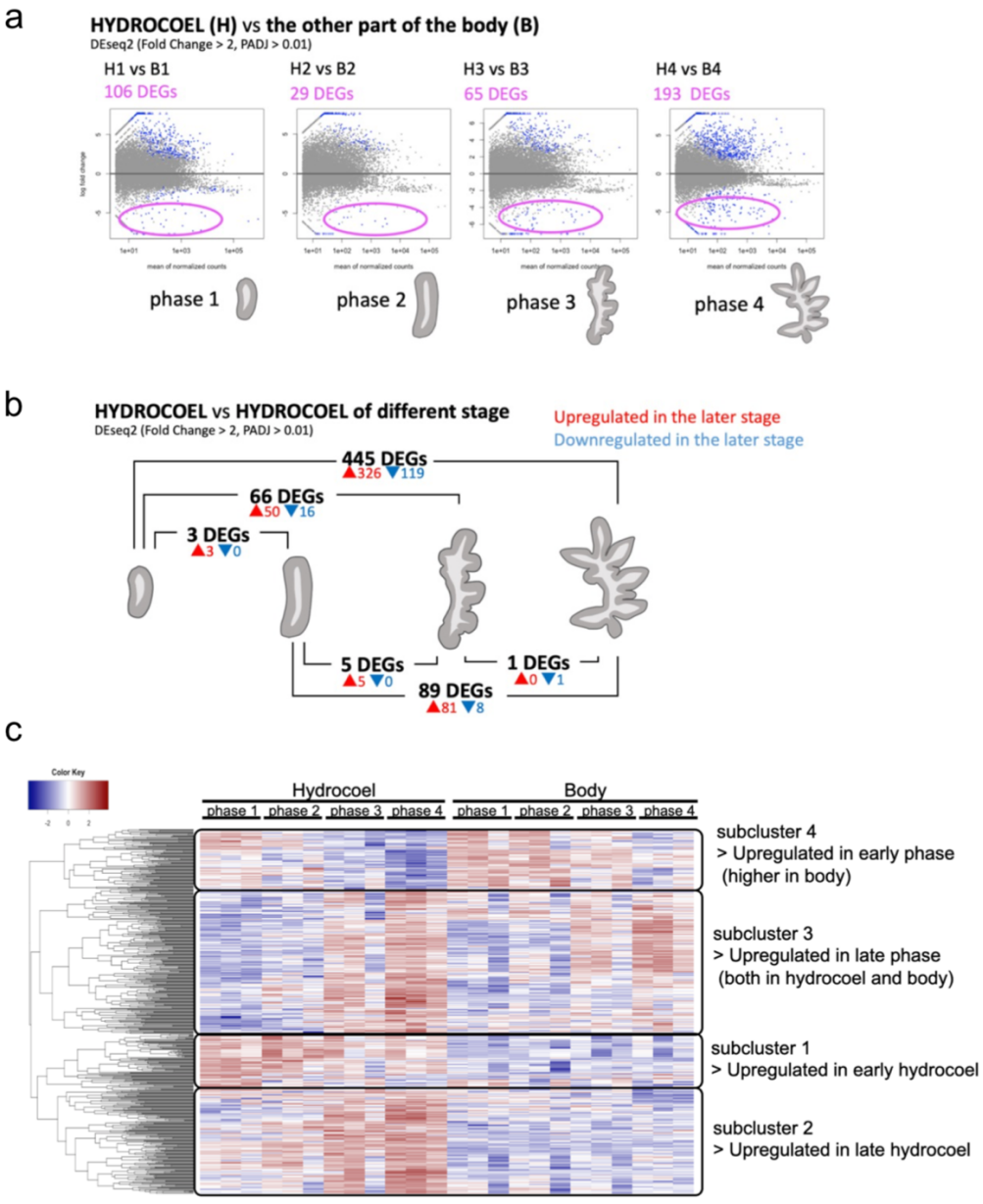

Figure 3-3. Differentially expression analysis.

(a) In each phase, Highly expressed DEGs compared to body were obtained (fold change > 2, padj > 0.01). (b) DEGs between hydrocoel of different phases were obtained (fold change > 2, padj > 0.01). (c) Hierarchical clustering of DEGs obtained in (a) and (b). The tendency in expression patter of four clusters are shown in the figure.

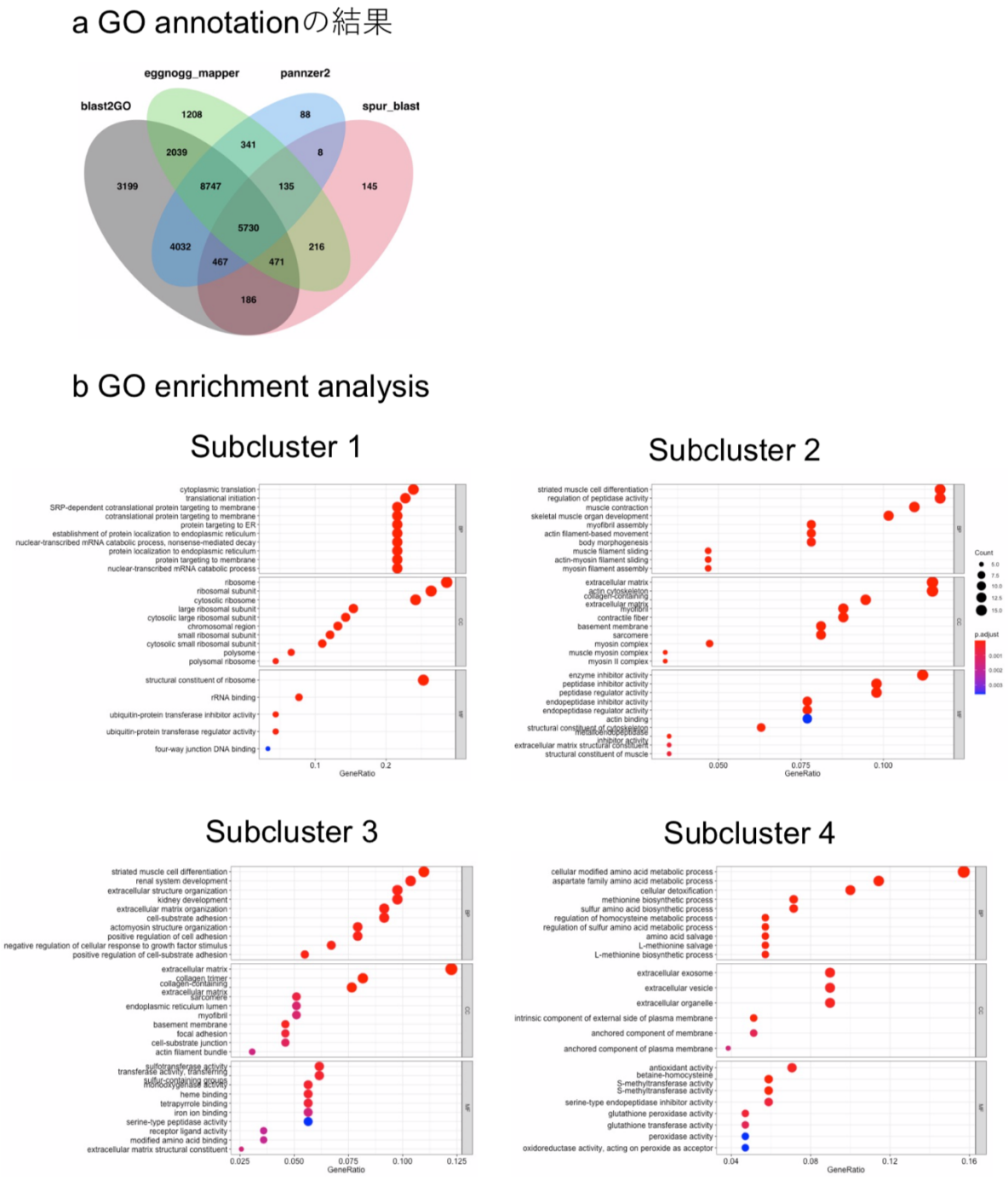

Figure 3-4. GO term annotation and enrichment analysis.

(a) The number of *A. japonicus* genes which annotated by four different methods. spur_blast means reciprocal blast against sea urchin *S. purpuratus*. (b) GO enrichment analysis of four clusters obtained in Fig. 3-3c.

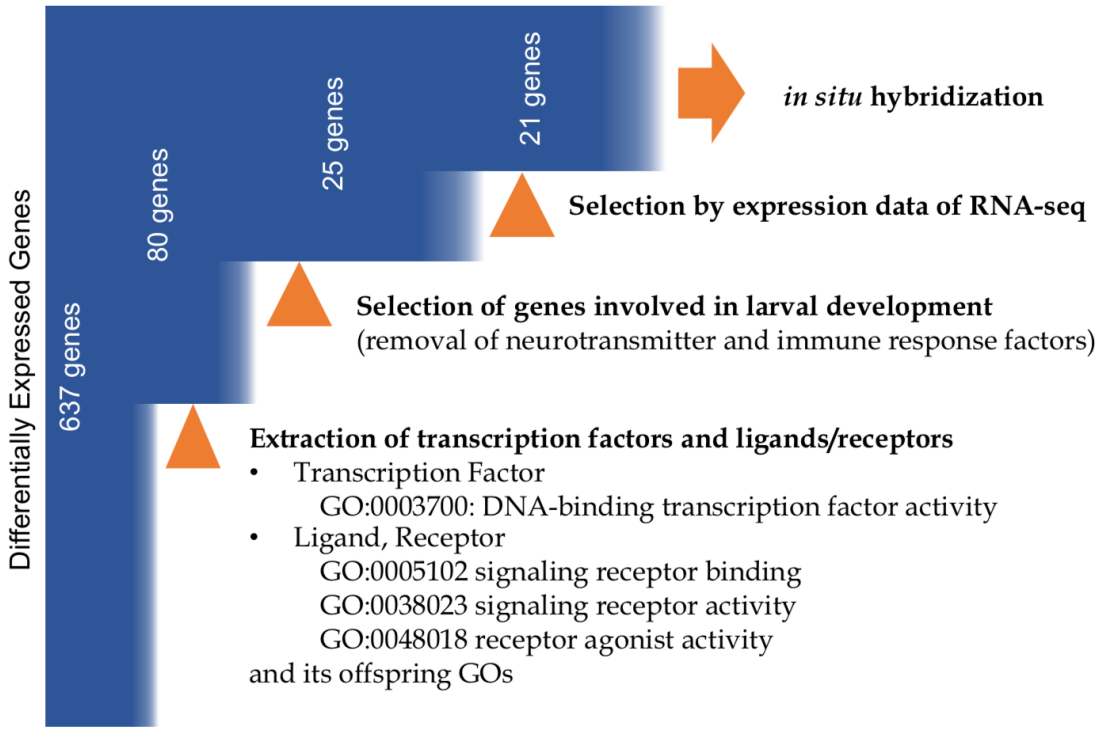

Figure 3-5. Candidate selection based on RNA-seq data and GO term.

Process of candidate selection for genes involved in the pettern formation and regulation of morphogenesis in the hydrocoel. Out of 637 DEGs selected in Fig. 3-3, genes annotated with GO term as transcription factors, ligands or receptors were selected. Genes related to neurotransmission and immune response or genes highly expressed in the body were removed.

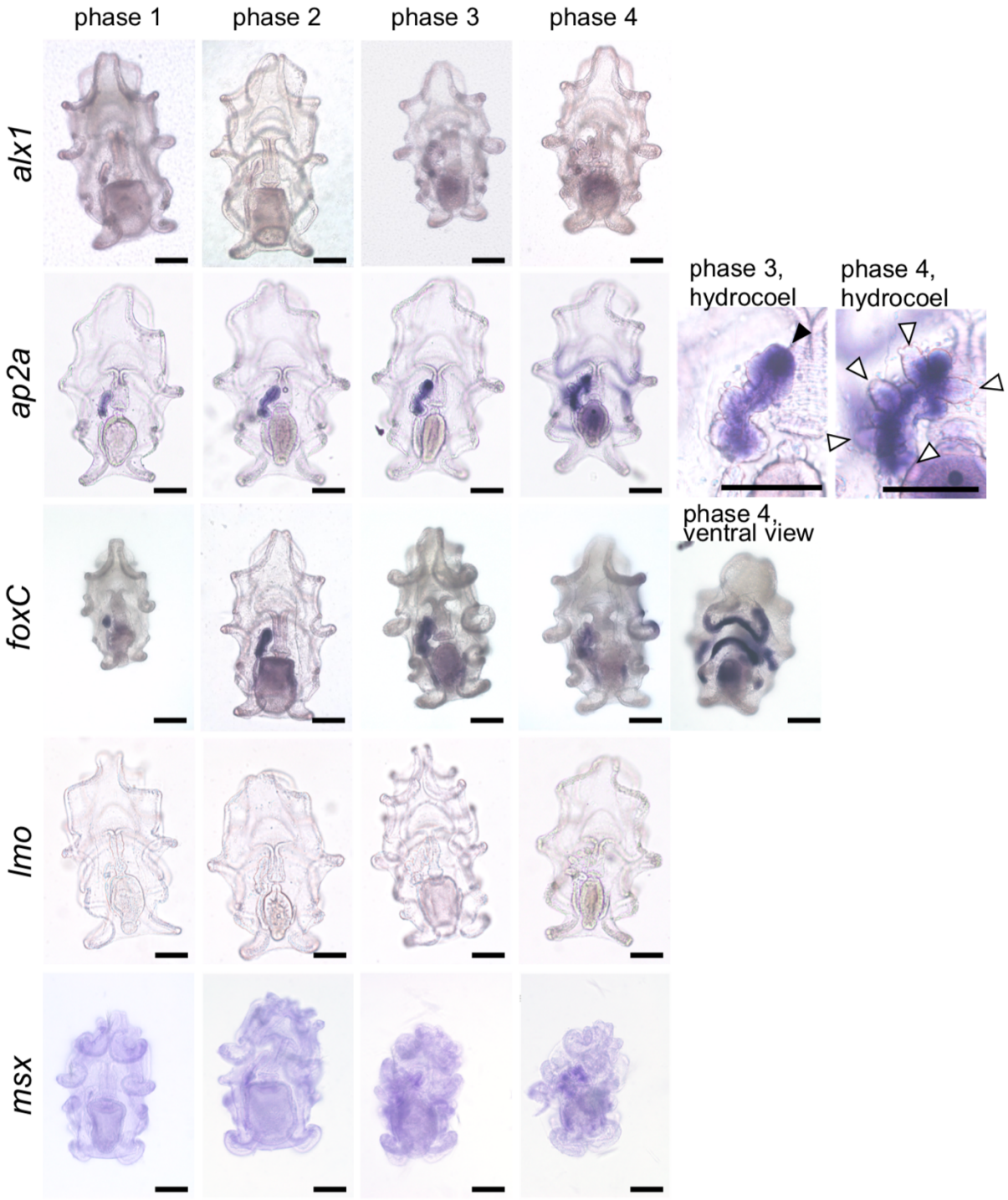

Figure 3-6. Expression pattern of candidate genes (1).

The results of *in situ* hybridization from phases 1 to 4 are presented. Unless otherwise noted, images show dorsal view, anterior top. Scale: 100 μm。 List of genes investigated is presented in Table 3-1. In this panel, expression patterns of transcription factors *alx1, ap2a, foxC, lmo* and *msx* are presented.

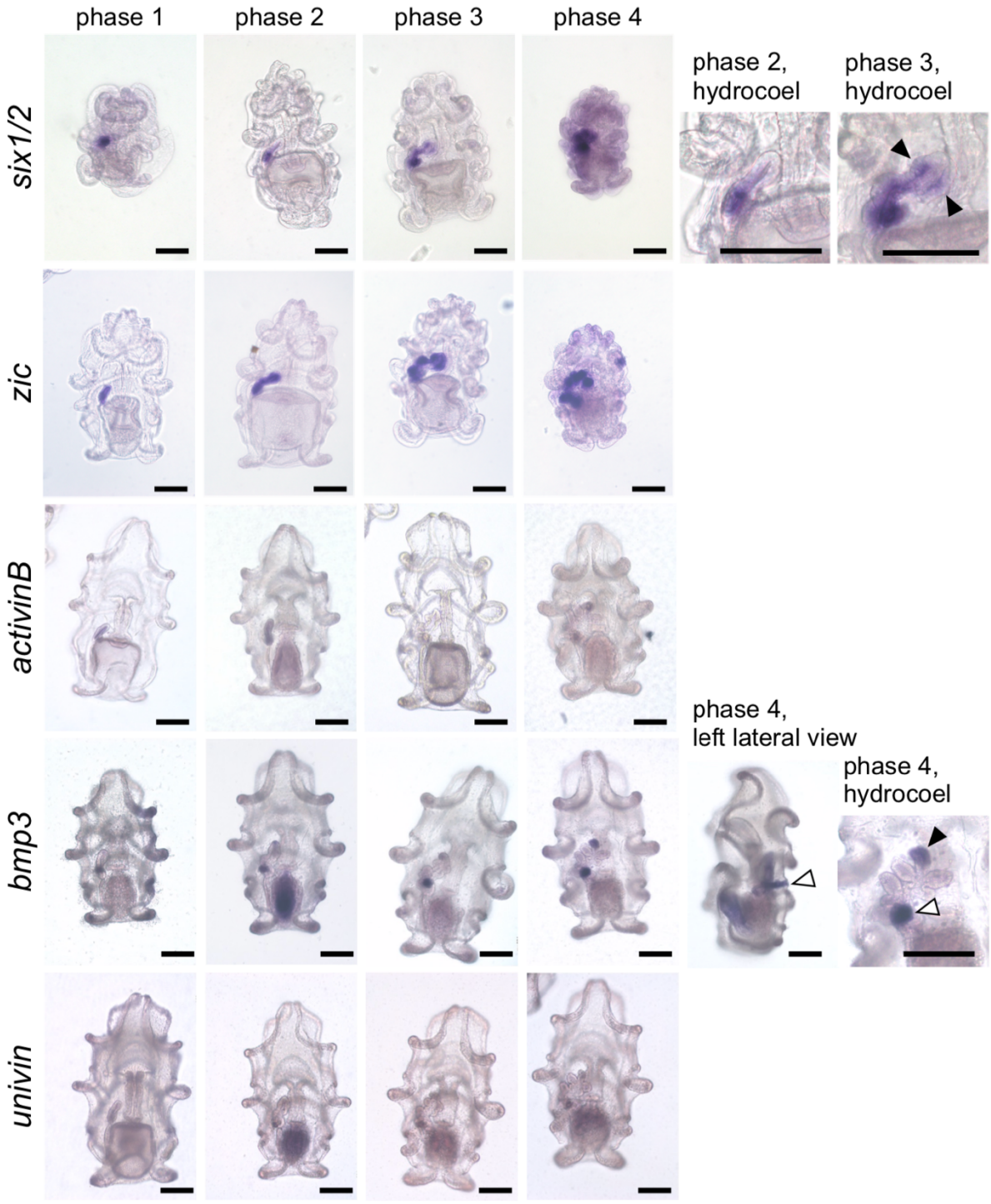

Figure 3-7. Expression pattern of candidate genes (2).

The results of *in situ* hybridization from phases 1 to 4 are presented. Unless otherwise noted, images show dorsal view, anterior top. Scale: 100 μm。 List of genes investigated is presented in Table 3-1. In this panel, expression patterns of transcription factors *six1/2, zic* and that aof ligand in TGF-β super family pathway *activinB, bmp3* and *univin* are presented.

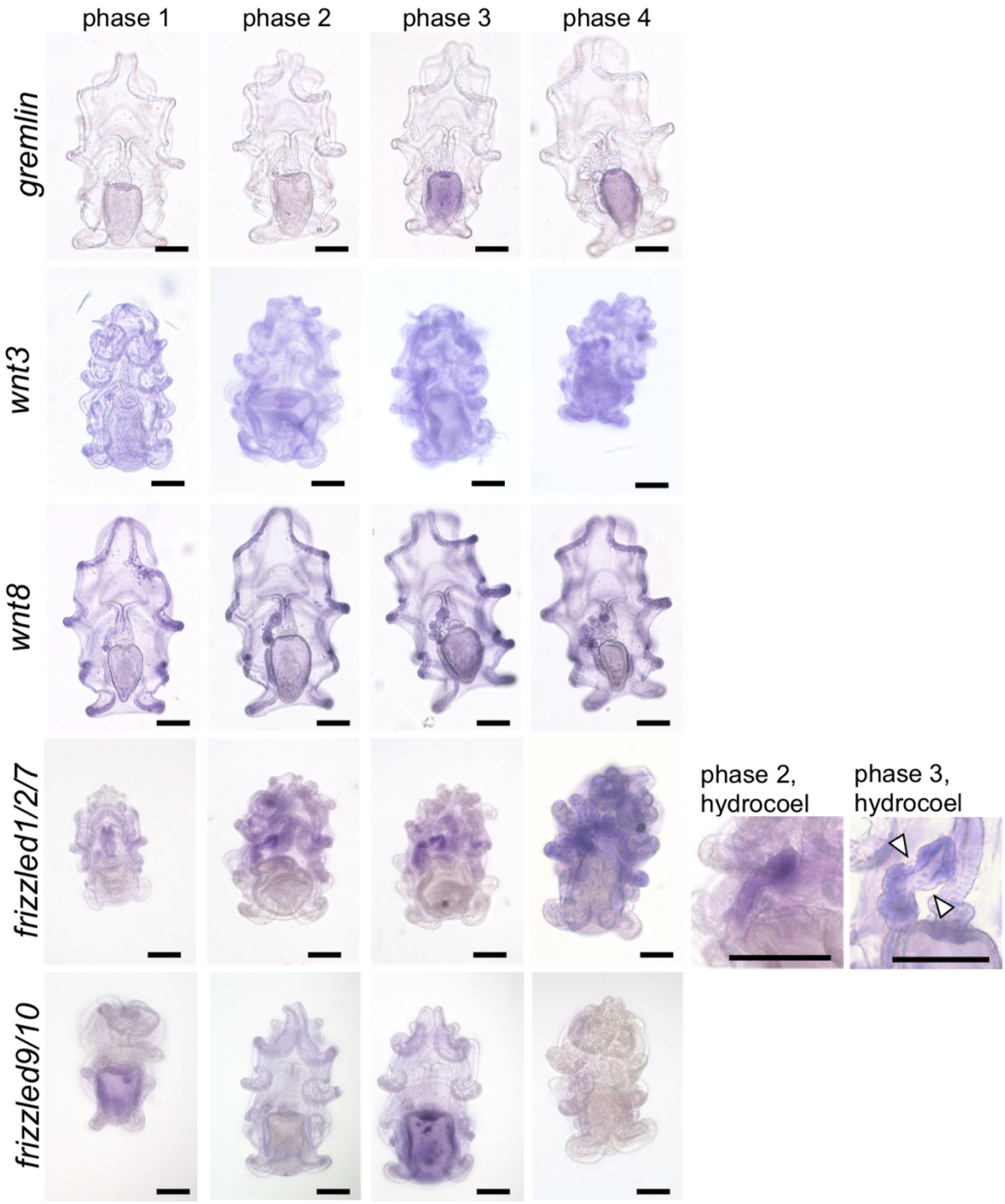

Figure 3-8. Expression pattern of candidate genes (3).

The results of *in situ* hybridization from phases 1 to 4 are presented. Unless otherwise noted, images show dorsal view, anterior top. Scale: 100 μm。 List of genes investigated is presented in Table 3-1. In this panel, expression patterns of BMP antagonist *gremlin* and that of factors in Wnt pathway *wnt3, wnr8, frizzled1/2/7* and *frizzled9/10* are presented.

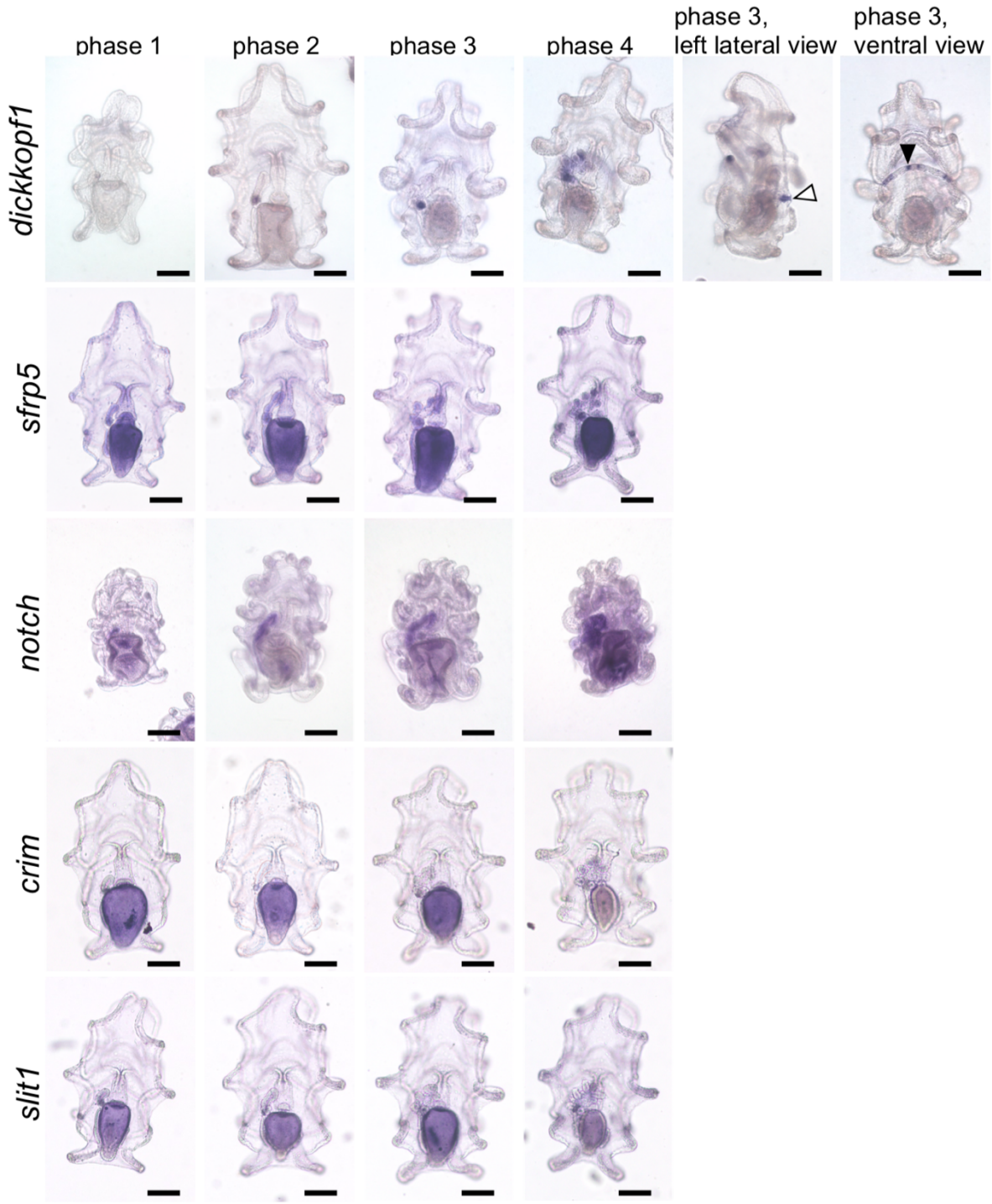

Figure 3-9. Expression pattern of candidate genes (4).

The results of *in situ* hybridization from phases 1 to 4 are presented. Unless otherwise noted, images show dorsal view, anterior top. Scale: 100 μm。 List of genes investigated is presented in Table 3-1. In this panel, expression patterns of Wnt antagonist *dickkopf, sfrp5* and that of receptor *notch,* ligand *crim* and *slit1* are presented.

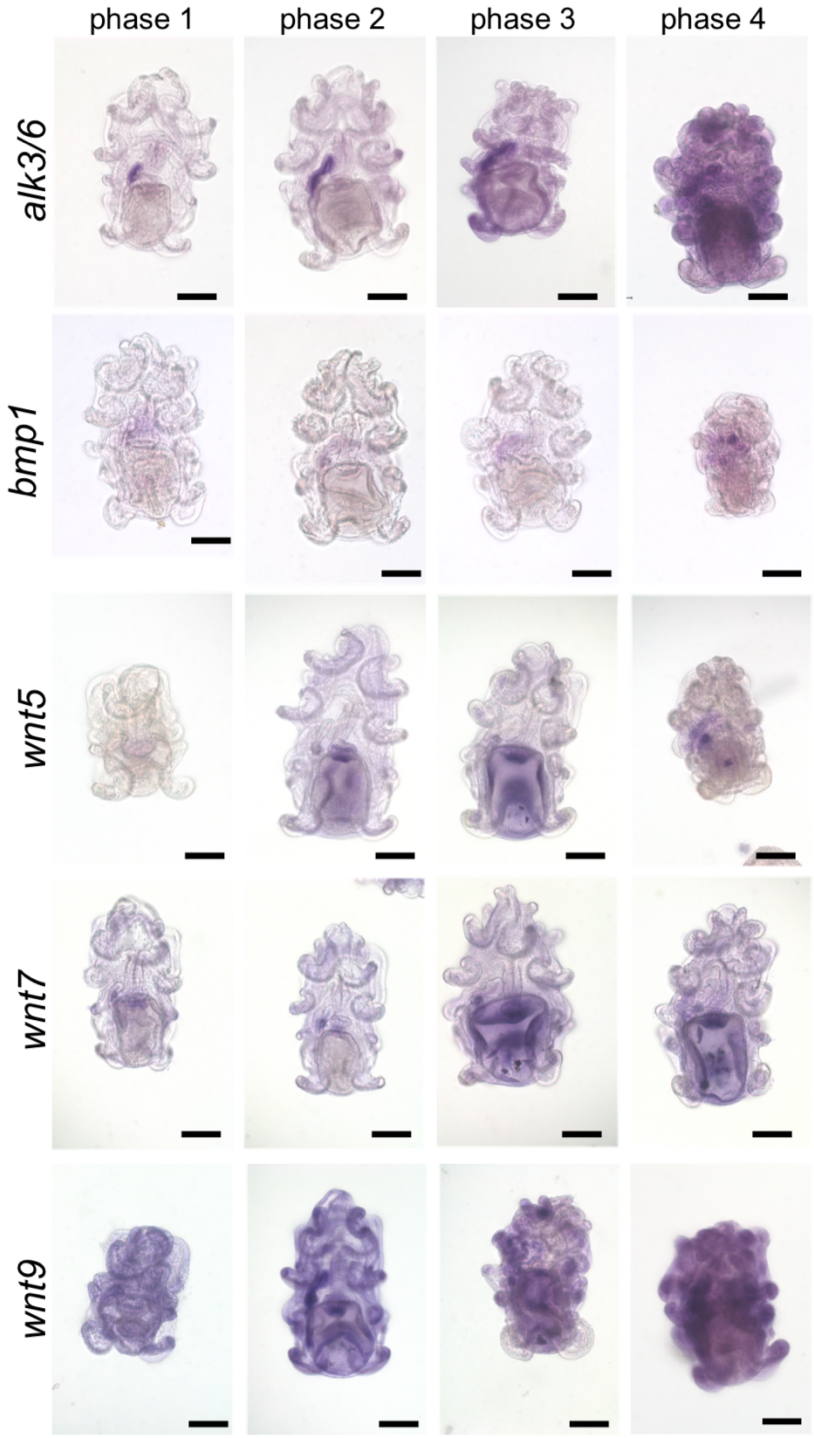

Figure 3-10. Expression pattern of genes related to TGF-β super family, Wnt and Notch pathway (1).

The results of *in situ* hybridization from phases 1 to 4 are presented. Unless otherwise noted, images show dorsal view, anterior top. Scale: 100 μm。 List of genes investigated is presented in Table 3-2. In this panel, expression patterns of *alk3/6, bmp1* in TGF-β super family pathway and *wnt5, wnt7, wnt9* in Wnt pathway.

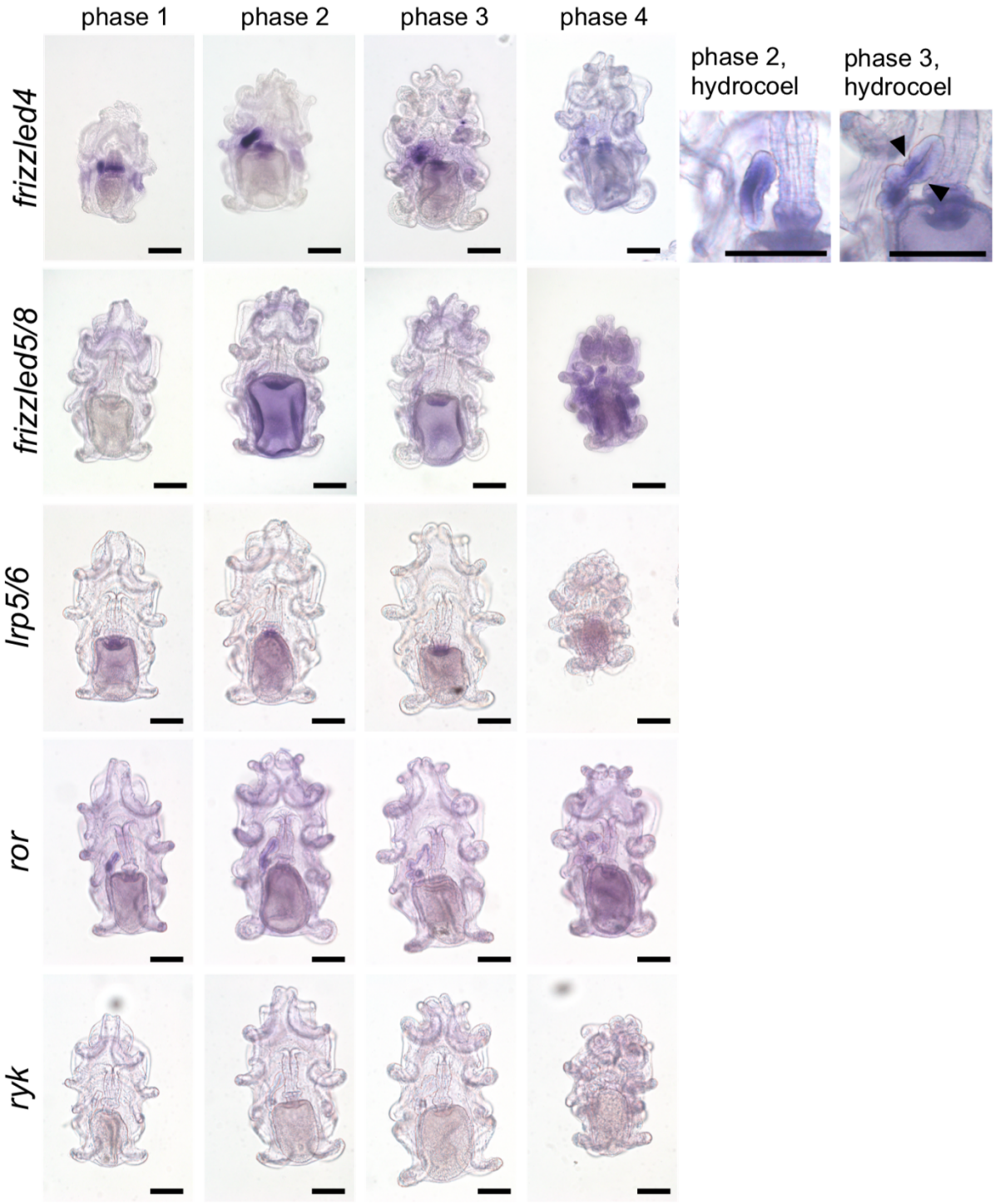

Figure 3-11. Expression pattern of genes related to TGF-β super family, Wnt and Notch pathway (2).

The results of *in situ* hybridization from phases 1 to 4 are presented. Unless otherwise noted, images show dorsal view, anterior top. Scale: 100 μm。 List of genes investigated is presented in Table 3-2. In this panel, expression patterns of *frizzled4, frizzled5/8, lrp5/6, ror* and *ryk* in Wnt pathway.

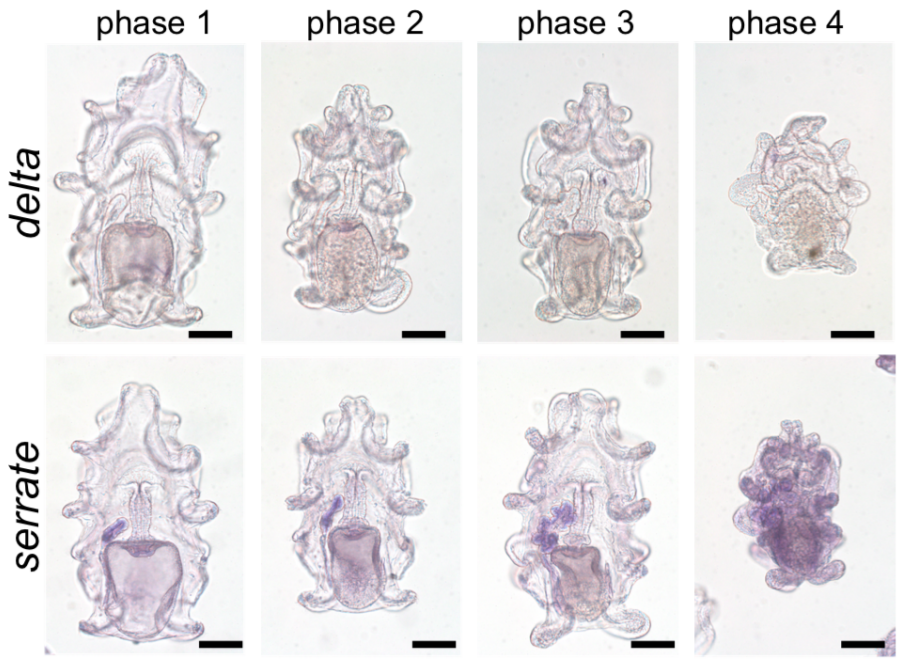

Figure 3-12. Expression pattern of genes related to TGF-β super family, Wnt and Notch pathway (3).

The results of *in situ* hybridization from phases 1 to 4 are presented. Unless otherwise noted, images show dorsal view, anterior top. Scale: 100 μm。 List of genes investigated is presented in Table 3-2. In this panel, expression patterns of *delta* and *serrate* in Notch pathway.

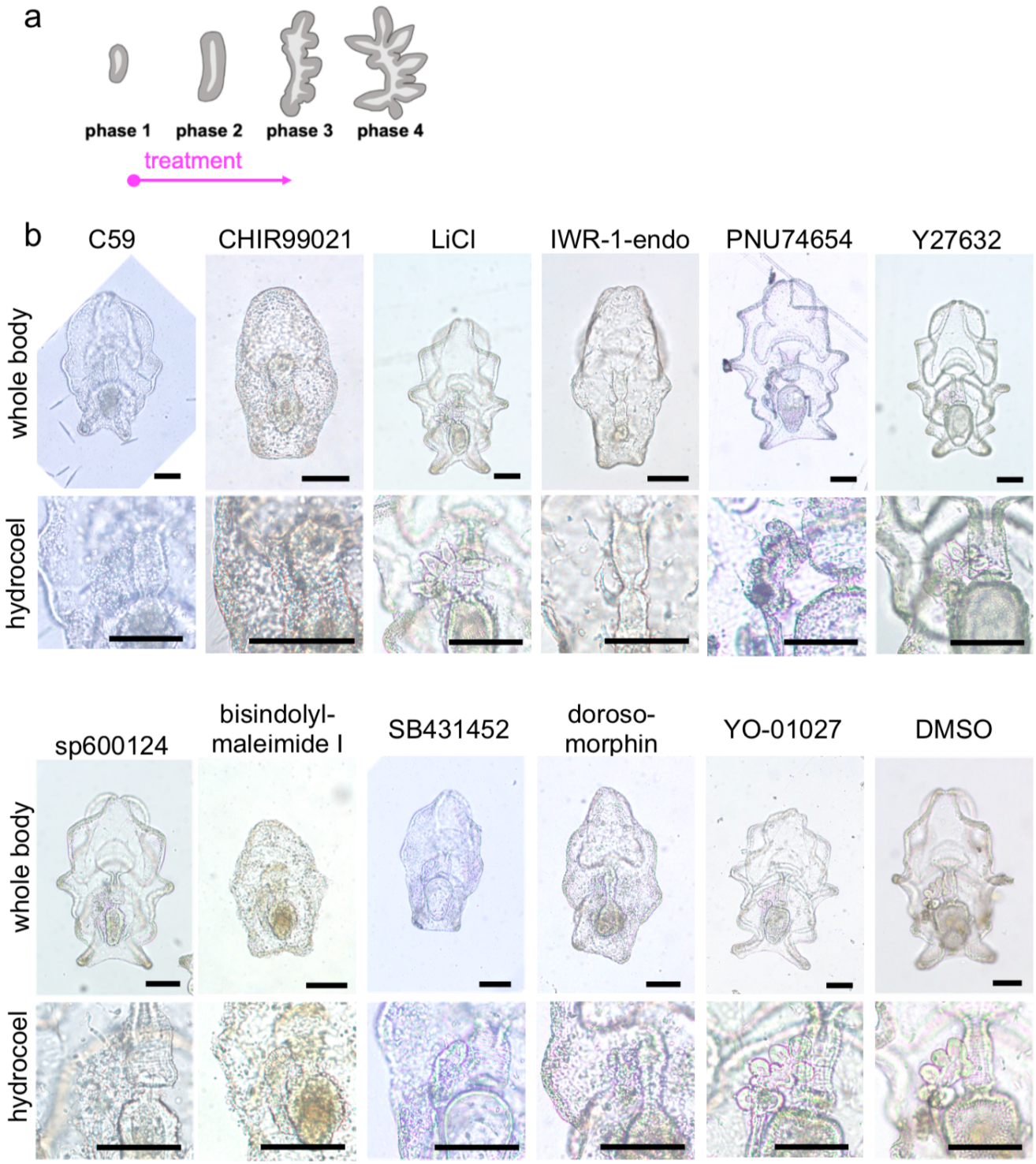

Figure 3-13. Phenotype of chemical treatment.

(a) Treatment was initiated at phase 1 and larvae were kept until they showed a clear phenotype or became phase 4. (b) Phenotype of treatment. Whole body（dorsal view, anteritor top） are presented in upper row and magnified images of the hydrocoel are presented in lower row. Scale: 100 μm

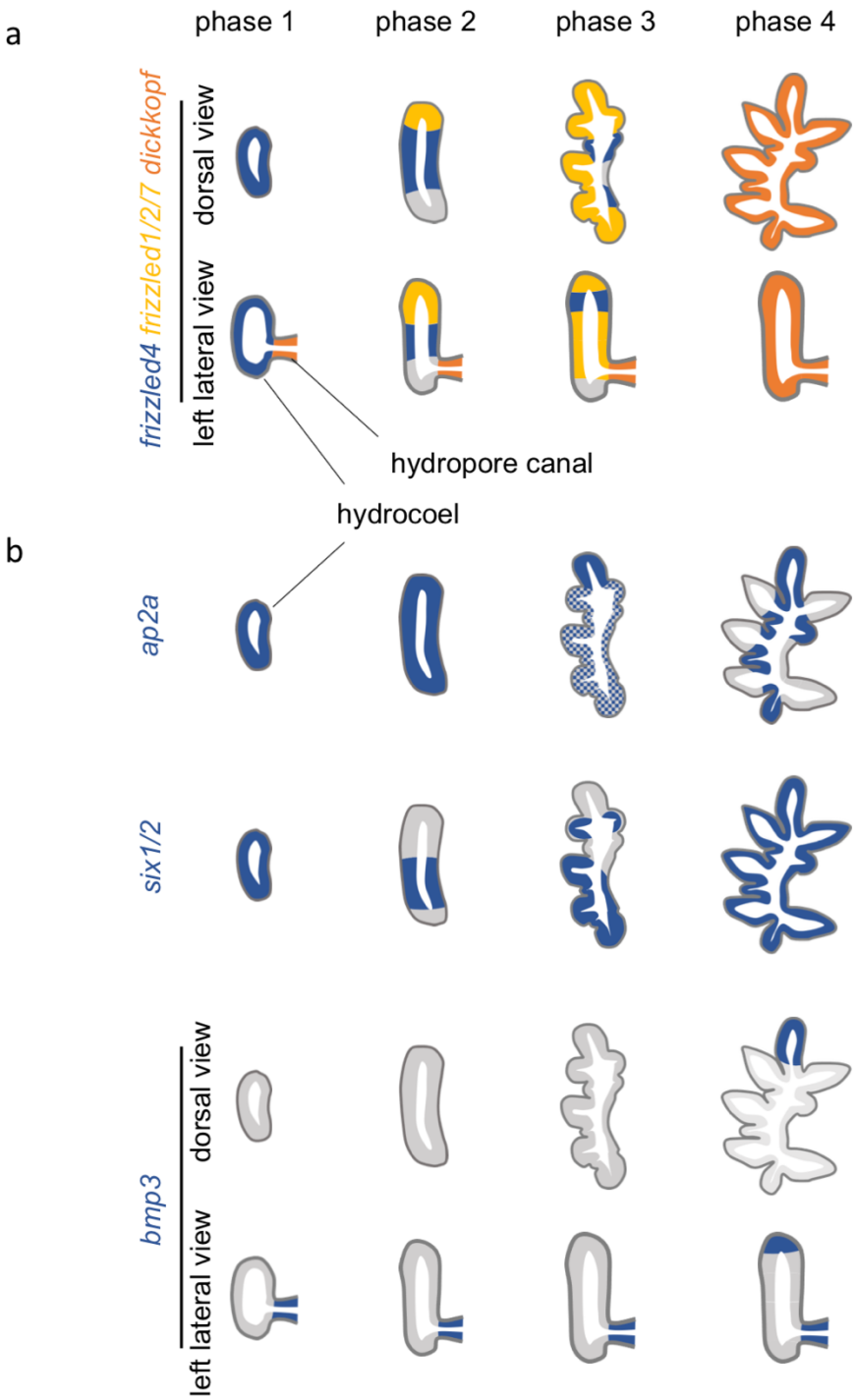

Figure 3-14 Schematic illustration of genes which showed heterogeneous expression in the hydrocoel.

Expression pattern is based on Fig. 3-6 to 3-12. Only the hydrocoel and hydropore canalare presented. (a) Expression pattern of Wnt related genes *(frizzled4, frizzled1/2/7, dickkopf)*. (b) Expression pattern of other genes with heterogeneous expression in the hydrocoel *(ap2a, six1/2, bmp3)*.

General Discussion

Highlights of this thesis and insights from results

In this study, to clarify the developmental mechanism of the pentaradial body plan in a sea cucumber species, I focused on the hydrocoel, that is the first pentaradial structure formed during development (Fig. G-1).

In Chapter 1, I demonstrated that the hydrocoel induces the pentamery of other tissues, resulting in the formation of a pentaradial body plan. The importance of the hydrocoel in the development of the pentaradial body plan has long been pointed out (Hyman, 1955). Although it has been known that the hydrocoel has the potential to induce the formation of adult tissues (Minsuk and Raff, 2002a), the fact that the pentaradial structure of the hydrocoel is essential for the establishment of pentamery in adult tissues is firstly shown in this study. This result indicates that the pentaradial pattern formation in the hydrocoel is the primary axis determination of the pentaradial body plan.

In Chapter 2, it was suggested that the sequential radial cell intercalation from the tip to the proximal part of the hydrocoel lobe is the driving force of hydrocoel lobe formation. In other words, the pentameric hydrocoel lobe is thought to be formed by spatiotemporally controlled cell migration.

In Chapter 3, several transcription factors and *frizzled*, receptors for Wnt, were found to be expressed with heterogeneity inside the hydrocoel, implying the involvement of these genes in the pentaradial pattern formation of hydrocoel. In addition, inhibition of the Wnt-PCP-JNK pathway resulted in the loss of hydrocoel tissue integrity and failure in hydrocoel lobe formation. Although the mechanism underlying the morphogenesis of the

hydrocoel had been completely unknown (Byrne et al., 2016a), these results demonstrate that the Wnt pathway is involved in the hydrocoel morphogenesis and suggested that regional differentiation of the hydrocoel occur during the hydrocoel development.

In summary, this study showed that the pentaradial body plan of echinoderms is formed by the hydrocoel controlling the pentamery of adult tissues and suggested that the morphogenesis of the pentaradial hydrocoel itself is achieved by cell migration controlled through mechanisms including the Wnt pathway.

On the acquisition of the pentaradial body plan of echinoderms

As mentioned above, inductive role of the hydrocoel in the body axis formation and the mechanisms underlying pentaradial morphogenesis in the hydrocoel were thought to be the key in the development of the pentaradial body plan. If so, how were these developmental mechanisms acquired in the ancestor of extant echinoderms?

There is a homology in the structure of planktonic larvae between echinoderms and hemichordates, the sister group of echinoderms. Larvae of hemichordates also have a mesodermal coelom (mesocoel) homologous to the hydrocoel (Peterson et al., 2000). However, in hemichordates, the mesocoel forms bilaterally symmetrical collar, a part of bilateral adult body (Kaul-Strehlow and Stach, 2013). To understand the evolutionary process of the pentaradial pattern formation, it is important to examine the mechanisms underlying pentaradial pattern formation were co-opted from conserved mechanisms in bilaterians, or novel genes or regulatory mechanisms were acquired in the ancestor of echinoderms. Comparison of the expression patterns in other echinoderms and hemichordates of genes that are suggested to be involved in hydrocoel pattern formation

in this study will provide deeper insights for this question. Another background to the acquisition of the pentaradial body plan is why the hydrocoel acquired the ability to rearrange the bilateral larvae to pentaradial juvenile. During metamorphosis, many species of echinoderms rotate their internal organs perpendicular to the larval anteroposterior axis and the mouth is newly formed on the left side. It is said that this body torsion in ancestral echinoderms allowed them to diverge from bilateral framework and establish a new body axis (Smith, 2008). On the other hand, in sea cucumbers including *A. japonicus*, which are considered to be the derived group, the degree of body torsion is small, and larval left-right axis remains in the body arrangement even after metamorphosis (Smirnov, 2014b). Investigations on the conflict between original LR axis and pentaradial axis in sea cucumbers will deepen our understanding in the acquisition of novel pentaradial symmetry.

On the conservation and diversification of pentaradial body plan

Echinoderms present diverged morphology although the pentaradial symmetry is conserved. One theory that explains the principles behind the diversification of echinoderm morphology is the extraxial-axial theory (David and Mooi, 1998). The extraxial-axial theory postulates that changes in the ratio of pentaradial axial regions associated with water vascular system to extraxial regions, which covers out of the axial regions, are associated with the diversification of echinoderm morphology. In this study, I found that the hydrocoel regulates the pentamery of other tissues, and when this finding is applied to extraxial-axial theory, it can be said that extraxial-axial ratio means the balance between the region under the influence of hydrocoel and the region out of

influence. In other words, the changes in the regions under influence of the hydrocoel can be a parameter which explains the diversification of echinoderm body plan.

On the other hand, it is also interesting that the pentaradial symmetry has been basically conserved despite the diversification in echinoderm morphology. Interestingly, the hydrocoel pentamery has been basically conserved despite the diversification in echinoderm morphology. Even in a development of multiarmed sea star *Coscinasterias acutispina,* whose juvenile has six arms, the number of hydrocoel lobes is five at first and the sixth lobe is added later (Shibata et al., 2010). It is possible that the patterning mechanism in the hydrocoel cannot make the patterns other than multiples of five and thus pentaradial symmetry might be widely conserved among echinoderms. Once the exact mechanisms underlying pentameral pattern formation is clarified, the phenotypic variations of perturbation experiments on the pattern formation will provide the important insights to this issue. In the consideration of evolution, echinoderms are thought to have undergone triradiate symmetry (Smith and Zamora, 2013) suggesting that the patterning mechanism also possible to create a triplet pattern with some modification. Mathematical model will help us in analyzing the conservation and diversification of the pattern formation mechanism. For example, the patterning of digits and finger joints in vertebrate limbs is known to proceed based on the Turing model, and simulations have been used to not only verify the patterning mechanism, but also to identify critical parameters in the diversification of patterns (Raspopovic et al., 2014; Scoons et al., 2020). Thus, by using the findings of this study as a starting point, we can expect to gain evolutionary and developmental insights into the diversification and conservation of echinoderm body plans.

As I have discussed, elucidation of developmental mechanisms underlying the

pentaradial body plan relates to the acquisition, diversification, and conservation of the body plan. Detailed investigation of molecular basis of developmental mechanisms and the comparative analysis to identify the critical change in the gene regulatory network will provide us novel insights into the background of animal body plan diversification.

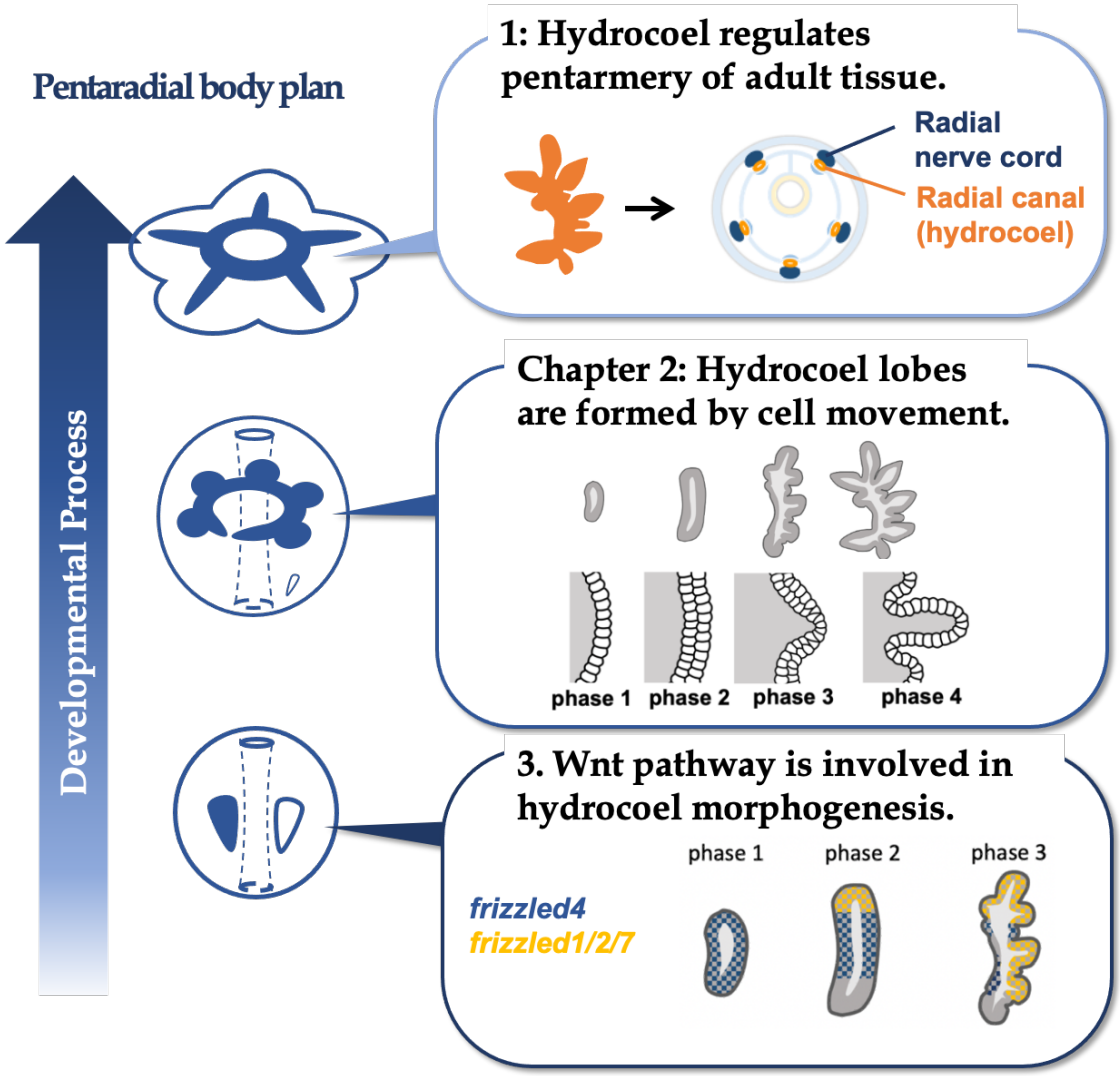

Figure G1. Graphical abstract of this thesis.

Acknowledgement

I would like to express my deepest gratitude to my supervisor, Professor. Toru Miura, for his encouragement, advice, and discussion through this study. I also would like to appreciate to Dr. Mariko Kondo for her guidance and support through my master course.

I am also grateful to Dr. Naoki Irie and Dr. Yui Uchida for discussion and support for RNA-seq analysis; Mr. Takafumi Ikeda and Dr. Toru Kawanishi for their encouragement and advice on embryology and RNA-seq analysis; Dr. Gary Wessel and PRIMO lab members for their technical support and discussion for functional experiment; Ms. Akiko Nagai and Dr. Akihito Omori for encouragement and advice on developmental experiments of echinoderms; Dr. Hiroyuki Takeda, Dr. Takema Fukatsu, Dr. Toshihiko Fujita for reviewing this thesis and precious advice. I would like to express my gratitude to Y. Harumoto and the staff of Aquamarine Fukushima, Fukushima Ocean Science Museum and Dr. Daisuke Shibata or assisting us at the time of sampling.

I would like to express my gratitude to Dr. Manabu Yoshida, Dr. Daisuke Kurokawa, Dr. Masanori Okanishi, Mr. Hisanori Kohtsuka and all the alumni and colleagues of Misaki Marine Biological Station for lots of advice, important discussion, support in experiments and field sampling and encouragements in days at MMBS.

Finally, I would like to appreciate to my parents, Mr. Munetaka Udagawa, Ms. Natsuko Udagawa, my brothers, Mr. Nobuyuki Udagawa, Mr. Seiji Udagawa and my grandmothers, Ms. Reiko Udagawa and Ms. Sachiko Miki for their understanding, supports and heartful encouragement through my Ph.D. course.

References

Adachi, S., Niimi, I., Sakai, Y., Sato, F., Minokawa, T., Urata, M., Sehara-fujisawa, A., Kobayashi, I., Yamaguchi, M., 2018. Anteroposterior Molecular Registries in Ectoderm of the Echinus Rudiment 1297–1307. https://doi.org/10.1002/dvdy.24686

Andrikou, C., Iovene, E., Rizzo, F., Oliveri, P., Arnone, M., 2013. Myogenesis in the sea urchin embryo: the molecular fingerprint of the myoblast precursors. Evodevo 4, 33. https://doi.org/10.1186/2041-9139-4-33

Andrikou, C., Pai, C.Y., Su, Y.H., Arnone, M.I., 2015. Logics and properties of a genetic regulatory program that drives embryonic muscle development in an echinoderm. Elife 4, 1–22. https://doi.org/10.7554/eLife.07343

Bennett, B.L., Sasaki, D.T., Murray, B.W., O'Leary, E.C., Sakata, S.T., Xu, W., Leisten, J.C., Motiwala, A., Pierce, S., Satoh, Y., Bhagwat, S.S., Manning, A.M., Anderson, D.W., 2001. SP600125, an anthrapyrazolone inhibitor of Jun N-terminal kinase. Proc. Natl. Acad. Sci. U. S. A. 98, 13681–13686. https://doi.org/10.1073/pnas.251194298

Bolger, A.M., Lohse, M., Usadel, B., 2014. Trimmomatic: A flexible trimmer for Illumina sequence data. Bioinformatics 30, 2114–2120. https://doi.org/10.1093/bioinformatics/btu170

Burke, R.D., Osborne, L., Wang, D., Murabe, N., Yaguchi, S., Nakajima, Y., 2006. Neuron-Specific Expression of a Synaptotagmin Gene in the Sea Urchin Strongylocentrotus purpuratus 251, 244–251. https://doi.org/10.1002/cne.20939

Byrne, M., Koop, D., Morris, V.B., Chui, J., Wray, G.A., Cisternas, P., 2018. Expression of genes and proteins of the pax-six-eya-dach network in the metamorphic sea urchin: Insights into development of the enigmatic echinoderm body plan and sensory structures. Dev. Dyn. 247, 239–249. https://doi.org/10.1002/dvdy.24584

Byrne, M., Martinez, P., Morris, V., 2016a. Evolution of a pentameral body plan was not linked to translocation of anterior Hox genes: The echinoderm HOX cluster revisited. Evol. Dev. 18, 137–143. https://doi.org/10.1111/ede.12172

Carlson, M., Pagès, H., 2020. AnnotationForge: Tools for building SQLite-based annotation data packages [WWW Document]. R Packag. version 1.32.0.

Cary, G.A., Hinman, V.F., 2017. Echinoderm development and evolution in the post-genomic era. Dev. Biol. 427, 203–211. https://doi.org/10.1016/j.ydbio.2017.02.003

Chen, B., Dodge, M.E., Tang, W., Lu, J., Ma, Z., Fan, C.W., Wei, S., Hao, W., Kilgore, J., Williams, N.S., Roth, M.G., Amatruda, J.F., Chen, C., Lum, L., 2009. Small molecule-mediated disruption of Wnt-dependent signaling in tissue regeneration and cancer. Nat. Chem. Biol. 5, 100–107. https://doi.org/10.1038/nchembio.137

Chou, A.H., Howard, B.D., 2002. Inhibition by Wnt-1 or Wnt-3a of nerve growth factor-induced differentiation of PC12 cells is reversed by bisindolylmaleimide-I but not by several other PKC inhibitors. Oncogene 21, 6348–6355. https://doi.org/10.1038/sj.onc.1205791

Cobb, J.L.S., 1985. The neurobiology of the ectoneural/hyponeural synaptic connection in an echinoderm. Biol. Bull. 168, 432–446. https://doi.org/10.2307/1541523
Conesa, A., Götz, S., García-Gómez, J.M., Terol, J., Talón, M., Robles, M., 2005. Blast2GO: A universal tool for annotation, visualization and analysis in functional genomics research. Bioinformatics 21, 3674–3676. https://doi.org/10.1093/bioinformatics/bti610
Croce, J., Duloquin, L., Lhomond, G., McClay, D.R., Gache, C., 2006. Frizzled5/8 is required in secondary mesenchyme cells to initiate archenteron invagination during sea urchin development. Development 133, 547–557. https://doi.org/10.1242/dev.02218
Cui, M., Siriwon, N., Li, E., Davidson, E.H., Peter, I.S., 2014. Specific functions of the Wnt signaling system in gene regulatory networks throughout the early sea urchin embryo. Proc. Natl. Acad. Sci. U. S. A. 111, E5029–E5038. https://doi.org/10.1073/pnas.1419141111
David, B., Mooi, R., 1998. Major events in the evolution of echinoderms viewed by the light of embryology. Echinoderms San Fr. 21–28.
Demilly, A., Steinmetz, P., Gazave, E., Marchand, L., Vervoort, M., 2013. Involvement of the Wnt/β-catenin pathway in neurectoderm architecture in Platynereis dumerilii. Nat. Commun. 4. https://doi.org/10.1038/ncomms2915
Dolmatov, I.Y., Ginanova, T.T., Frolova, L.T., 2016. Metamorphosis and definitive organogenesis in the holothurian Apostichopus japonicus. Zoomorphology 135, 173–188. https://doi.org/10.1007/s00435-015-0299-y
Dolmatov I . Yu ., Yushin V . V, 1993. Larval development of Eupentacta fraudatrix (Holothuroidea , Dendrochirota). Asian Mar. Biol. 10, 123–132.
Dush, M.K., Nascone-Yoder, N.M., 2013. Jun N-terminal kinase maintains tissue integrity during cell rearrangement in the gut. Dev. 140, 1457–1466. https://doi.org/10.1242/dev.086850
Ettensohn, C.A., 1985. Gastrulation in the sea urchin embryo is accompanied by the rearrangement of invaginating epithelial cells. Dev. Biol. 112, 383–390. https://doi.org/10.1016/0012-1606(85)90410-5
Ewald, A.J., Huebner, R.J., Palsdottir, H., Lee, J.K., Perez, M.J., Jorgens, D.M., Tauscher, A.N., Cheung, K.J., Werb, Z., Auer, M., 2012. Mammary collective cell migration involves transient loss of epithelial features and individual cell migration within the epithelium. J. Cell Sci. 125, 2638–2654. https://doi.org/10.1242/jcs.096875
Ferkowicz, M.J., Raff, R.A., 2001. Wnt gene expression in sea urchin development: Heterochronies associated with the evolution of developmental mode. Evol. Dev. 3, 24–33. https://doi.org/10.1046/j.1525-142X.2001.00084.x
Garner, S., Zysk, I., Byrne, G., Kramer, M., Moller, D., Taylor, V., Burke, R.D., 2016. Neurogenesis in sea urchin embryos and the diversity of deuterostome neurogenic mechanisms. Dev. 143, 286–297. https://doi.org/10.1242/dev.124503
Hao, J., Daleo, M.A., Murphy, C.K., Yu, P.B., Ho, J.N., Hu, J., Peterson, R.T., Hatzopoulos, A.K., Hong, C.C., 2008. Dorsomorphin, a selective small molecule inhibitor of BMP signaling, promotes cardiomyogenesis in embryonic stem cells. PLoS One 3. https://doi.org/10.1371/journal.pone.0002904
Harada, Y., Shoguchi, E., Taguchi, S., Okai, N., Humphreys, T., Tagawa, K., Satoh,

N., 2002. Conserved Expression Pattern of BMP-2/4 in Hemichordate Acorn Worm and Echinoderm Sea Cucumber Embryos . Zoolog. Sci. 19, 1113–1121. https://doi.org/10.2108/zsj.19.1113
Hardin, J.D., Cheng, L.Y., 1986. The mechanisms and mechanics of archenteron elongation during sea urchin gastrulation. Dev. Biol. 115, 490–501. https://doi.org/10.1016/0012-1606(86)90269-1
Hasebe, T., Fujimoto, K., Kajita, M., Fu, L., Shi, Y.B., Ishizuya-Oka, A., 2017. Thyroid Hormone-Induced Activation of Notch Signaling is Required for Adult Intestinal Stem Cell Development During Xenopus Laevis Metamorphosis. Stem Cells 35, 1028–1039. https://doi.org/10.1002/stem.2544
Heisenberg, C.P., Bellaïche, Y., 2013. Forces in tissue morphogenesis and patterning. Cell 153, 948. https://doi.org/10.1016/j.cell.2013.05.008
Hinck, L., Silberstein, G.B., 2005. The mammary end bud as a motile organ. Breast Cancer Res. 7, 245–251. https://doi.org/10.1186/bcr1331
Huerta-Cepas, J., Forslund, K., Coelho, L.P., Szklarczyk, D., Jensen, L.J., Von Mering, C., Bork, P., 2017. Fast genome-wide functional annotation through orthology assignment by eggNOG-mapper. Mol. Biol. Evol. 34, 2115–2122. https://doi.org/10.1093/molbev/msx148
Hyman, L.H., 1955. The Invertebrates: Echinodermata, the Coelomate Bilateria. Volume IV.
Inman, G.J., Nicolás, F.J., Callahan, J.F., Harling, J.D., Gaster, L.M., Reith, A.D., Laping, N.J., Hill, C.S., 2002. SB-431542 is a potent and specific inhibitor of transforming growth factor-β superfamily type I activin receptor-like kinase (ALK) receptors ALK4, ALK5, and ALK7. Mol. Pharmacol. 62, 65–74. https://doi.org/10.1124/mol.62.1.65
Kamei, Y., Suzuki, M., Watanabe, K., Fujimori, K., Kawasaki, T., Deguchi, T., Yoneda, Y., Todo, T., Takagi, S., Funatsu, T., Yuba, S., 2009. Infrared laser–mediated gene induction in targeted single cells in vivo. Nat. Methods 6, 79–81. https://doi.org/10.1038/nmeth.1278
Kato, S., Tsurumaru, S., Taga, M., Yamane, T., Shibata, Y., Ohno, K., Fujiwara, A., Yamano, K., Yoshikuni, M., 2009. Neuronal peptides induce oocyte maturation and gamete spawning of sea cucumber, Apostichopus japonicus. Dev. Biol. 326, 169–176. https://doi.org/10.1016/j.ydbio.2008.11.003
Kaul-Strehlow, S., Stach, T., 2013. A detailed description of the development of the hemichordate Saccoglossus kowalevskii using SEM, TEM, Histology and 3D-reconstructions. Front. Zool. 10, 1. https://doi.org/10.1186/1742-9994-10-53
Keller, R.E., 1980. The cellular basis of epiboly: An SEM study of deep-cell rearrangement during gastrulation in Xenopus laevis. J. Embryol. Exp. Morphol. VOL.60, 201–234. https://doi.org/10.1242/dev.60.1.201
Kikuchi, M., Omori, A., Kurokawa, D., Akasaka, K., 2015. Patterning of anteroposterior body axis displayed in the expression of Hox genes in sea cucumber Apostichopus japonicus. Dev. Genes Evol. 225, 275–286. https://doi.org/10.1007/s00427-015-0510-7
Kim, D., Paggi, J.M., Park, C., Bennett, C., Salzberg, S.L., 2019. Graph-based genome alignment and genotyping with HISAT2 and HISAT-genotype. Nat. Biotechnol. 37, 907–915. https://doi.org/10.1038/s41587-019-0201-4
Kimberly, E.L., Hardin, J., 1998. Bottle cells are required for the initiation of primary

invagination in the sea urchin embryo. Dev. Biol. 204, 235–250. https://doi.org/10.1006/dbio.1998.9075
Kimura, E., Deguchi, T., Kamei, Y., Shoji, W., Yuba, S., Hitomi, J., 2013. Application of infrared laser to the zebrafish vascular system:Gene induction, tracing, and ablation of single endothelial cells. Arterioscler. Thromb. Vasc. Biol. 33, 1264–1270. https://doi.org/10.1161/ATVBAHA.112.300602
Koop, D., Cisternas, P., Morris, V.B., Strbenac, D., Yang, J.Y.H., Wray, G.A., Byrne, M., 2017. Nodal and BMP expression during the transition to pentamery in the sea urchin Heliocidaris erythrogramma: insights into patterning the enigmatic echinoderm body plan. BMC Dev. Biol. 17, 4. https://doi.org/10.1186/s12861-017-0145-1
Koyanagi, M., Haendeler, J., Badorff, C., Brandes, R.P., Hoffmann, J., Pandur, P., Zeiher, A.M., Kühl, M., Dimmeler, S., 2005. Non-canonical Wnt signaling enhances differentiation of human circulating progenitor cells to cardiomyogenic cells. J. Biol. Chem. 280, 16838–16842. https://doi.org/10.1074/jbc.M500323200
Li, J., Chatzeli, L., Panousopoulou, E., Tucker, A.S., Green, J.B.A., 2016. Epithelial stratification and placode invagination are separable functions in early morphogenesis of the molar tooth. Dev. 143, 670–681. https://doi.org/10.1242/dev.130187
Li, Y., Kikuchi, M., Li, X., Gao, Q., Xiong, Z., Ren, Y., Zhao, R., Mao, B., Kondo, M., Irie, N., Wang, W., 2018. Weighted gene co-expression network analysis reveals potential genes involved in early metamorphosis process in sea cucumber Apostichopus japonicus. Biochem. Biophys. Res. Commun. 495, 1395–1402. https://doi.org/10.1016/j.bbrc.2017.11.154
Li, Y., Omori, A., Flores, R.L., Satterfield, S., Nguyen, C., Ota, T., Tsurugaya, T., Ikuta, T., Ikeo, K., Kikuchi, M., Leong, J.C.K., Reich, A., Hao, M., Wan, W., Dong, Y., Ren, Y., Zhang, S., Zeng, T., Uesaka, M., Uchida, Y., Li, X., Shibata, T.F., Bino, T., Ogawa, K., Shigenobu, S., Kondo, M., Wang, F., Chen, L., Wessel, G., Saiga, H., Cameron, R.A., Livingston, B., Bradham, C., Wang, W., Irie, N., 2020. Genomic insights of body plan transitions from bilateral to pentameral symmetry in Echinoderms. Commun. Biol. 3, 1–10. https://doi.org/10.1038/s42003-020-1091-1
Liu, S., Sun, J., Ru, X., Hamel, J.-F., Mercier, A., 2015. Broodstock Conditioning and Spawning. Dev. Aquac. Fish. Sci. 39, 101–110.
Love, M.I., Huber, W., Anders, S., 2014. Moderated estimation of fold change and dispersion for RNA-seq data with DESeq2. Genome Biol. 15, 1–21. https://doi.org/10.1186/s13059-014-0550-8
Lowe, C.J., Wu, M., Salic, A., Evans, L., Lander, E., Stange-Thomann, N., Gruber, C.E., Gerhart, J., Kirschner, M., 2003. Anteroposterior patterning in hemichordates and the origins of the chordate nervous system. Cell 113, 853–865. https://doi.org/10.1016/S0092-8674(03)00469-0
Lu, J., Ma, Z., Hsieh, J.C., Fan, C.W., Chen, B., Longgood, J.C., Williams, N.S., Amatruda, J.F., Lum, L., Chen, C., 2009. Structure-activity relationship studies of small-molecule inhibitors of Wnt response. Bioorganic Med. Chem. Lett. 19, 3825–3827. https://doi.org/10.1016/j.bmcl.2009.04.040
Luo, Y.J., Su, Y.H., 2012. Opposing Nodal and BMP Signals Regulate Left-Right

Asymmetry in the Sea Urchin Larva. PLoS Biol. 10. https://doi.org/10.1371/journal.pbio.1001402
Mashanov, V.S., Zueva, O.R., Heinzeller, T., Aschauer, B., Dolmatov, I.Y., 2007. Developmental origin of the adult nervous system in a holothurian: an attempt to unravel the enigma of neurogenesis in echinoderms. Evol. Dev. 9, 244–256. https://doi.org/10.1111/j.1525-142X.2007.00157.x
Mehta, S., Hingole, S., Chaudhary, V., 2021. The Emerging Mechanisms of Wnt Secretion and Signaling in Development. Front. Cell Dev. Biol. 9, 714746.
Milano, J., McKay, J., Dagenais, C., Foster-Brown, L., Pognan, F., Gadient, R., Jacobs, R.T., Zacco, A., Greenberg, B., Ciaccio, P.J., 2004. Modulation of Notch processing by γ-secretase inhibitors causes intestinal goblet cell metaplasia and induction of genes known to specify gut secretory lineage differentiation. Toxicol. Sci. 82, 341–358. https://doi.org/10.1093/toxsci/kfh254
Minsuk, S.B., Raff, R.A., 2002a. Pattern formation in a pentameral animal: Induction of early adult rudiment development in sea urchins. Dev. Biol. 247, 335–350. https://doi.org/10.1006/dbio.2002.0704
Morris, V.B., 2016. Analysis of coelom development in the sea urchin Holopneustes purpurescens yielding a deuterostome body plan . Biol. Open 5, 348–358. https://doi.org/10.1242/bio.015925
Morris, V.B., 2007. Origins of radial symmetry identified in an echinoderm during adult development and the inferred axes of ancestral bilateral symmetry. Proc. R. Soc. B Biol. Sci. 274, 1511–1516. https://doi.org/10.1098/rspb.2007.0312
Nakajima, Y., Kaneko, H., Murray, G., Burke, R.D., 2004. Divergent patterns of neural development in larval echinoids and asteroids. Evol. Dev. 6, 95–104. https://doi.org/10.1111/j.1525-142X.2004.04011.x
Nakano, H., Murabe, N., Amemiya, S., Nakajima, Y., 2006. Nervous system development of the sea cucumber Stichopus japonicus. Dev. Biol. 292, 205–212. https://doi.org/10.1016/j.ydbio.2005.12.038
Neumann, N.M., Perrone, M.C., Veldhuis, J.H., Huebner, R.J., Zhan, H., Devreotes, P.N., Brodland, G.W., Ewald, A.J., 2018. Coordination of Receptor Tyrosine Kinase Signaling and Interfacial Tension Dynamics Drives Radial Intercalation and Tube Elongation. Dev. Cell 45, 67-82.e6. https://doi.org/10.1016/j.devcel.2018.03.011
Okuyama, T., Yokoi, S., Abe, H., Isoe, Y., Suehiro, Y., Imada, H., Tanaka, M., Kawasaki, T., Yuba, S., Taniguchi, Y., Kamei, Y., Okubo, K., Shimada, A., Naruse, K., Takeda, H., Oka, Y., Kubo, T., Takeuchi, H., 2014. A Neural Mechanism Underlying Mating Preferences for Familiar Individuals in Medaka Fish. Science (80-.). 343, 91–94. https://doi.org/10.1126/SCIENCE.1244724
Omori, A., Kikuchi, M., Kondo, M., 2018b. Larval and Adult Body Axes in Echinoderms, in: Kobayashi, K., Kitano, T., Iwao, Y., Kondo, M. (Eds.), Reproductive and Developmental Strategies. Springer, Tokyo, pp. 763–789. https://doi.org/10.1007/978-4-431-56609-0_34
Pertea, M., Pertea, G.M., Antonescu, C.M., Chang, T.C., Mendell, J.T., Salzberg, S.L., 2015. StringTie enables improved reconstruction of a transcriptome from RNA-seq reads. Nat. Biotechnol. 33, 290–295. https://doi.org/10.1038/nbt.3122
Peterson, K.J., Arenas-Mena, C., Davidson, E.H., 2000. The A/P axis in echinoderm ontogeny and evolution: Evidence from fossils and molecules. Evol. Dev. 2, 93–

101. https://doi.org/10.1046/j.1525-142X.2000.00042.x
Piacentino, M.L., Ramachandran, J., Bradham, C.A., 2015. Late Alk4/5/7 signaling is required for anterior skeletal patterning in sea urchin embryos. Dev. 142, 943–952. https://doi.org/10.1242/dev.114322
Pond, K.W., Doubrovinski, K., Thorne, C.A., 2020. WNT/β-catenin signaling in tissue self-organization. Genes (Basel). 11, 1–18. https://doi.org/10.3390/genes11080939
Proffitt, K.D., Madan, B., Ke, Z., Pendharkar, V., Ding, L., Lee, M.A., Hannoush, R.N., Virshup, D.M., 2013. Pharmacological inhibition of the Wnt acyltransferase PORCN prevents growth of WNT-driven mammary cancer. Cancer Res. 73, 502–507. https://doi.org/10.1158/0008-5472.CAN-12-2258
Qiu, T., Zhang, T., Hamel, J.F., Mercier, A., 2015. Development, Settlement, and Post-settlement Growth. Dev. Aquac. Fish. Sci. 39, 111–131. https://doi.org/10.1016/B978-0-12-799953-1.00008-8
Raff, R.A., 1996. The Shape of Life. The University of Chicago Press, Chicago., Chicago.
Raff, R.A., Byrne, M., 2006. The active evolutionary lives of echinoderm larvae. Heredity (Edinb). 97, 244–252. https://doi.org/10.1038/sj.hdy.6800866
Range, R.C., 2018. Canonical and non-canonical Wnt signaling pathways de fi ne the expression domains of Frizzled 5 / 8 and Frizzled 1 / 2 / 7 along the early anterior- posterior axis in sea urchin embryos. Dev. Biol. 444, 83–92. https://doi.org/10.1016/j.ydbio.2018.10.003
Raspopovic, J., Marcon, L., Russo, L., Sharpe, J., 2014. Digit patterning is controlled by a Bmp-Sox9-Wnt Turing network modulated by morphogen gradients. Science (80-.). 345, 566–570. https://doi.org/10.1126/science.1252960
Riento, K., Ridley, A.J., 2003. Rocks: Multifunctional kinases in cell behaviour. Nat. Rev. Mol. Cell Biol. 4, 446–456. https://doi.org/10.1038/nrm1128
Rozhnov, S., 2014. Symmetry of echinoderms: From initial bilaterally-asymmetric metamerism to pentaradiality. Nat. Sci. 06, 171–183. https://doi.org/10.4236/ns.2014.64021
Sasagawa, Y., Hayashi, T., Danno, H., Uno, K.D., Imai, T., Ueda, H.R., 2013. Quartz-Seq: a highly reproducible and sensitive single-cell RNA-Seq reveals non-genetic gene expression heterogeneity Genome Biology. Genome Biol. 14, 1–17. https://doi.org/10.1186/gb-2013-14-4-r31
Scoones, J.C., Hiscock, T.W., 2020. A dot-stripe Turing model of joint patterning in the tetrapod limb. Development 147. https://doi.org/10.1242/dev.183699
Sharma, T., Ettensohn, C.A., 2011. Regulative deployment of the skeletogenic gene regulatory network during sea urchin development INTRODUCTION. Development 138, 2581–2590. https://doi.org/10.1242/dev.065193
Shibata, D., Moriyama, Y., Komatsu, M., Hirano, Y., 2010. Development of the fissiparous and multiarmed seastar, Coscinasterias acutispina (Stimpson). Echinoderms Durham - Proc. 12th Int. Echinoderm Conf. 17, 479–486. https://doi.org/10.1201/9780203869543-c74
Shoguchi, E., Harada, Y., Numakunai, T., Satoh, N., 2000. Expression of the Otx gene in the ciliary bands during sea cucumber embryogenesis. Genesis 27, 58–63. https://doi.org/10.1002/1526-968X(200006)27:2<58::AID-GENE20>3.0.CO;2-8

Smiley, S., 1986. Metamorphosis of Stichopus californicus (Echinodermata: Holothuroidea) and its phylogenetic implications. Biol. Bull. 171, 611–631. https://doi.org/10.2307/1541627
Smirnov, A. V., 2014a. Sea cucumbers symmetry (Echinodermata: Holothuroidea). Paleontol. J. 48, 1215–1236. https://doi.org/10.1134/s0031030114120107
Smith, A.B., 2008. Deuterostomes in a twist: The origins of a radical new body plan. Evol. Dev. 10, 493–503. https://doi.org/10.1111/j.1525-142X.2008.00260.x
Smith, A B, Peterson, K.J., Wray, G., Littlewood, D.T.J., 2004. From bilateral symmetry to pentaradiality: The phylogeny of hemichordates and echinoderms. Assem. Tree Life.
Smith, Andrew B., Peterson, K.J., Wray, G., Littlewood, D.T.J., 2004. From Bilateral Symmetry to Pentaradiality The Phylogeny of Hemichordates and Echinoderms, in: Cracraft, J., Donoghue, M.J., Editors (Eds.), Assembling the Tree of Life. Oxford University Press, New York, pp. 365–383.
Smith, A.B., Zamora, S., 2013. Cambrian spiral-plated echinoderms from Gondwana reveal the earliest pentaradial body plan. Proc. R. Soc. B Biol. Sci. 280, 13–15. https://doi.org/10.1098/rspb.2013.1197
Smith, M.M., Smith, L.C., Cameron, R.A., Urry, L.A., 2008. The larval stages of the sea urchin, Strongylocentrotus purpuratus. J. Morphol. 269, 713–733. https://doi.org/10.1002/jmor.10618
Smith, M.S., Collins, S., Raff, R.A., 2009. Morphogenetic mechanisms of coelom formation in the direct-developing sea urchin Heliocidaris erythrogramma. Dev. Genes Evol. 219, 21–29. https://doi.org/10.1007/s00427-008-0262-8
Spurlin, J.W.I., Nelson, C.M., 2017. Building branched tissue structures : from single cell guidance to coordinated construction. Philos. Trans. R. Soc. B 372, 20150527.
Stephens, L., 1986. The Effects of Aphidicolin on Morphogenesis and Differentiation in the Sea Urchin Embryo. Dev. Biol. 118, 64–69.
Su, Y.H., 2014. Telling left from right: Left-right asymmetric controls in sea urchins. Genesis 52, 269–278. https://doi.org/10.1002/dvg.22739
Sumrall, C.D., Wray, G.A., 2007. Ontogeny in the fossil record: diversification of body plans and the evolution of “aberrant” symmetry in Paleozoic echinoderms. Paleobiology 33, 149–163. https://doi.org/10.1666/06053.1
Szabó, A., Cobo, I., Omara, S., McLachlan, S., Keller, R., Mayor, R., 2016. The Molecular Basis of Radial Intercalation during Tissue Spreading in Early Development. Dev. Cell 37, 213–225. https://doi.org/10.1016/j.devcel.2016.04.008
Taguchi, S., Tagawa, K., Humphreys, T., Satoh, N., 2002. Group B Sox genes that contribute to specification of the vertebrate brain are expressed in the apical organ and ciliary bands of hemichordate larvae. Zoolog. Sci. 19, 57–66. https://doi.org/10.2108/zsj.19.57
ten Tusscher, K.H., Hogeweg, P., 2011. Evolution of networks for body plan patterning; interplay of modularity, robustness and evolvability. PLoS Comput. Biol. 7. https://doi.org/10.1371/journal.pcbi.1002208
Törönen, P., Medlar, A., Holm, L., 2018. PANNZER2: A rapid functional annotation web server. Nucleic Acids Res. 46, W84–W88. https://doi.org/10.1093/nar/gky350

Tu, Q., Cameron, R.A., Worley, K.C., Gibbs, R.A., Davidson, E.H., 2012. Gene structure in the sea urchin Strongylocentrotus purpuratus based on transcriptome analysis. Genome Res. 22, 2079–2087. https://doi.org/10.1101/gr.139170.112
Vidavsky, N., Addadi, S., Schertel, A., Ben-Ezra, D., Shpigel, M., Addadi, L., Weiner, S., 2016. Calcium transport into the cells of the sea urchin larva in relation to spicule formation. Proc. Natl. Acad. Sci. U. S. A. 113, 12637–12642. https://doi.org/10.1073/pnas.1612017113
Vonica, A., Weng, W., Gumbiner, B.M., Venuti, J.M., 2000. TCF is the nuclear effector of the β-catenin signal that patterns the sea urchin animal-vegetal axis. Dev. Biol. 217, 230–243. https://doi.org/10.1006/dbio.1999.9551
Wei, Z., Angerer, L.M., Angerer, R.C., 2016. Neurogenic gene regulatory pathways in the sea urchin embryo. Dev. 143, 298–305. https://doi.org/10.1242/dev.125989
Wei, Z., Angerer, R.C., Angerer, L.M., 2011. Direct development of neurons within foregut endoderm of sea urchin embryos 108, 1–5. https://doi.org/10.1073/pnas.1018513108
Wessel, G.M., Zhang, W., Klein, W.H., 1990. Myosin heavy chain accumulates in dissimilar cell types of the macromere lineage in the sea urchin embryo. Dev. Biol. 140, 447–454. https://doi.org/10.1016/0012-1606(90)90093-X
Williams, J.M., Daniel, C.W., 1983. Mammary ductal elongation: Differentiation of myoepithelium and basal lamina during branching morphogenesis. Dev. Biol. 97, 274–290. https://doi.org/10.1016/0012-1606(83)90086-6
Woo, S.P., Ogawa, A., Tan, S.H., Yasin, Z., Kajihara, H., Fujita, T., 2017. A taxonomic revision of the genus Apostichopus (Holothuroidea: Stichopodidae) from Japan. Zootaxa 4350, 121–135. https://doi.org/10.11646/zootaxa.4350.1.7
Wu, T., Hu, E., Xu, S., Chen, M., Guo, P., Dai, Z., Feng, T., Zhou, L., Tang, W., Zhan, L., Fu, X., Liu, S., Bo, X., Yu, G., 2021. clusterProfiler 4.0: A universal enrichment tool for interpreting omics data. Innovation(China) 2, 100141. https://doi.org/10.1016/j.xinn.2021.100141
Yaguchi, J., Takeda, N., Inaba, K., Yaguchi, S., 2016. Cooperative Wnt-Nodal Signals Regulate the Patterning of Anterior Neuroectoderm. PLoS Genet. 12, 1–27. https://doi.org/10.1371/journal.pgen.1006001
Yankura, K.A., Koechlein, C.S., Cryan, A.F., Cheatle, A., Hinman, V.F., 2013. Gene regulatory network for neurogenesis in a sea star embryo connects broad neural specification and localized patterning. Proc. Natl. Acad. Sci. 110, 8591–8596. https://doi.org/10.1073/pnas.1220903110
Yoshida, W., Tamai, A., Yanaka, T., Ishida, S., 2001. Normal development and artificial breeding of sea cucumber (Stichopus japonicus Selenka) from Mutsu Bay. Bull. Fac. Agric. Life Sci., Hirosaki Univ. 4, 16–23.
Yu, P.B., Hong, C.C., Sachidanandan, C., Babitt, J.L., Deng, D.Y., Hoyng, S.A., Lin, H.Y., Bloch, K.D., Peterson, R.T., 2008. Dorsomorphin inhibits BMP signals required for embryogenesis and iron metabolism. Nat. Chem. Biol. 4, 33–41. https://doi.org/10.1038/nchembio.2007.54
Zeng, C.-W., Kamei, Y., Shigenobu, S., Sheu, J.-C., Tsai, H.-J., 2021. Injury-induced Cavl-expressing cells at lesion rostral side play major roles in spinal cord regeneration. Open Biol. 11, 200304. https://doi.org/10.1098/RSOB.200304
Zhang, X., Sun, L., Yuan, J., Sun, Y., Gao, Y., Zhang, L., Li, S., Dai, H., Liu, C., Yu,

Y., Liu, S., Lin, W., Guo, K., Jin, S., Xu, P., Storey, B., Huan, P., Zhang, T., Zhou, Y., Zhang, J., Lin, C., Li, X., Xing, L., Huo, D., Sun, M., Wang, L., Mercier, A., Li, F., Yang, H., Xiang, J., 2017. The sea cucumber genome provides insights into morphological evolution and visceral regeneration.